1-1-2015

Quantification Of Auto-Ignition In Diesel Engines

Umashankar M. Joshi
Wayne State University,

QUANTIFICATION OF AUTO-IGNITION IN DIESEL ENGINES

by

UMASHANKAR JOSHI

DISSERTATION

Submitted to the Graduate School

of Wayne State University,

Detroit, Michigan

in partial fulfillment of the requirements

for the degree of

DOCTOR OF PHILOSOPHY

2015

MAJOR: MECHANICAL ENGINEERING

Approved by:

_____

Advisor Date

_____

_____

_____

_____

DEDICATION

I dedicate this work to my grandparents.

ACKNOWLEDGMENTS

I would like to express my deepest and heartfelt gratitude to my advisor Prof. Naeim Henein. I am indebted to him for the opportunity he gave me to work in the Center for Automotive Research at Wayne State. I have benefitted a lot from his guidance and vast knowledge in this field. The experience of working with him has not only been limited to professional and technical knowledge, I have learnt from him that hard work, patience and perseverance are key to a person's overall development.

I would also like to thank Dr Trilochan Singh, Dr. Dinu Taraza, Dr. Marcis Jansons, and Dr Peter Schihl for their important inputs and feedbacks. I would like to thank Dr. Ziliang Zheng for being a great colleague and friend, and for being there always to help me in testing, data analysis and simulations. I am also grateful to the technical support given by Lidia, Eugene and Marvin for the repair and maintenance works done for the lab. A special thanks to the colleagues in the Center for Automotive Research for their help and support, especially Chandrasekharan Jayakumar, Amit Shrestha and Rolando Ferrer.

Last but not the least; I would like to thank my parents and wife for their support and encouragement. Without them it would not have been possible.

Umashankar Joshi

August 2015, Detroit MI

TABLE OF CONTENTS

LIST OF FIGURES

LIST OF TABLES

NOMENCLATURE

AMR	Adaptive Mesh Refinement
CN	Cetane Number
CTL	Coal-to-Liquid
CI	Compression Ignition
CR	Compression Ratio
CFD	Computational Fluid Dynamics
CFR	Co-operative Fuel Research
CAD	Crank Angle Degree
CuRHR	Cumulative Rate of Heat Release
DCN	Derived Cetane Number
E_a	Apparent Activation Energy
ECU	Engine Control Module
EGR	Exhaust Gas Recirculation
FACE	Fuels for Advanced Combustion Engine
FP	Fuel Pressure
GTL	Gas-to-Liquid
HCN	High Cetane Number
HSDI	High Speed Direct Injection
HCCI	Homogeneous Charge Compression Ignition
ID	Ignition Delay

IQT	Ignition Quality Tester
IMEP	Indicated Mean Effective Pressure
IPK	Isomerized Paraffinic Kerosene
JP-8	Jet Propellant 8
KH-RT	Kelvin-Helmholts/Rayleigh-Taylor
LLNL	Lawrence Livermore National Lab
LCN	Low Cetane Number
LTC	Low Temperature Combustion
NL	Needle Lift
NTC	Negative Temperature Coefficient
PNGV	Partnership for Next Generation Vehicles
PCCI	Premixed Charge Compression Ignition
PRF	Primary Reference Fuel
RANS	Reynolds Averaged Navier-Stokes
RHR	Rate of Heat Release
SI	Spark Ignition
SOI	Start of Injection
SOC	Start of Combustion
ULSD	Ultra Low Sulfur Diesel
TDC	Top Dead Center
WSU	Wayne State University

CHAPTER 1

SCOPE OF THE WORK

1.1 Introduction

Diesel engines form a bulk of the heavy duty engines used in the field of power generation, transportation, construction, marine and agricultural applications owing to its high thermal and combustion efficiency. The high compression ratio, reduced pumping losses and overall lean burn mixture due to heterogeneous combustion improves it efficiency compared to spark ignited (SI) engines. However, the rising problem of global warming and climate change is forcing the government to bring in first-ever efficiency standards for trucks [1] to reduce CO_2 emissions, the need of the hour is to make diesel engines more efficient. Also, to reduce American dependency on foreign crude imports and strengthen energy security there is a need to make the engines flexible to run on alternate fuels.

The fundamental concept on which compression ignition (CI) engines work is to form an air-fuel mixture at high temperatures and pressures so that it auto-ignites [2]. This phenomenon of auto-ignition is one of the basic distinctions between diesel engines and gasoline (SI) engines. In SI engines due to its detrimental effects it is essential to avoid auto-ignition as much as possible; on the other hand, in CI engines it plays a major role in the combustion, performance, fuel economy and emissions.

Therefore, it is highly desirable to have a better understanding of the auto-ignition processes in order to have better control of the engine.

This dissertation covers the effect of ignition delay definitions, effective temperatures and engine conditions on global activation energy, essentially a measure of auto-ignition characteristics of fuels. Furthermore, based on these findings a correlation between the Derived Cetane Number (DCN) and the apparent activation energy of the fuels has been developed.

1.2 Dissertation Framework

The dissertation starts with a review of previous investigations on auto-ignition and combustion behavior of fuels in engines, in chapter 2. This review would also include the various ignition delay correlations previously developed. In addition, each chapter will have its own literature review, specific to its requirements. Chapter 3 has a detailed description of the test cell which includes the engine, accessory systems and instrumentation. In chapter 4, we will discuss about the preliminary results and their comparison to results obtained in previous work [3, 4]. This will be the foundation work for this research and will provide the objective for further investigations.

The major part of this research work is covered in chapters 5-7. In chapter 5, an effort has been made to find out the most suitable ignition delay definition for auto-ignition studies. Since, ID is the time period between SOI and SOC any change in the definition of those two would result in change in ID definition. Furthermore, ID values are used in Arrhenius plots based on which global activation energy of combustion

would be calculated, variations in ID value would result in variation in global activation energy value of a fuel as well. Thus, changes in SOI and SOC would indirectly result in changes in global activation energy values of fuel. The chapter focuses on how much would be the effect of different SOI and SOC definitions on global activation energy.

Chapter 6 concentrates on the other important parameter that affects calculation of global activation energy value i.e. temperature. In homogeneous charge and gas phase reactors it is convenient to use initial temperature in ignition delay correlations for calculating global activation energy, since the change in temperature would be due to chemical reactions only. However in heterogeneous combustion, physical delay also plays an important part in auto-ignition and is included in ID period, as a result it becomes important to have an effective temperature which would be a good representation of the physical and chemical processes taking place during ID period. Researchers have remained divided in defining the effective temperature for heterogeneous combustion during ID period [4-8]. The effect of different effective temperatures on global activation calculations has been discussed in this chapter.

In engines the temperature during auto-ignition can be changed either by varying the intake air temperature or by changing the SOI. Besides changing temperature, each method also affects cylinder pressure, wall impingement, swirl pattern and air fuel mixing. However, global activation energy is most sensitive to temperature and it is interesting to see the results of these two totally different approaches of temperature control on it. In chapter 7, the effect of these two methods on global activation energy has been studied for different fuels. It also includes CFD and 0-dimensional simulation

results which helps us in a deeper understanding of the factors affecting the processes during ID period and leading to auto-ignition.

The final chapter – chapter 8, gives the conclusions for the thesis and some recommendations for the future work.

CHAPTER 2

LITERATURE REVIEW

2.1 Introduction

From being stationary power source to driving heavy duty trucks and tractors, ships and submarines, cranes, locomotives, and electric generators the diesel engine has changed a lot since it was invented by Rudolf Diesel in 1893. Although, we have been able to achieve 55% efficiency [2, 9, 10] in the low speed marine and electric power generation engines, we still lag in increasing the efficiency beyond 45% for the medium and high speed engines used in trucks and locomotives. In addition, the stringent standards set by government to reduce carbon emissions would further compel the industry to better the efficiency of diesel engines.

Besides the need to improve fuel economy, the reducing global oil reserves also poses risk to the energy independence and security of the country. This has led to widespread research into use of alternative fuels for diesel engine applications. Alternative fuels range from renewable fuels like bio-diesel [11-14] and ethanol [15-19] to non-renewable synthetically manufactured fuels like S-8 [20, 21] and Sasol IPK [22-24]. The synthetic fuels are manufactured by the Fischer-Tropsch (F-T) process from natural gas or coal: hence called Gas-to-Liquid (GTL) [25-28] and Coal-to-Liquid (CTL) [29, 30] fuels respectively. Owing to such a vast difference in sources from which the fuels are derived, they show a large variation in the physical and chemical properties. In

order to design future CI engines and modify existing engines there is a need for computer simulations of the diesel cycle using different fuels. This requires the quantification of the auto-ignition process in terms of correlations for the ignition delay period which is known to affect all aspects of diesel engine operation. Several correlations have been developed for the ignition delay period using different equipment and definitions. Almost all of these correlations include the activation energy which quantifies the sensitivity of the auto-ignition process to variations in the charge temperature. While different values for the activation energy have been reported in the literature, all previous researchers considered the activation energy to be independent of the charge pressure and density.

This investigation reviews different definitions used to specify the end for the ignition delay period, the instrumentation used for its measurement and the values of the activation energy reported in the literature. In addition, the dependence of the activation energy on the temperature in the different combustion regimes will be examined.

2. Literature Review

2.1 Ignition Delay Period

In 1914, Dixon et al [31] discovered for the first time that when a combustible fuel-air mixture is compressed in a glass cylinder it starts burning after some initial delay. This time delay for the start of combustion is now popularly referred to as ignition delay. The ignition delay time in diesel engines was not measured until 1920 by Hawk

[32]. The difference between these two measurements, done by Dixon and Hawk, would be the presence of a noticeable physical delay time in diesel engines. Although initially researchers [33-35] denied the presence of physical delay in diesel engine combustions, but later its presence was recognized by the works of Tausz and Schulte [36-38] and further confirmed by Rothrock and Waldron [39, 40] and Miller [41].

The initial stages in the ignition delay period, is predominantly dominated by physical processes like spray breakup, air entrainment, droplet formation and evaporation, and air-fuel mixing. Therefore, it is referred to as physical ignition delay period. In the latter half, the chemical reactions takeover the physical processes and become more dominant, and this stage is referred to as chemical ignition delay period. Although there are chemical reactions taking place during the physical delay period as well, their heat release rate is negligible compared to the scale and effect of physical processes. Thus, the ignition delay period in diesel engines consists of two stages and the total ignition delay is a sum of the physical and chemical ignition delay period.

2.1.1 Physical Ignition Delay

In 1936, Wenzel [42] made a theoretical analysis to calculate physical delay based on heating and vaporization of droplets in diesel engines. The comparisons of his results to experimental ignition delay values showed great variations which he attributed to wrong assumptions or to the presence of chemical delay period.

Yu, et al [43] in 1956 studied physical delay period by injecting fuel in a single cylinder GM-71 engine with nitrogen instead of air. The changes in pressure were measured by the hot motored technique in alternate fired and misfired cycles. The

maximum drop in cylinder pressure was observed to be dependent on cetane number of a fuel rather than volatility.

Hurn, et al [44] in 1956 conducted tests in a constant volume bomb on fuels with different volatilities. Different charge gases were also tried to see their influence on vaporization and fuel droplet heating. They observed that there was a presence of long delay period before the start of chemical heat release, which they attributed to the time required to heat and evaporate the fuel droplets. He concluded that the surrounding air properties had more effect than the fuel volatility and structure on the physical delay period.

In the same year, El-Wakil et al [45] analyzed the processes of jet break up and droplet evaporation. They observed that a condition of adiabatic saturation is developed around the spray core irrespective of the fuel properties although fuel/air ratio varied depending on the fuel used. Under adiabatic saturation condition all fuels have almost equal opportunity to reach a temperature and fuel/air ratio suitable for auto-ignition and combustion.

Sitkei [46] in 1963 found the value of physical delay in his tests, as a constant value of 0.5 msec at a an injection pressure of 125 atm. Lyn and Valdmanis [47] in 1966 conducted tests in a pre-chamber engine to study the effect of injection pressure, nozzle size and injection rate on physical delay period. They observed that increase in injection pressure from 200 to 350 atm and increase in nozzle size from 0.3 to 0.6 mm resulted in negligible change in ignition delay period. In 1971, Henein [48] defined the end of physical delay as the time when stoichiometric mixture is formed at the surface of a

stagnant droplet. Based on this assumption the physical delay for a 4 μm cetane droplet was calculated to be 0.02 msec.

Pederson [49] in 1974 studied the effect of injection pressure and nozzle hole diameter in an open chamber engine. He too observed similar results as Lyn and Vladmanis. He further analyzed the evaporation behavior in a moving droplet, and unlike Henein he defined end of physical delay as the time when stoichiometric mixture is formed in the wake of the moving droplet. Based on the calculation he arrived at a value of 0.04 msec for the physical delay period at 1530 °R gas temperature.

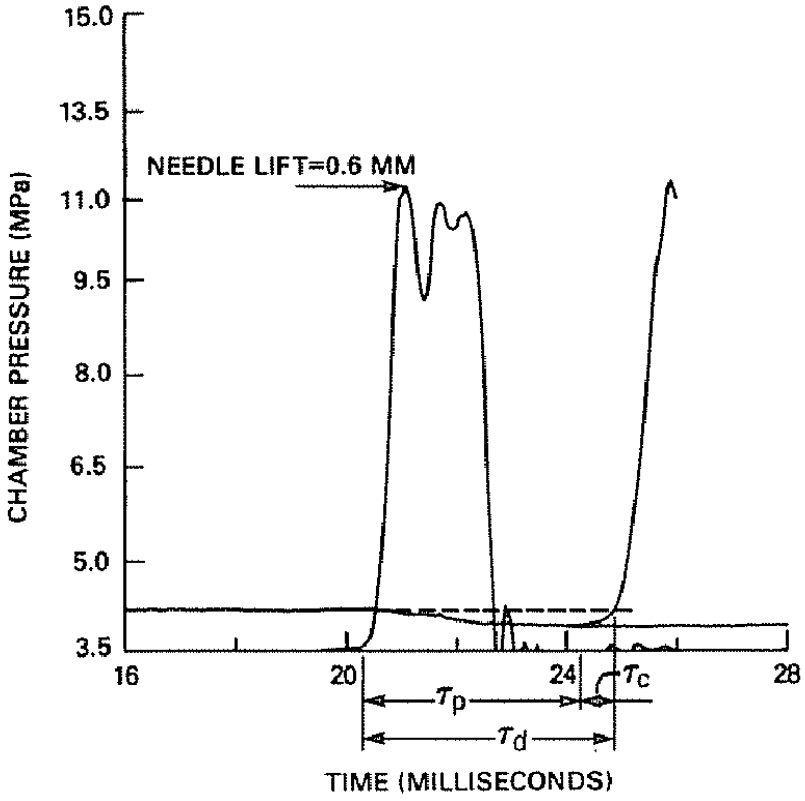

Figure 2.1: Pressure trace for a blend of hexadecane and HMN in both air and nitrogen [50]

In 1985, Ryan [50] separated physical and chemical delay periods in a constant volume vessel by injecting fuels separately in air and nitrogen. The lack of exothermic reactions in the inert atmosphere of nitrogen would show the presence of just the physical processes whereas when fuel is injected in air it will show both physical and chemical processes. When pressure traces from both these tests are superimposed, the point at which they detach from each other would mark the end of physical delay period and start of chemical delay period (Fig. 2.1). His test results showed that a major part of the total ignition delay period is physical delay period and a small portion of it is chemical delay.

From the review of physical delays it is evident in engines the physical delay is very small compared to the total ignition delay period. On the other hand, in constant volume chambers like the IQT physical delay has a significant presence and cannot be neglected.

2.1.2 Chemical Ignition Delay

The chemical ignition delay has been studied extensively with advent of modern computation and simulations. Flynn et al [51] modeled iso-octane and n-heptane at conditions based on tests done by Dec [52] for laser diagnostics. They observed that the steps in the auto-ignition process and the intermediate species formed for both the fuels were same. The only difference being the rate of the reactions, which is affected by the low temperature heat release of the fuel. In addition to the low temperature heat release the intermediate temperature heat release also affects the ignition quality of the fuels [53].

Chen et al [54] and Westbrook [55] classified the oxidation processes of hydrocarbons into three important regimes: low temperature, intermediate temperature and high temperature regimes.

2.1.2.1 Low temperature regime

According to Westbrook [55], at low temperatures, a hydrogen atom is removed from a hydrocarbon molecule to form an alkyl radical (R). This alkyl radical gets attached to an oxygen molecule to form a RO_2 molecule which further isomerizes to form QOOH (Q = C_nH_{2n}) radical.

$$R + O_2 + M = RO_2 + M \qquad (1)$$

$$RO_2 = QOOH \qquad (2)$$

QOOH can decompose to form an olefin and HO_2 molecule, or a cyclic ether and OH molecule.

$$QOOH = QO + OH \qquad (3)$$

$$QOOH = Q + HO_2 \qquad (4)$$

QOOH also has a chance to attach with another O_2 molecule and form O_2QOOH. This molecule breaks down into a ketohydroperoxide and OH molecule.

$$QOOH + O_2 = O_2QOOH \qquad (5)$$

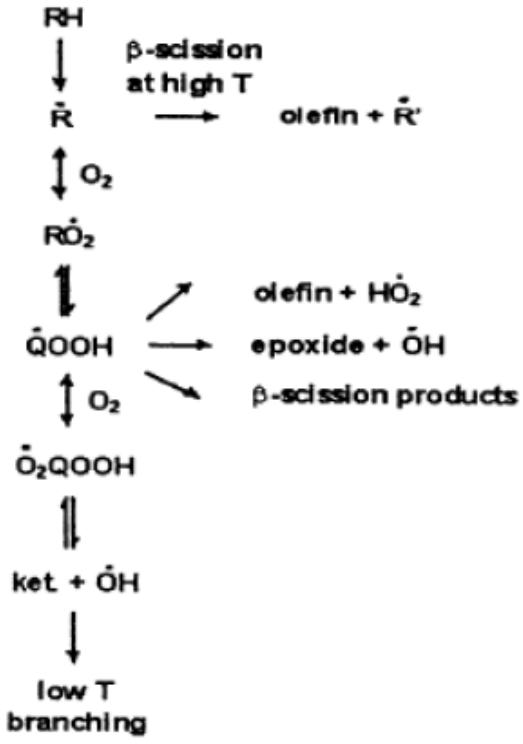

Figure 2.2: Schematic of hydrocarbon oxidation [56]

Ketohydroperoxide decomposes at around 800 K which is lower than the H_2O_2 decomposition temperature range; hence it marks the end of the low temperature combustion regime. Fig. 2.2 shows a schematic of hydrocarbon oxidation similar to the one explained by Westbrook [55].

2.1.2.2 Intermediate temperature regime

In the temperature range of 850 to 1200 K, OH formation to sustain chain branching is dependent on the following reactions:

$$H + O_2 + M = HO_2 + M \qquad (5)$$

$$RH + HO_2 = R + H_2O_2 \quad (6)$$

$$H_2O_2 + M = OH + OH + M \quad (7)$$

2.1.2.3 High temperature regime

At temperatures higher than 1200 reaction (8) takes over reaction (5) and becomes the most important reaction controlling combustion rate.

$$H + O_2 = O + OH \quad (8)$$

The final stage in the high temperature regime is the oxidation of CO by OH radical with release of CO_2 and H_2O.

$$CO + OH = CO_2 + H_2O \quad (9)$$

The H atom required to start this reaction is released from thermal decomposition of alkyl radicals, which is possible at only higher temperatures.

2.1.2.4 Negative Temperature Coefficient (NTC) and Thermal-Ignition Preparation regime

Kuwahara et al [57] based on 0-D simulations of n-heptane and di-methyl ether proposed a four stage oxidation process for fuels which show cool flame (Fig. 2.3). At higher initial temperatures the secondary oxygen addition competes with the branching of QOOH, and causing reduction in reaction rates leading to NTC regime. The NTC regime is followed by the thermal ignition preparation stage, in which the branching chain reactions are overtaken by the HO_2 formation reactions. This stage starts at around 950 K and continues until the temperature rises till 1500 K leading to high temperature combustion.

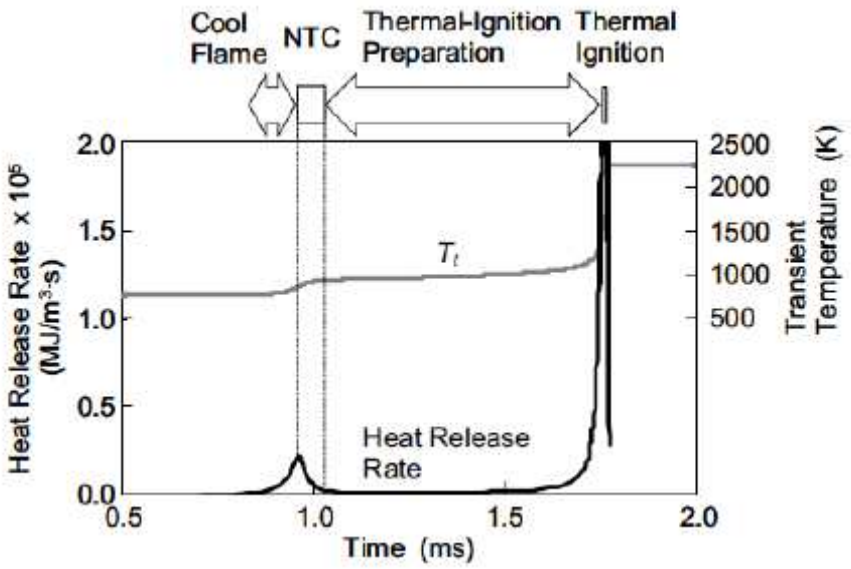

Figure 2.3: Different stages of auto-ignition using Heat Release Rate trace [57]

The reactions involved in the thermal ignition preparation regime form a reaction loop involving H_2O_2, termed as "H_2O_2 loop reactions".

$$H_2O_2 + M = OH + OH + M \qquad (7)$$

$$OH + HCHO = HCO + H_2O \qquad (10)$$

$$HCO + O_2 = HO_2 + CO \qquad (11)$$

$$2\ HO_2 = H_2O_2 + O_2 \qquad (12)$$

The loop reactions release around 473 kJ of energy which aids in the rise of temperature leading to high temperature combustion. The overall reaction for the loop is given as:

$$2\ HCHO + O2 = 2\ H2O + 2\ CO + 473\ kJ \qquad (13)$$

Yao et al [58] developed a reduced mechanism for n-heptane (35 species and 41 reactions) based on the original mechanism developed by Lawrence Livermore National Lab (LLNL) under HCCI conditions. The 0-D modeling results showed n-heptane has a two stage auto-ignition behavior. Stein et al [59] developed and studied oxidation of surrogates for jet fuels and arrived at similar conclusions.

2.2 Ignition Delay Correlations

One of the earliest ignition delay correlations was developed by Boerlage and Broeze [60] in 1931, based on tests conducted on a slow speed, direct injection, four stroke, single cylinder diesel engine for pressure range of 375-600 psi (25-42 bar). Their simple correlation suggested pressure rise delay was a hyperbolic function of compression pressure.

$$ID_P = \frac{K}{P} \tag{2.1}$$

In their following work [61] in which they compared combustion of cetene ($C_{16}H_{32}$) and tetra-isobutylene ($C_{16}H_{32}$), two compounds with similar chemical formula but different structure of molecules, they observed tetra-isobutylene has poor ignition quality than cetene. This led them to conclude that besides compression pressure, thermal stability and molecular structure also affects the pressure rise delay.

The most widely used form of correlation for ignition delay is the one developed by Wolfer in 1938 [62], based on data from constant volume bombs of two different shapes, cylindrical and spherical. The tests were performed at a pressure of 118-389 psi (8-27 bar) in the cylindrical bomb and 172-705 psi (11-49 bar) in the spherical bomb,

and an overall temperature range of 600-947 °F (333-526 K). The equation is applicable to fuels with CN ≥ 50.

$$ID_P = \frac{0.44 e^{\frac{4650}{T}}}{P^{1.19}} \tag{2.2}$$

where, P is in atmospheres and T in degrees Kelvin.

He further stated that fuel injection pressure, nozzle diameter, turbulence, combustion chamber design, fuel/air ratio and fuel temperatures above 100 °C have a minimum effect on ignition delay value. In fact, the effect of air turbulence on ignition delay was investigated by Small [63] in a similar spherical bomb. He also concluded that static and turbulent air produced comparable pressure rise delay.

In 1939, Schmidt [64] provided a formula for the initial lag period for a simple reaction between molecules of two gases without involving intermediate reactions.

$$ID_{Ch} = \frac{e^{+\frac{E}{RT}}\sqrt{T}}{P} a'B \tag{2.3}$$

where,

P and T = initial pressure and temperature, respectively.

a’ = factor dependent on air-fuel ratio

B = factor that allows for the reduction in ignition delay from the increased rate of burning during the delay period, which is due to the temperature rise during the interval

In order for this equation to represent the chemical ignition delay in engine combustion, he added an exponential power to pressure to accommodate for the chain reactions happening due to intermediate species. The equation was further reduced to a form (Eq. 2.4) of Wolfer equation, as it was observed that exponential factor was more dominant than T, a' and B.

$$ID = \frac{ce^{\frac{b}{T}}}{P^n} \tag{2.4}$$

In the same year, Bauer [65] introduced an equation in which the ignition delay is a function of T log P.

$$ID = F_{n'}(TlogP) \tag{2.5 a}$$

OR

$$ID = F_n(Pe^T) \tag{2.5 b}$$

where,

P = pressure in atmospheres

T = temperature in Kelvin

The formula was found by trial and error, and was believed to be reasonably accurate in predicting illumination delay for an optical engine of 3.375 in bore and 5 in stroke. It is interesting to note that contrary to the correlations developed by Wolfer and Schmidt, ignition delay is a function of e^T rather than $e^{1/T}$. Their work found support in the 1941 research of West and Taylor [66] done on a single cylinder open chamber diesel engine. They showed there existed a relationship between ignition delay and T log P, similar to shown in Fig. 2.4.

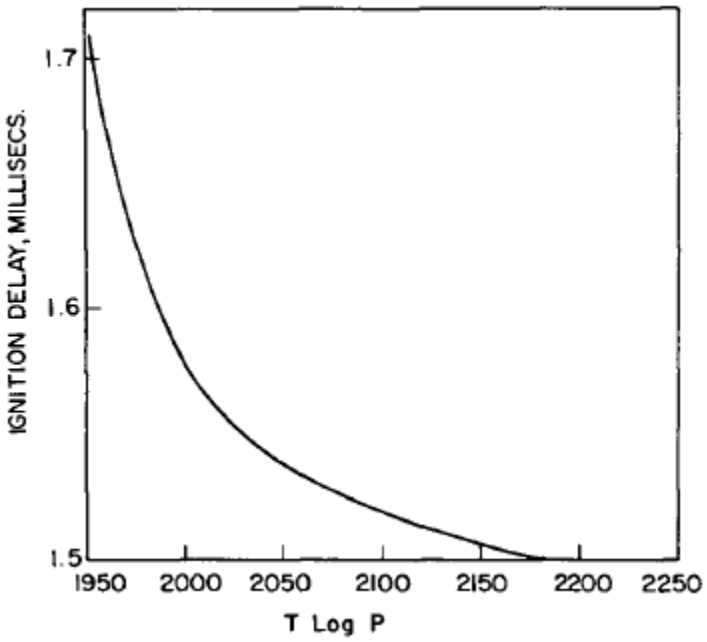

Figure 2.4: Relation between ID_P and T log P, by West et al. [66]

Tests were conducted by Starkman [67] in 1946, on a CFR diesel engine and a bomb of volume equal to the clearance volume of the engine. He found that with the increase in pressure, temperature and fuel/air ratio pressure rise delay is reduced, and that the engine has shorter delay than the constant volume bomb. In 1949 Elliott [68], made a detailed analysis of the results of Mueller [69] and Wolfer which were reproduced by Jost [70], to find the effect of temperature on the pressure rise delay. His formulae for ignition delay of methylnaphthalene and cetane were in the form of sum of physical and chemical delays, and which agreed well with the results of Starkman.

For methylnaphthalene the formula is:

$$ID = 0.977e^{\frac{1070}{T}} + 2.18 \times 10^{-14}e^{\frac{14510}{T}} \tag{2.6}$$

For cetane the formula is:

$$ID = 0.710e^{\frac{1070}{T}} + 3.47 \times 10^{-14} e^{\frac{17620}{T}} \quad (2.7)$$

Hurn and Hughes [71] in 1952 conducted tests on a constant volume bomb of size 2.5 in diameter and 3.5 in length, by varying the temperature 850-1050 F (472–583 K), pressure 275-675 psi (18-46 bar), oxygen concentration 15-40% and CN of fuels 37.2-53.7. They found that there exists an optimum oxygen concentration at which the pressure rise delay is minimum, and that the delay difference between different fuels decreases at high temperatures and pressures.

Garner, et al [72] in 1957 measured the effect of compression ratio on illumination delay in a CFR diesel engine. They observed that there existed an ideal compression ratio at which the lowest illumination delay was reached at all fuel-air ratios, which was 23:1 for low CN napthenic gas oil and 25:1 for high CN paraffinic secondary reference fuel. In their continuing work [73] of 1961 they found that a constant preflame energy is released by a given fuel, which is directly proportional to the ignition delay time.

In the following year Tsao, et al [74] investigated effect of engine speed, fuel injection per cycle, fuel CN, intake air temperature and pressure on the temperature rise delay in a modified CFR engine. The in cylinder gas temperature was measured using an infrared technique called “Null Method”. Based on their results they developed the first empirical relationship to have besides temperature and pressure, engine speed as a factor affecting ignition delay.

$$ID = \left(\frac{123}{P} + 0.415\right)\left\{\left(\frac{-36.3}{T} + 0.0222\right)N + \left[\left(\frac{47.45 \times 10^3}{T} - 26.66\right) + \left(\frac{T}{1000} - 1.45\right)\left(\frac{1000 - N}{60}\right)\right]\right\} \quad (2.8)$$

where,

ID_T = ignition delay time, msec

P = gas pressure at point of injection, psi

T = gas temperature at point of injection, °R

N = engine speed, rpm

In 1963, Sitkei [46] performed tests on an air cell engine and on a pre-combustion chamber engine, and measured the illumination delay as a sum of physical delay and three part chemical delay:

$$ID = ID_{Ph} + ID_{CF} + ID_{BF} + ID_{EF} \quad (2.9)$$

where,

ID_{CF} = Ignition delay of the cold flame

ID_{BF} = Ignition delay of the blue flame

ID_{EF} = Ignition delay of the explosion flame

He found that ID_{BF} and ID_{EF} are inseparable and can be put together as $ID_{(B+E)F}$, whereas ID_{Ph} was estimated to be 0.5 msec. The final formula after evaluation was:

$$ID = 0.5 + \frac{0.135e^{\frac{7800}{RT}}}{P^{0.7}} + \frac{4.8e^{\frac{7800}{RT}}}{P^{1.8}} \quad (2.10)$$

where, P is in atmospheres and T in degree Kelvin.

Starting from 1962 to 1966, Lyn and Valdmanis [47, 75] conducted tests on two engines and studied Schlieren photographs of combustion behavior. Based on data obtained using motored engine technique coupled with single shot injection; they concluded that injection timing, in-cylinder pressure and temperature are the most important factors affecting ignition delay period. These are followed by injection pressure, nozzle specifications and swirl ratio which have secondary effects, and the least affecting parameter is fuel quantity which is a measure of overall fuel/air ratio.

In 1967, Henein and Bolt [76] studied the effect of fuel/air ratio, injection pressure, cooling water temperature, cylinder pressure and turbulence on illumination delay and pressure rise delay in a modified single cylinder diesel engine. The test results showed that pressure rise delay is smaller than illumination delay and is more reproducible as well. The factors affecting both the delays most are air pressure, fuel/air ratio and cooling water temperature. On the other hand, illumination delay is affected a lot by injection pressure whereas pressure delay showed negligible effect. They gave an ignition delay correlation similar to the one given by Wolfer and Schmidt.

$$ID_P = \frac{C}{P^n} \tag{2.11}$$

Under the test conditions C and n were found to be 64740 and 1.774, respectively.

In their continuing work, Henein and Bolt [77] in 1969 investigated the effect of engine speed on ignition delay. They found that initially ignition delay seems to decrease with increase in speed; however, after the correction for the increase in-cylinder temperature, the trend was found to be opposite. In another study [78], they

performed tests on the effect of air charge temperature on pressure rise delay of different fuels like gasoline, CITE, and diesel. It was observed that with increase in intake temperature, low CN fuel showed a large reduction in ignition delay than a high CN fuel, as shown in Fig. 2.5. However, at extremely high temperatures the ignition delay values for all the fuels were found to be close, similar to the results previously obtained by Hurns and Hughes [71].

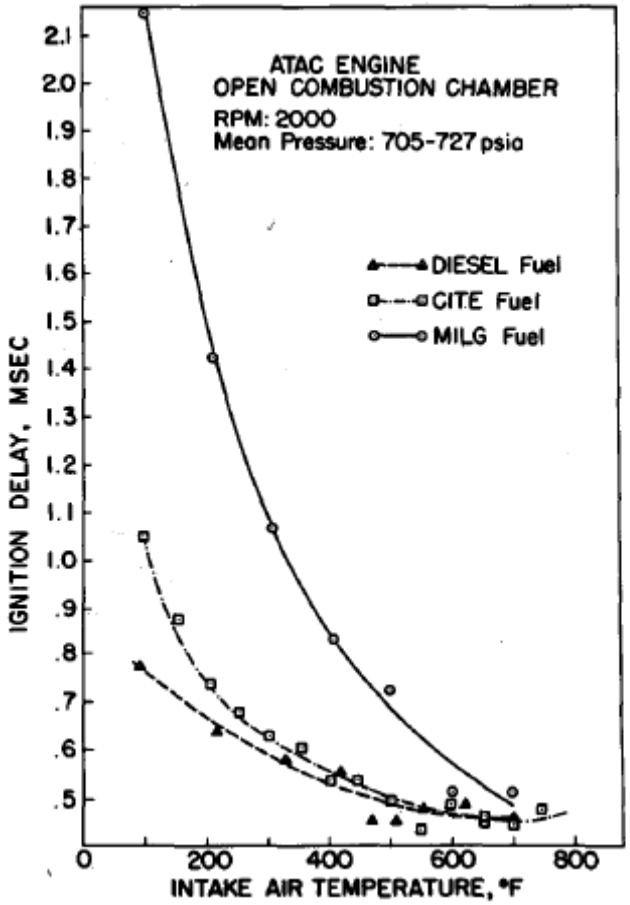

Figure 2.5: Effect of gas temperature on ignition delay of different fuels [78]

Based on the experimental data for three fuels with different CN they developed a correlation between the ignition delay and apparent activation energy, E_a.

$$ID_P = Ce^{\frac{E_a}{RT_m}} \tag{2.12}$$

It was observed that fuels with longer ignition delay (lower CN) have higher activation energy, and the ones with shorter ignition delay (high CN) have lower activation energy. Thus, they were able to come up with a straight line relationship between CN and apparent activation energy.

$$E_a = 15500 - 230(CET - 15) \tag{2.13}$$

Stringer [79] in 1970 conducted tests on a constant pressure flow rig using 21 primary reference fuels with a CN range 0-100. The tests were performed at a pressure of 40 atm and temperatures of 790-922 °K. He arrived at a correlation similar to the Wolfer's equation and calculated values of apparent activation energy (E_a), pre-exponential factor (C) and pressure exponential factor (n) for all the fuels tested.

$$ID_P = \frac{Ce^{\frac{E_a}{RT}}}{P^n} \tag{2.14}$$

In 1974, Pederson [49] measured ignition delay for hexadecane (CN=100) in an open chamber engine. The tests were conducted at wide range of mean gas temperature (590–755 °K), pressure (20-31 atm) and fuel temperature (300-450 °K). He formulated ignition delay time as a sum of physical and chemical delay periods (Eq. 2.15). The physical delay period is said to be affected by mean gas temperature and pressure, droplet diameter and velocity, and fuel temperature.

$$ID_P = 0.00642e^{x} + 53.34e^{\frac{1231}{T_m}} \tag{2.15}$$

$$x = \left[3.53\left(\frac{T_m}{823}\right)\right]\left[0.22\left(\frac{P}{34}\right) + 0.78\right]\left(\frac{d}{25}\right)^{1.77} \tag{2.16}$$

$$\left[1.74 - \left(\frac{0.74T_f}{293}\right)\right]\left(\frac{v}{20}\right)^{-0.17}$$

where,

P (atm) = Mean gas pressure during ignition delay period

T_m (K) = Mean gas temperature during ignition delay period

v (m/sec) = Droplet velocity

d (μm) = Droplet diameter

T_f (°K) = Fuel temperature

Hiroyasu [80] in 1977 measured illumination delay in a constant volume bomb and gave an ignition delay formula which included ambient oxygen concentration as a factor. The investigations were done using primary reference fuels with 0-100 CN at temperatures 300-450 °K and pressure 1-40 atm.

$$ID_{II} = \frac{A\varphi^c}{P^n} e^{\frac{D}{T}} \tag{2.17}$$

In 1987, Ryan and Stapper [81] investigated effect of temperature and CN on physical and chemical delay period in a constant volume vessel. The results showed that the chemical delay period was found to be sensitive to temperature whereas physical delay is not affected much by temperature and CN. They too proposed a correlation for the total ignition delay similar to one used by previous researchers.

$$\tau_D = Ae^{\frac{B}{T}} \tag{2.18}$$

Ryan and Callahan [82] further modified their equation by studying the effect of other parameters on ignition delay period in a bomb.

$$\tau_D = b_0(O_2)^{b_1}(Fuel)^{b_2}\rho^{b_3}e^{\frac{b_4}{T}} \quad (2.19)$$

where,

τ_D = ID in msec

O_2, F = Oxygen and fuel concentration respectively in moles/m^3

ρ = Gas density in kg/m^3

T = Gas temperature in K

b_i = regression coefficients

Henein and Akasaka [83] in 1987 measured ignition delay for different fuels in a CFR engine and studied the effect of fuel properties and engine conditions on the delay time. It was observed that CN is a good measure for combustion behavior for fuels with higher CN, but for low CN fuels physical properties and chemical composition also need to be taken into consideration. Also, it was observed that all fuels are capable of producing two-stage combustion depending on the compression ratio (C.R.) they are tested at. Even high cetane fuels can exhibit two-stage combustion at very low C.R.'s, as shown in Figure 2.6.

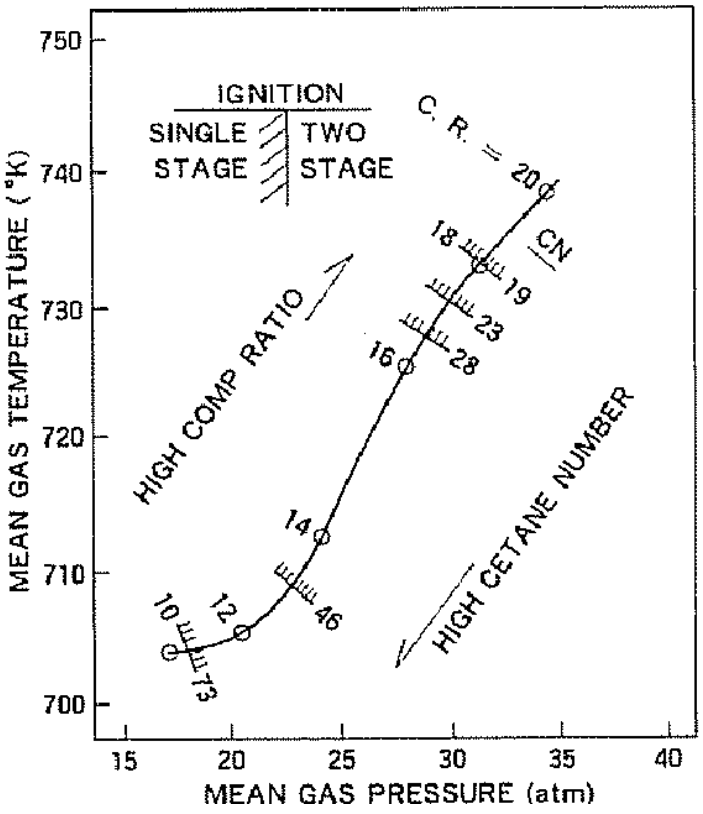

Figure 2.6: Effect of mean gas temperature and pressure on two-stage ignition [83]

Therefore, they proposed ignition delay as a function of engine parameters and fuel properties.

$$ID = Fn(T_m, P_m, CN, S) \tag{2.20}$$

where,

T_m, P_m = Mean temperature and pressure during ignition delay period

CN = Fuel cetane number

S = Fuel specific property affecting spray formation, evaporation and mixing.

In 1990, Kwon et al [84] conducted a series of tests to study the effect of mean cylinder temperature and pressure on ignition delay period in a diesel engine. The tests

were performed at varying start of injection, nozzle hole diameter, swirl ratio, injection pressure, combustion chamber shape and engine speed. Unlike Henein and Bolt [76], they observed that illumination delay is always shorter than pressure rise delay. However, they agreed with Wolfer [62] on the negligible effect of swirl ratio, engine speed, injection pressure, and nozzle hole diameter on ID.

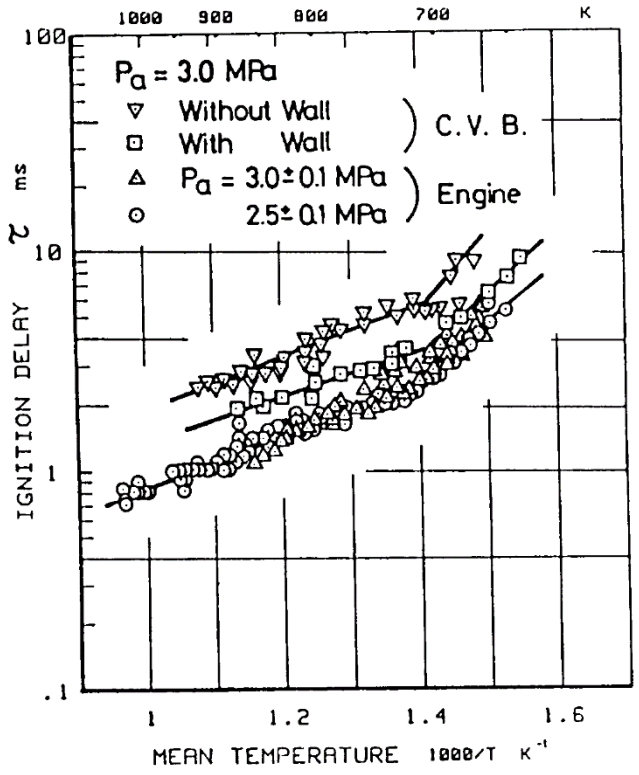

Figure 2.7: Comparison of Ignition Delays obtained from the Engine and the Bomb [84]

They also studied the effect of wall impingement on ignition delay by inserting a combustion chamber to a constant volume bomb, referred to as cavity wall. It was observed that wall impingement reduces ignition delay time which was attributed to better mixture formation. Furthermore, a plot of ignition delay and mean temperature

during delay period shows that at about 715 K there is sharp change in slopes of line, representing a change in apparent activation energy (Fig. 2.7). Based on these results they developed separate correlations for ignition delay for the two temperature regimes, in the pressure range of 2.5-3 MPa.

$$\tau = 5.23 \times 10^{-2} e^{\frac{2780}{T}} \qquad T \geq 715\ K \tag{2.21}$$

$$\tau = 2.16 \times 10^{-4} e^{\frac{6710}{T}} \qquad T < 715\ K \tag{2.22}$$

Taylor et al [85] in 2004 performed tests determining ignition delay time in the IQT (Ignition Quality tester) using different fuels and pure hydrocarbons. The Arrhenius plot showing log of ignition delay and inverse of temperature was plotted, and it gave a non-linear relationship between ID and temperature. This was attributed to the combined presence of physical and chemical processes during the ignition delay period in heterogeneous combustion.

In his continuing work, Taylor [86] in 2006 investigated the effect of temperature, pressure and oxygen concentration on ID in IQT. He observed that with an increase in ambient temperature, pressure and oxygen concentration the ID value decreased, based on which he developed a global rate model.

$$Rate = \frac{1}{ID} = A \cdot \exp\left[\frac{E_a}{RT}\right] \cdot [O_2]^b \tag{2.23}$$

where,

$O_2 = \frac{P}{RT} \cdot X_{O_2}$ = molar concentration of O_2

b = reaction order for oxygen concentration

The effect of charge dilution and injection timing on ID time in an optical engine was studied by Kook et al [8] in 2005. Similar to Taylor they observed that besides temperature; pressure and oxygen concentration also has a considerable affect on ID. Therefore, they used an ID expression which included a factor for pressure and oxygen concentration.

$$\tau_{id} = A \cdot p^{-n_1} {X_{O_2}}^{-n_2} e^{\frac{E_a}{RT}} \tag{2.24}$$

For the tested diesel fuel the values for A, n_1, n_2 and E_a/R obtained were 12.254, 1, 1.2 and 3242.4 K, respectively.

In 2010, Bogin et al [87] conducted tests in the IQT using Fuels for Advanced Combustion Engine (FACE) fuels which have a wide range of physical and chemical properties. They also arrived on an ID correlation similar to the one obtained by Taylor et al [85, 86] and regression analysis was used to determine the values for the four parameters A, b, c and E_a for all the nine fuels.

$$ID = A \cdot P^b \cdot {X_{O_2}}^c \cdot e^{\frac{E_a}{RT}} \tag{2.25}$$

Rothamer and Murphy [88] in 2013 performed tests on a 2.44 L heavy-duty single-cylinder diesel engine using five fuels. They provided an ID correlation which included the effect of density along with temperature.

$$\tau_{id} = A\rho^{n_1} e^{\frac{E_a}{RT}} \tag{2.26}$$

In the same year, Jayakumar [4] conducted tests on a single cylinder diesel engine at variable intake temperature conditions for ULSD, JP-8 (HCN), JP-8 (LCN) and S-8. The intake temperatures were increased with an increment of 10 °C in the range

30-110 °C. The log ignition delay value calculated at each test point was plotted against the inverse of the mean temperature during ignition delay period. The ignition delay correlation was of the form used by Henein and Bolt [78].

$$\tau_{id} = Ae^{\frac{E_a}{RT}} \tag{2.27}$$

The global activation energy values for all the tested fuels are listed in Table 2.1. It should be noted that the apparent activation energy for ULSD is much lower than the values reported for diesel fuels in previous investigations.

Table 5.2: Global activation energy values for different fuels [4]

Definition	E_a (KJ/mole)
ULSD	1.975
JP-8 (HCN)	5.305
S-8	2.034
JP-8 (LCN)	2.106

In 2014, Zheng [3] measured ignition delay for 6 fuels in IQT, and separated chemical and physical ignition delay using the method previously used by Ryan [50]. He plotted Arrhenius plots using total ignition delay, physical delay and chemical delay. The global activation energy was calculated as slope of the lines from these plots. He proposed total ignition delay time as a sum of physical delay and chemical delay.

$$ID_{total} = A_{phy} \cdot e^{\frac{E_{phy}}{R_u T_{mean\,phy}}} + A_{chem} e^{\frac{E_{chem}}{R_u T_{mean\,chem}}} \tag{2.28}$$

He observed that apparent activation energy calculated using chemical delay (E_{chem}) has an inverse relationship to DCN, whereas the other two delays do not show a

specific trend. Based on this observation he proposed a correlation between apparent activation and DCN.

$$E_a = \frac{1860}{DCN + 30} \tag{2.29}$$

From the literature review it is evident that several definitions for the delay period were used and the measurements were made in a variety of test equipment and environments. These ignition delays were correlated to the compressed air properties, engine operating conditions and fuel properties. In constant volume vessels the compressed air pressure and temperatures are constant before the start of combustion, and exhibit small variations during the ignition delay period. Arrhenius plots were developed from which activation energy values for fuels were calculated. Because of these differences, different values for the activation energy for the same fuel appear in the literature.

The goal of this investigation is to examine the conditions in the different equipment used to measure the ignition delay period and its definitions. The focus will be on the quantification of auto-ignition characteristics of fuels in the heterogeneous environment. Therefore, from engineering point of view it is necessary to understand how different ID definitions and engine conditions affects the calculation of the activation energy for a fuel. This is in the scope of this dissertation.

CHAPTER 3

EXPERIMENTAL SETUP

3.1 Introduction

The test cell (Fig. 3.1) comprises of a single cylinder engine coupled to a DC dynamometer, which controls the load and speed of the engine. The engine is fuelled from an independent common rail fuel injection system, capable of split injections, controlled by an open ECU. A separate cooling system comprising of cooling tower and radiator is used to deliver water to the cooling jacket surrounding the engine, to maintain constant engine wall and head temperatures. Engine oil is circulated to the engine, cam carrier and crank case using an isolated oil system. The engine is supplied with air from an independent compressed air system, thus controlling the intake air pressure. An air heater situated before the intake plenums helps control the intake air temperature. The entire intake and exhaust line is covered with insulation to reduce heat losses affecting engine performance and exhaust emission calculations respectively. A detailed description for the test cell is given in previous work [89, 90].

Figure 3.1: HSDI engine test cell

3.2 Test Cell Details

3.2.1 Engine Specifications

The test engine is a four stroke, four valve, small bore, single cylinder, high speed direct injection (HSDI) engine equipped with an intake swirl port, double overhead camshaft and a common rail injection system. It has a Mexican hat type combustion bowl chamber (Fig. 3.2) and is mounted with a centrally located 6 hole, mini-sac type nozzle. The engine specifications are listed in the Table 3.1.

Table 3.1 HSDI Engine Specifications

Displaced Volume	421.932 cc
Stroke	85 mm
Bore	79.5 mm
Connecting Rod	179 mm
Bowl Diameter	36.25 mm
Geometric Compression ratio	20:1
Number of Valves	4
Inlet Valve Open	353°
Intake valve Close	-140°
Exhaust Valve Open	155°
Exhaust Valve Close	-352°
Nozzle flow number	320
Nozzle hole diameter	0.131 mm
Nozzle hole length	0.6 mm
Nozzle Included Angle	145°

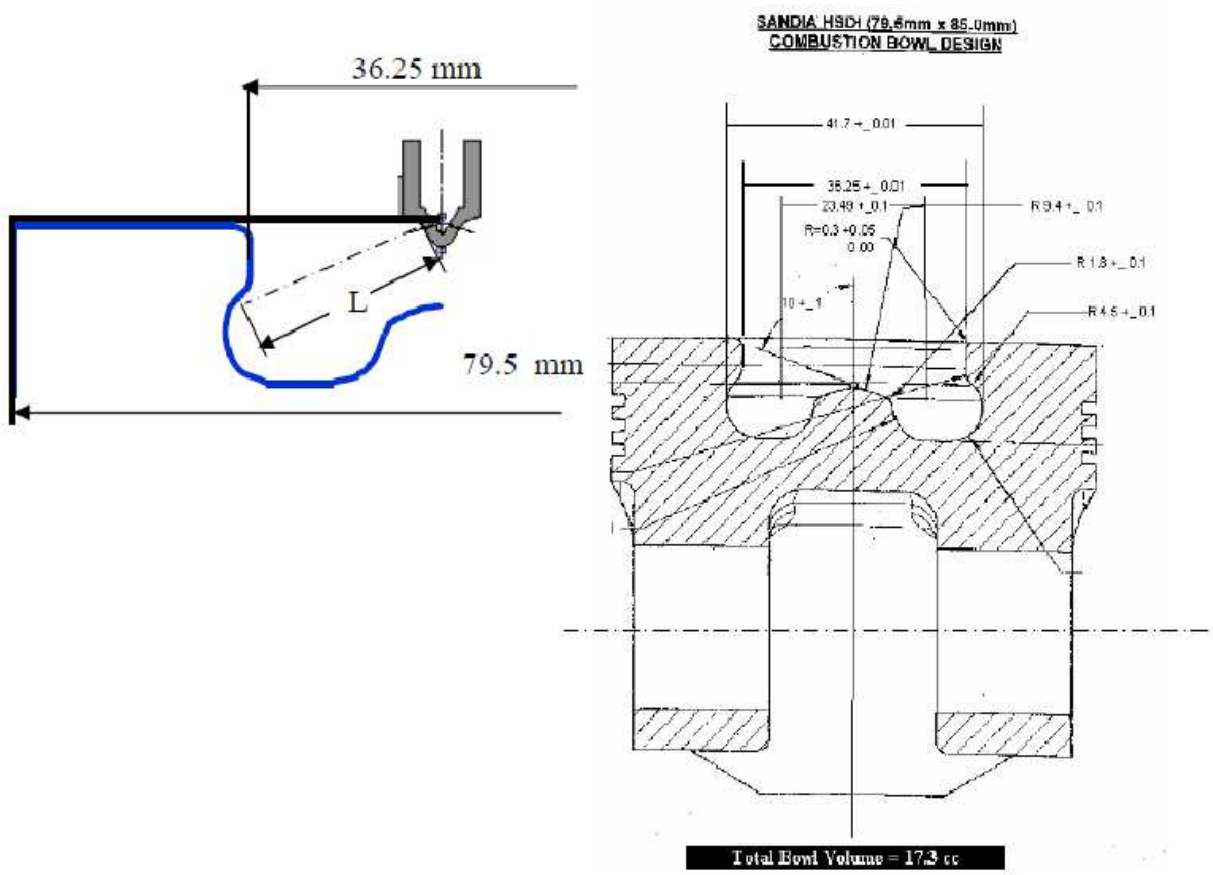

Figure 3.2: Combustion bowl and piston design [89]

3.2.2 Fuel Injection System

The common rail injection system used in the current test cell (Fig. 3.2) is capable of max injection pressure of 1350 bar. The fuel is stored in a tank under compressed nitrogen at 20 psi. The main purpose of using compressed nitrogen is to prevent fuel evaporation; however, it also improves the effectiveness of the low pressure pump. The fuel passes through a filter, vapor eliminator, flow meter and level controller before it enters the low pressure pump. The low pressure pump feeds into the first generation, high pressure, Bosch CP1 pump via a 3-way valve; which in case of any extra fuel flow, diverts it back. The high pressure pump maintains the necessary

pressure in the common rail, required for injection. The open ECU (not shown in Fig. 3.2) manufactured by Electro-Mechanical Associates, Inc. controls the pressure generated by the pump. The open ECU gives us the flexibility to change the injection timing and duration irrespective of the engine load. The current setting also allows us to split the injection into two separate injection events, if required. A fuel pressure sensor is placed upstream on the injector line to measure pressure drop during injection, applied as feedback control for the ECU to control the pump. The return line from injector and flow diversion from the 3-way valve passes through a heat exchanger, cooled by city water, to maintain the fuel temperature at ambient conditions. The level controller, into which the heat exchanger returns fuel, maintains the flow between returning fuel and new fuel coming from the fuel tank.

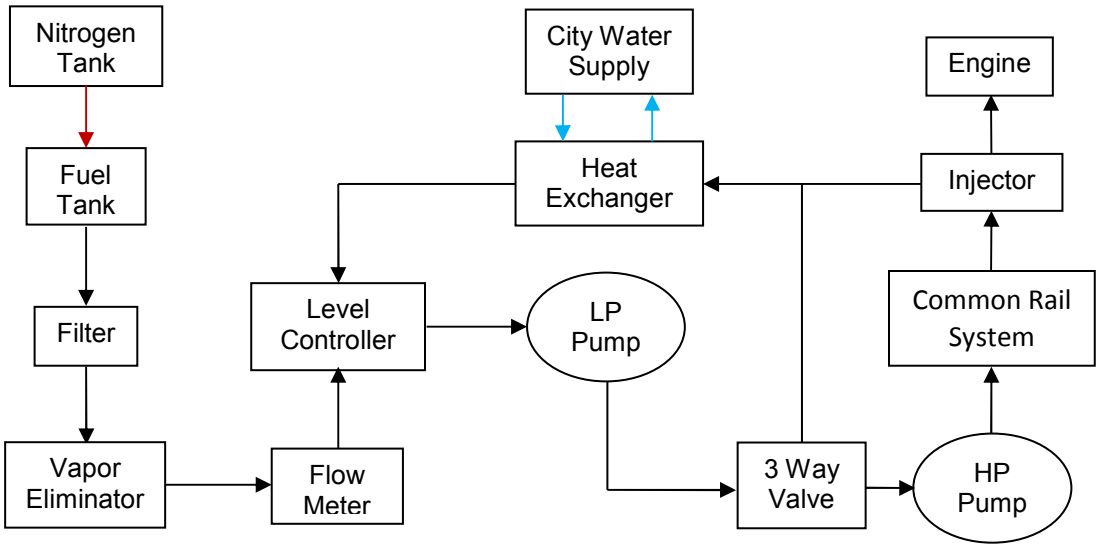

Figure 3.3: Line diagram of fuel injection system

3.2.3 Engine Cooling System

The engine cooling system consists of a distilled water system running through a jacket surrounding the engine walls and the cylinder head block (Fig. 3.3). Thus water

going into the engine is split into two branches: one going to the engine head jacket and other going to the wall jacket. The main goal for this system is to maintain the engine wall and head temperatures at a constant value, which is achieved by maintaining the water coming out at 180 °F always. A pair of heat exchangers is used in achieving the target temperature. A cooling heat exchanger cools the water coming out of the engine; however, the difference in the water temperature going in and coming out of the engine is just around 10 °F. The cooled water needs to be reheated by steam to around 170 °F. This also helps in eliminating fluctuations due to seasonal variation in temperature of city water. A centrifugal pump is at the centre of this system circulating the distilled water. K-type thermocouples are used at the engine inlets and outlet to measure water temperatures.

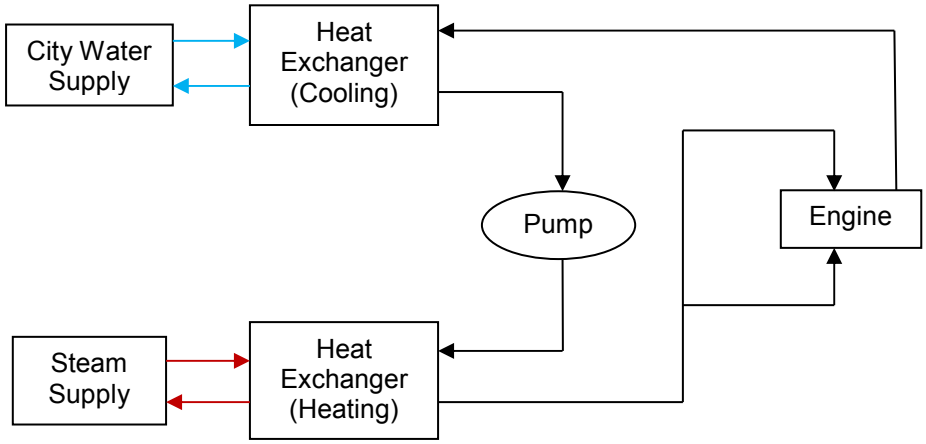

Figure 3.4: Line diagram for engine cooling system

3.2.4 Air Supply System

The engine is supplied with compressed air by a two stage air compressor capable of max pressure of 200 psi. The compressed air is stored in a high pressure tank situated in the basement. The air from the storage tank passes through a liquid

separator and air filter to eliminate any water and dust particles from it. The engine supply line consists of a secondary storage tank and air heater. The secondary storage tank helps in eliminating any fluctuations present in the system by acting as a buffer. The air heater helps in changing intake air temperature and provides flexibility with performing tests at different conditions.

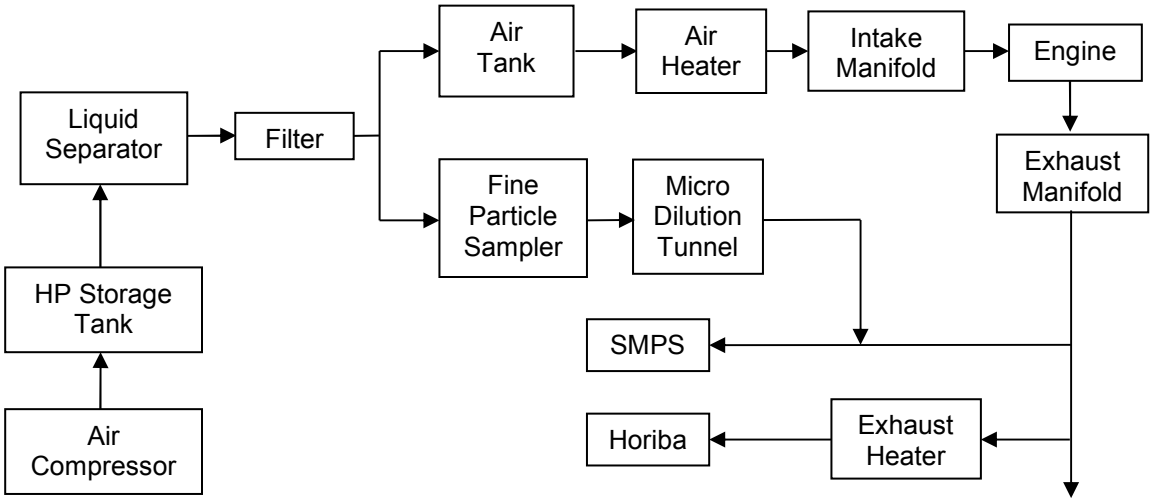

Figure 3.5: Line diagram of the air supply system

3.2.5 Oil System

The engine has a separate oil system which runs independent of it. It comprises of a oil pump, heat exchanger and a filter. The heat exchanger makes sure the engine oil is always at a fixed temperature of 120 °F, so that it does not lose its properties. The inlet going to the engine is split into two channels: (1) to the engine head lubricating the cams and accessories (2) to a piston jet lubricating the cylinder walls and piston. The extra oil is collected in the oil sump at the base of the engine block and re-circulated via the pump.

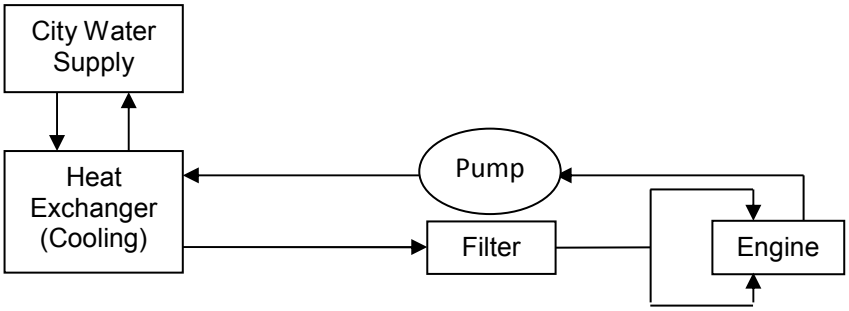

Figure 3.6: Line diagram for the oil system

CHAPTER 4

PRELIMINARY RESULTS

4.1 Introduction

Previously, researchers have calculated apparent activation energy values with large variations due to use of different equipments such as constant volume bombs, engines etc. More recently, work published for activation energy based on experiments on two same engines under the project Partnership for a New Generation of Vehicles (PNGV), one with optical access and the other metallic, have shown large variation. The differences in the two investigations include the definition of ID, effective temperature used for the ID period, and difference in the charge conditions at SOI and during ID period.

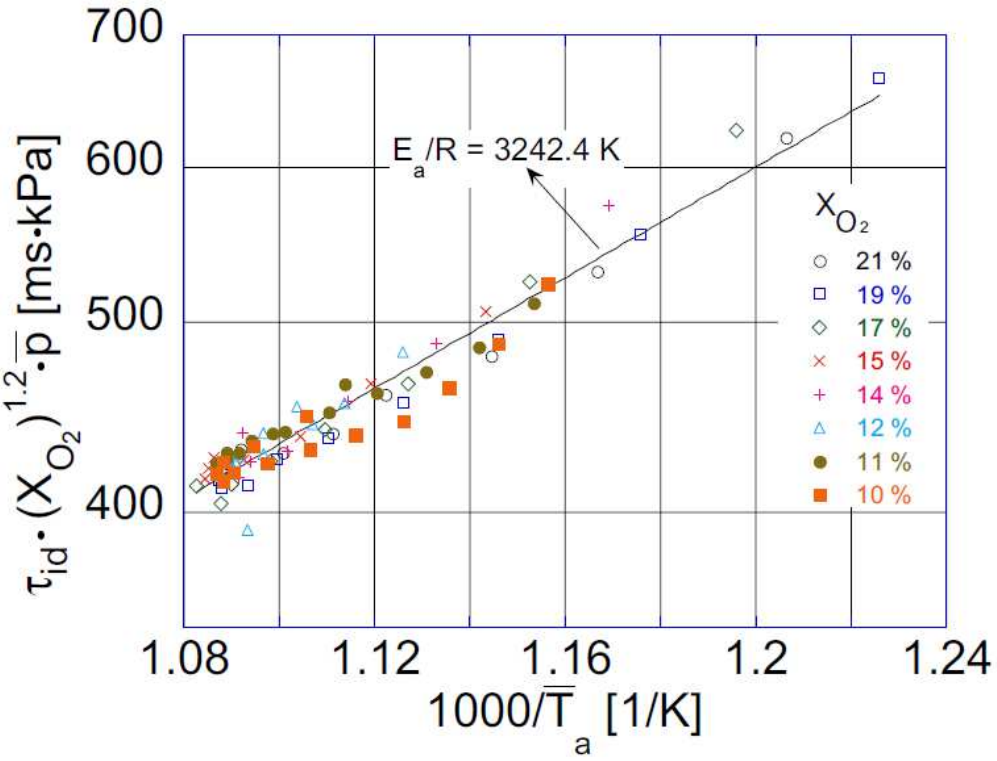

Figure 4.1: Correlation of ignition delay with average ambient pressure, temperature and O2 concentration [8]

Kook et al [8] conducted tests on a single cylinder optical engine using emission certification Diesel fuel (CN 47.1) at variable SOI conditions, keeping intake pressure and temperature constant. The tests were repeated at different oxygen concentrations by changing the EGR percentage. The Ea/R value for all the tests points combined together was found to be 3242 K (Fig. 4.1) which gives an activation energy value of 26957 J/mol.

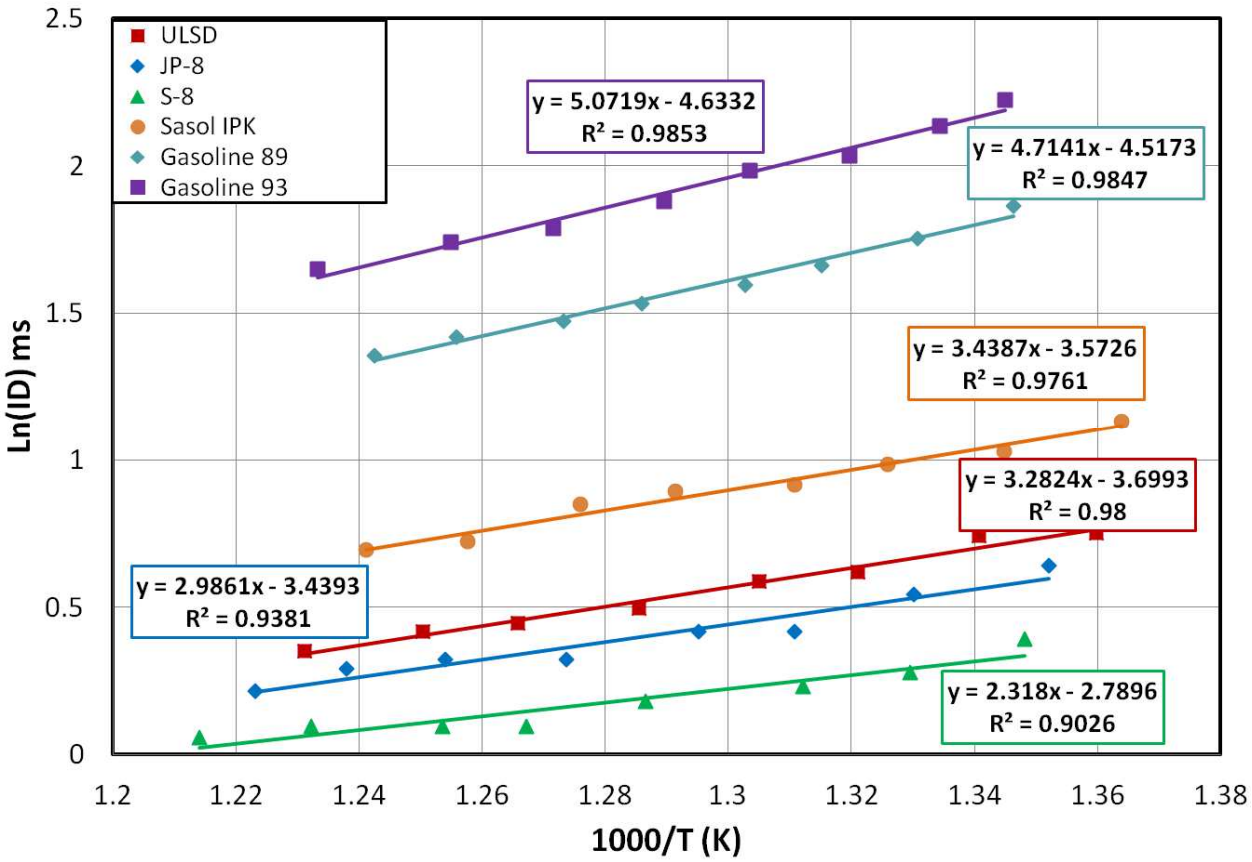

Figure 4.2: Arrhenius plot for chemical ignition delay measured in IQT versus the charge temperature before SOI for different fuels [3]

The activation energy values obtained by Kook et al are closer to the ones obtained by Zheng et al [3] for ULSD (Fig. 4.2). The values obtained by Zheng et al are based on data obtained from the constant volume IQT. However, the ID value used in calculating activation energy is the chemical delay time obtained by separating physical and chemical processes. Compared to engines, the constant volume chambers have longer physical delay time which affects the activation energy values a lot, hence it needs to be separated from chemical delay.

The tests on the metallic engine were done by Jayakumar et al [91], at a constant SOI and intake pressure while increasing the intake temperature. The tests were conducted at two load settings of 3 bar and 5 bar IMEP. The Ea/R value obtained for ULSD was very small compared to the above two investigations, about 237.6 K i.e. 1975.40 J/mol. In fact the activation energy values for all the fuels tested are very small and around 1/10th of the values obtained by Kook and Zheng (Fig. 4.3).

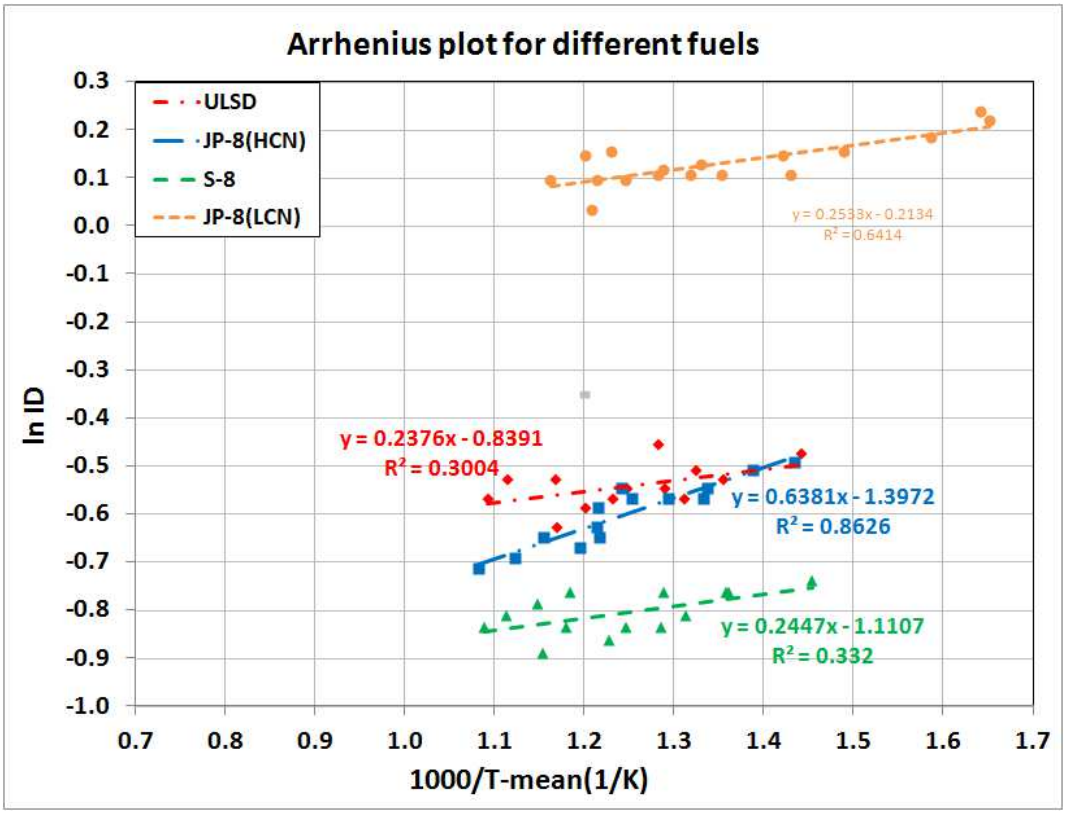

Figure 4.3: Arrhenius plot for different fuels [91]

Although Jayakumar et al covered a larger temperature range and their test points were at lower temperatures, it is interesting to observe they got apparent activation energy lower than Kook et al. It has been observed by researchers that global/apparent activation energy for fuels and pure hydrocarbons in heterogeneous

combustion shows a non-linear trend [85], in which global activation energy decreases with increase in temperature (Fig. 4.4). Based on this finding, the values obtained by Kook et al are expected to be lower than those reported by Jayakumar et al; however, this is not the case.

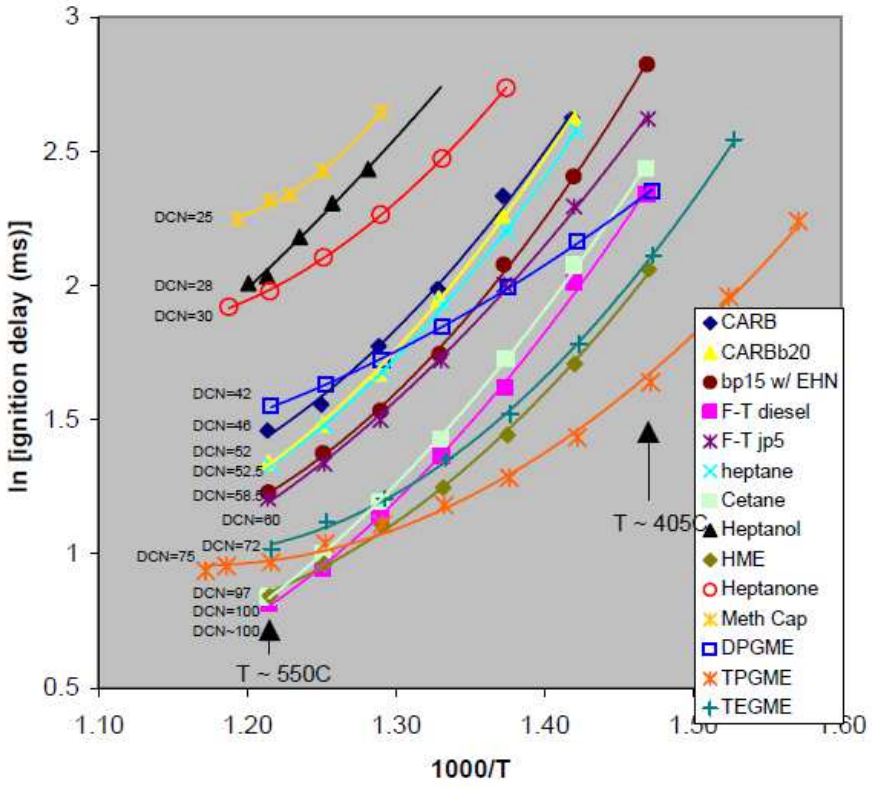

Figure 4.5: Ignition delay data versus the inverse of temperature for different fuels [85]

One of the objectives of this investigation is to find out the cause(s) of the lack of agreement in the activation energy values reported by Kook et al [8] and Jayakumer [91], while both were obtained in tests conducted on similar single-cylinder engines.

4.1 Preliminary Investigations

4.1.1 Tests on the metallic engine under the conditions of the optical engine

In order to compare between the results obtained on the two engines, tests were conducted on the metallic engine, under the same conditions of the optical engine. The test points chosen were the ones performed at 0% EGR i.e. 21% O_2 concentration. All the other parameters like intake temperature, intake pressure, injection pressure, swirl ratio, coolant temperature and load were kept the same. The SOI was varied from -7.6 to 3.3 CAD. The fuel used in the optical engine is ULSD with CN = 47.1. Then the fuel used in the metallic engine is JP8 of CN = 49. In addition, the same ID definition was used as the time period between SOI and the 10% of the mass burn fraction. Also, the effective temperature during ID period was considered to be the average of the temperatures at the SOI and SOC points. Furthermore, the y-axis of the Arrhenius plot was kept as the natural log of the multiple of ID value, average pressure and oxygen concentration. The results are plotted in Fig. 4.6.

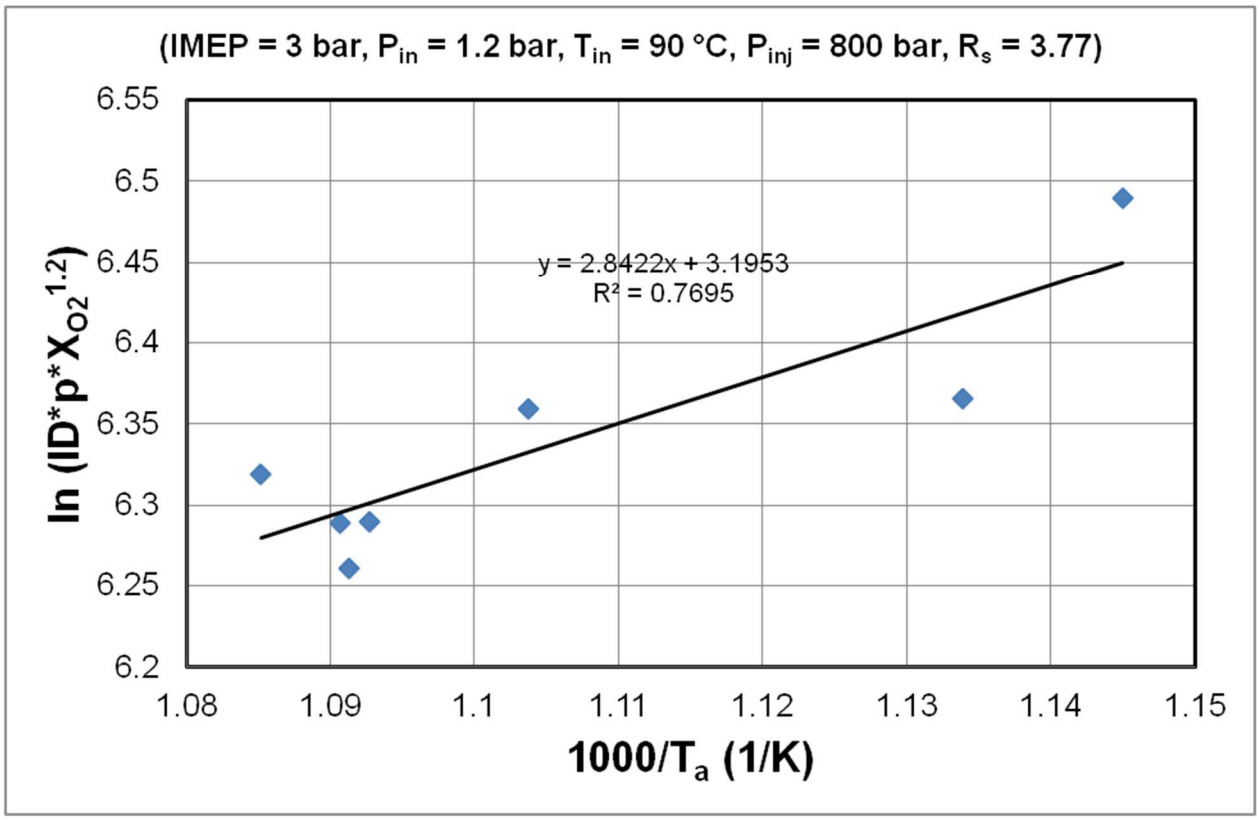

Figure 4.6: Arrhenius plot based on the approach of Kook et al

The E_a/R calculated from (Fig. 4.6), is 2842 K and the activation energy is 23630 J/mol. By repeating the test strategy and data analysis technique of Kook et al, the apparent activation energy value for JP8 is now higher than Jayakumar and is comparable to the values obtained by Zheng [92] in the IQT. Thus we can say that an activation energy value close to those obtained by Kook et al can be obtained from tests on other engines and with other fuels of close cetane numbers.

4.1.2 Tests on the metallic engine at variable intake temperatures and constant SOI

The data reported by Jayakumar et al were for tests conducted at variable intake temperature at constant SOI and intake pressure. However, the increase in temperature

at a fixed pressure reduces the density of air and the total mass of the air in the cylinder. If we assume that the same amount of fuel is needed to keep IMEP constant, the charge would have an overall higher equivalence ratio. Previous investigations showed the dependence of the ID on both the temperature and equivalence ratio [79, 80 and 82]. In the current investigation tests were conducted at different intake temperatures, while keeping a constant air-fuel ratio.

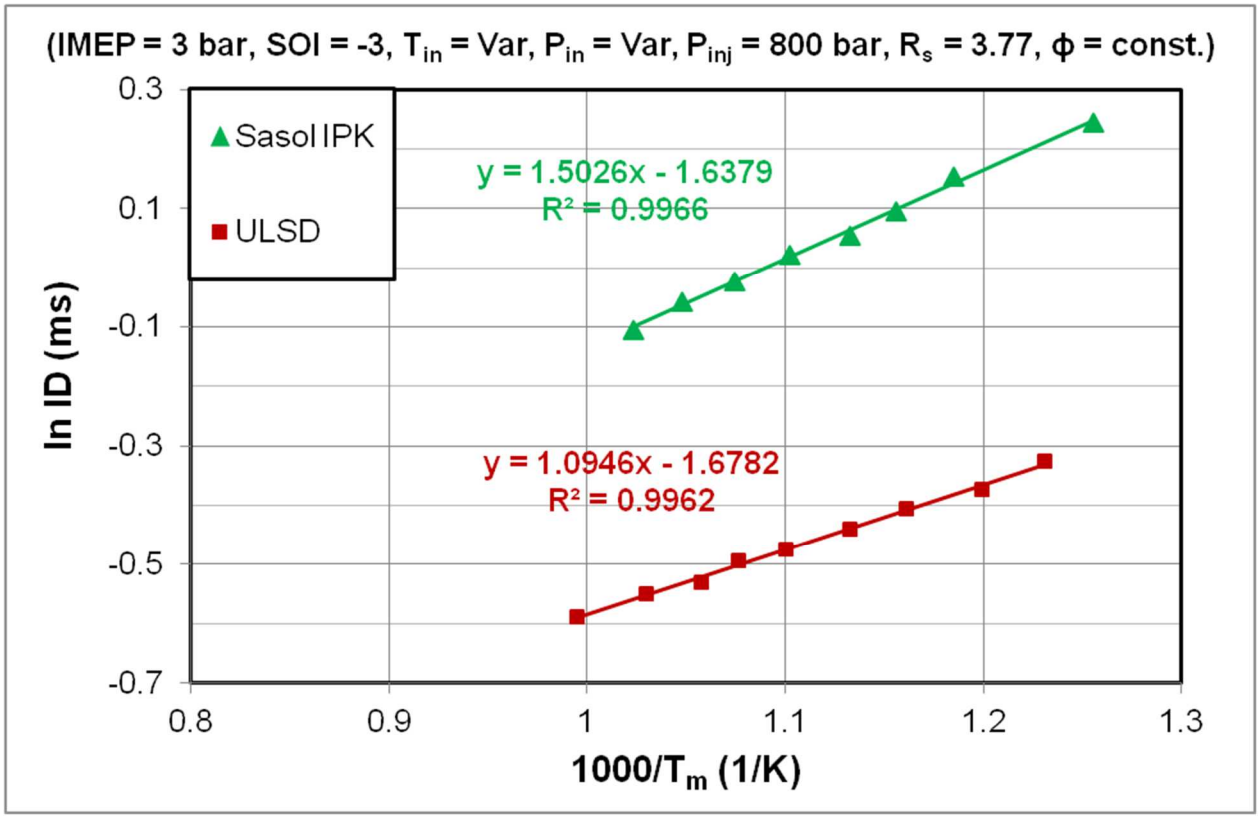

Figure 4.7: Arrhenius plot for ULSD and Sasol IPK based on tests done at constant SOI

Tests were done using ULSD and Sasol IPK in the metallic PNGV engine at fixed SOI of -3 CAD. The intake temperature and pressure was increased keeping the same

charge density at the given SOI. All the other parameters like injection pressure, swirl ratio, load and coolant temperature was kept same as previous tests.

In data analysis ID_{CA5} was used as the definition for ID and integrated mean of temperature during ID was used as the effective temperature. The Arrhenius plot using natural log of ID value vs. $1000/T_m$ was plotted and apparent activation energy was calculated. The E_a/R value for ULSD and Sasol IPK were 1095 K and 1503 K, which are higher than those previously reported by Jayakumar but still lower compared to Kook and Zheng.

So, it is evident that the activation energy values obtained by Kook and Jayakumar are affected by the test conditions. Also, there have been differences in ignition delay definitions, which show there is a need to study the sensitivity of global activation energy values to ID definitions. In engines, the temperature during the ignition delay period fluctuates a lot due to physical and chemical processes, and different methods are used to represent an effective temperature for the ID period. No previous record has been found of a research showing the sensitivity of activation energy to effective temperature method.

CHAPTER 5

IGNITION DELAY DEFINITIONS

5.1 Introduction

The events that occur immediately after injection and lead to auto-ignition include: spray breakup, droplet formation, fuel evaporation, air-fuel mixing, and endothermic and exothermic reactions. However, it is quite difficult to separate these events from each other as they always occur simultaneously in an engine. Therefore, ignition delay is used to collectively represent all these events and their effect on the start of combustion. The auto-ignition quality of different fuels has been rated by its cetane number (CN) determined in the CFR engine, according to ASTM D613 [93]. More recently, the Ignition Quality Tester (IQT), a constant volume vessel, has been used to determine the derived cetane number (DCN) to avoid the elaborate, time consuming and costly engine tests, according to ASTM D6890 [94]. The ignition delay period in these two standard tests and many investigations is considered as the time period between start of injection (SOI) and start of combustion (SOC). However, the ignition delay (ID) values determined from the SOI and SOC can be varied due to different instrumentation and definitions.

Ignition delay values are used in calculating apparent activation energies of different fuels in various test environments using the Arrhenius equation, Eq. (5.1).

$$ID = Ae^{\frac{E_a}{RT_m}} \quad (5.1)$$

where,

ID = ignition delay time

A = constant which depends on the fuel and combustion system characteristics

R_u = universal gas constant

E_a = apparent activation energy

T_m = mean temperature

Any change in the ignition delay value would affect the calculated apparent activation energy of the fuel. Hence an effort is made to study the effect of different ID definitions on the calculated global activation energy.

5.2 Literature Review

Most previous investigators agree that the ignition delay begins at the start of injection (SOI), and is usually measured by the needle lift (NL) of the injector [2]. Apart from needle lift, some researchers considered ID to start at the energizing of the injector [19], while others considered the drop in fuel pressure upstream the injector [95] as the SOI. So depending on the type of instrumentation the SOI definition will change but this would be a technical difference rather than conceptual. The major differences among researchers have been in the definition of the end of ignition delay, in other words the start of combustion (SOC).

In optical engines and other optically accessible combustion equipment, the ignition delay is termed as illumination delay. In such cases the start of combustion is determined by directly capturing the first visible radiation using photo sensors. In metal engines, on the other hand, it is difficult to determine the start of auto-ignition directly and a change in the slope of the pressure trace due to combustion has been considered to be the end of ignition delay [2]. Some investigations determine the end of ignition delay at certain points on the heat release rate trace.

As discussed above the basic phenomenon that signifies the start of combustion in metallic engines is a sudden rise in pressure trace, this simple event has been used to define the end of the ignition delay period. With the advent of computers and rapid computing speed it becomes convenient to use a formula to define and locate such a point, especially when there is a large amount of data to be processed. However, researchers have been unable to formulate the pressure rise delay as there is no standard method that defines the point in pressure trace that defines the sudden rise in pressure; hence, there are different approaches to locate the start of combustion.

Zaidi et al [96] defined SOC as the point where the pressure rate curve reaches its minimum value after SOI, whereas Assanis et al [97] stated that SOC is at a point where the second derivative of pressure curve reaches its first maximum after SOI. They chose these points as they coincided with the start of sudden pressure rise. However, these points coincide only in those cases where the fuel injection happens quite early in the compression stroke, but in cases where the fuel injection is close to TDC and combustion happens near TDC or late in the expansion stroke there is an offset between the two points. As shown in Fig. 5.1, the start of pressure rise is at

around 3.3 CAD while the minimum of pressure rate curve and first maximum of second derivative of pressure trace is at around 1.4 CAD and 4.3 CAD respectively. If the current definitions of SOC are used, the error in the ID value would be 1.9 CAD and 1 CAD respectively.

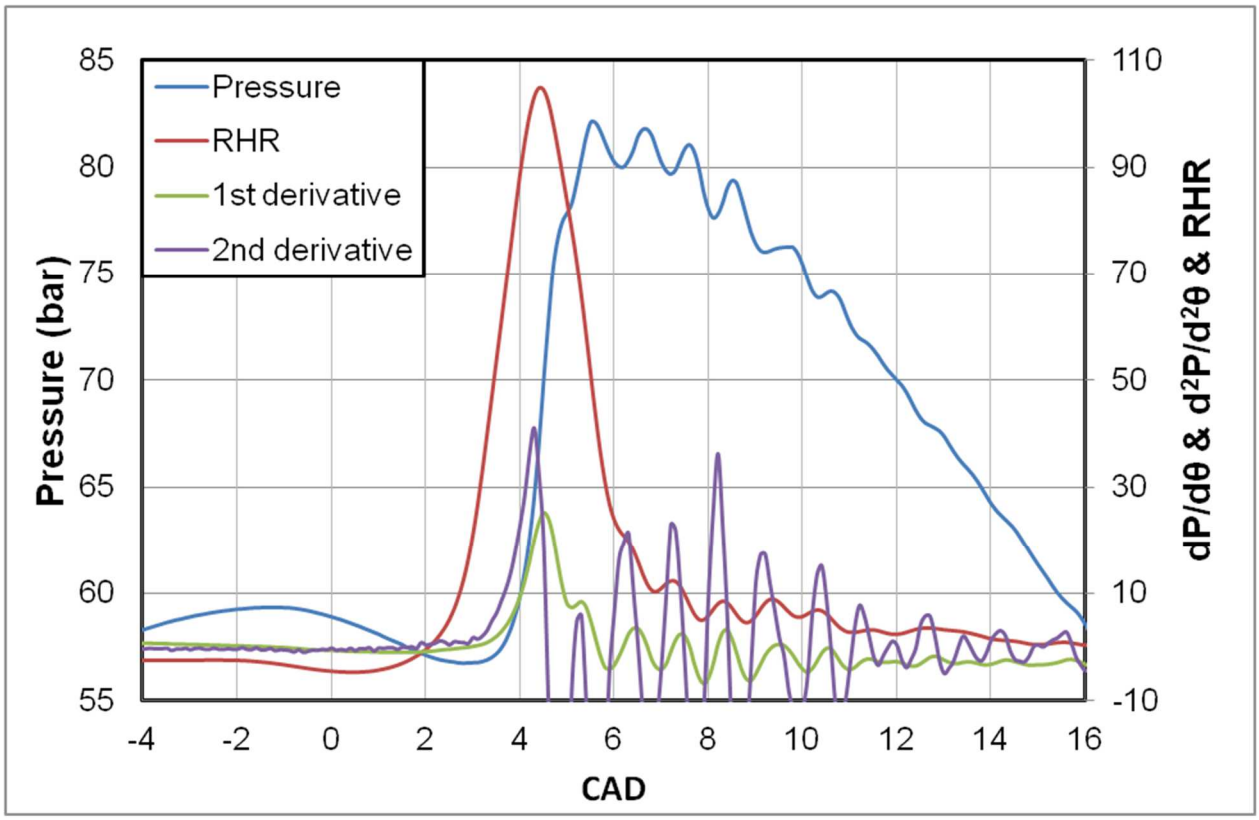

Figure 5.1: SOC location defined as the trough of first derivative of pressure trace

In another definition, Jayakumar et al [20] defined SOC as the lowest point on the pressure trace before it reaches peak combustion pressure (Fig. 5.2). However, this definition can only be applied in those cases where the pressure trace shows a considerable dip after injection, which happens mostly in such instances where the combustion takes place in the expansion stroke. As a result, this method cannot be applied to cases where the combustion takes place before top dead centre (TDC).

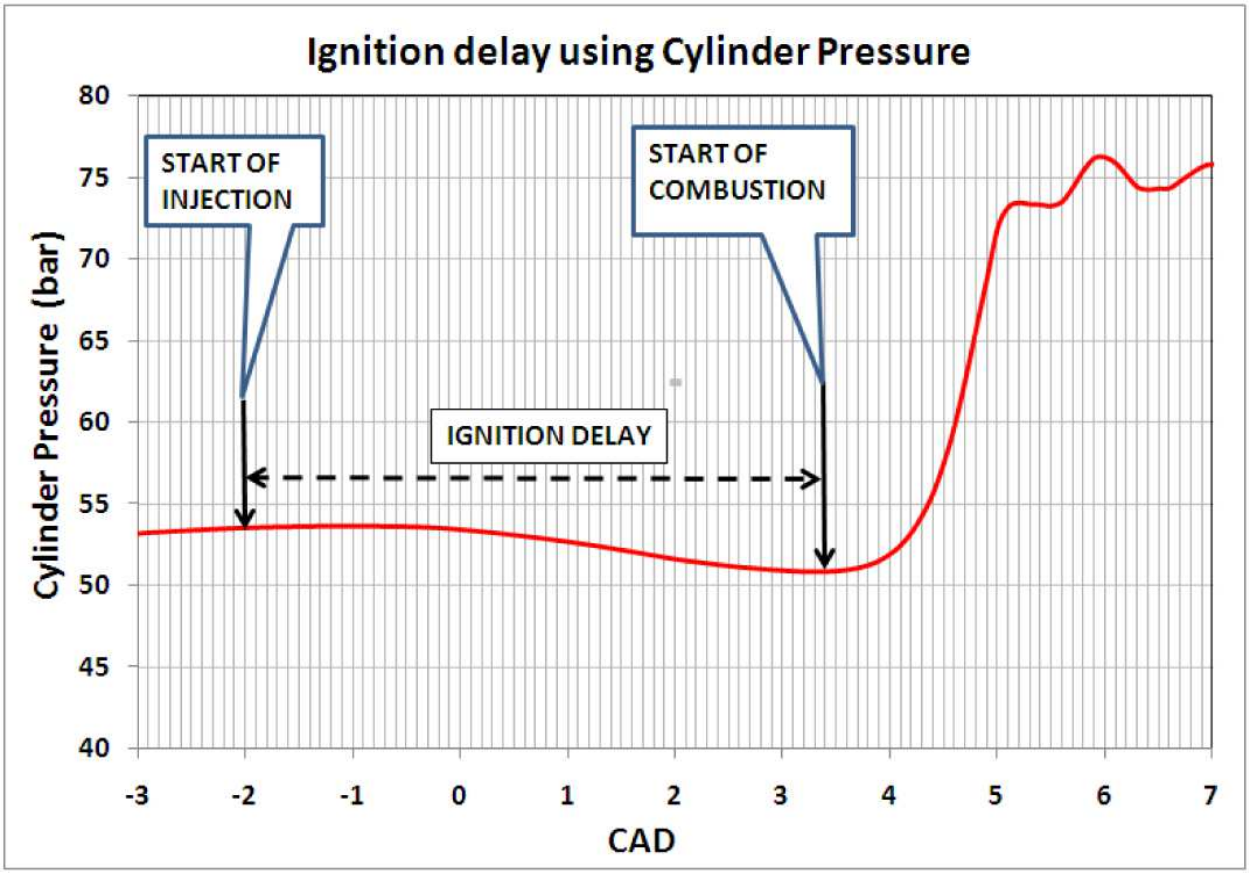

Figure 5.2: SOC location defined as the lowest point on pressure trace before pressure rise [20]

The problem to locate the start of pressure rise using a formula, applicable at all conditions, lead researchers to use other phenomenon to define SOC. Many researchers defined ignition delay using the rate of heat release (RHR) curve. The most common definition being used nowadays is the duration between the SOI and the point where the RHR curve crosses zero, and changes from negative to positive [12, 30, 98-101]. Although this definition is applicable at all SOI conditions, it still has a drawback. This method fails to include the two stage combustion shown by fuels with low CN, like Sasol IPK, and by regular fuels in advanced combustion modes like HCCI, PCCI, and LTC etc. The location of the cool flame and negative temperature coefficient

temperature (NTC) regimes, seen in two stage combustion, on the RHR curve is always after it has crossed zero; as a result, the ignition delay value in such cases is reduced considerably.

More recently, researchers have come up with new ignition delay definitions to include NTC and cool flame regimes. In one such approach, SOC is determined as the point where 10% mass burn fraction occurs that lies at 10% (CA10) of the cumulative RHR (CuRHR) curve [8, 102-104]. Similarly, in another approach, SOC is located at the 5% (CA5) of the CuRHR curve [105]. These methods have a wide applicability, and can be used to define ignition delay for HCCI, PCCI and LTC combustion modes as well.

In addition to the ignition delay definitions discussed above we have compared another definition in this study. As defined in the ASTM D6890 standard, the ignition delay for the IQT is the time delay between the SOI and the pressure recovery point [94]. In addition, when the CuRHR curve and the pressure curve are compared they show identical resemblance, and the pressure recovery point overlaps with CuRHR recovery point (Fig. 5.3). Thus, it can be said that the ignition delay for the IQT is the time delay between the SOI and the CuRHR recovery point. While it is hard to always get a pressure recovery point in engines, a CuRHR recovery point will be more realistic to detect in engines. The main purpose behind using this definition would be that it gives a common yardstick to compare data trends in two different environments: constant volume chamber and engines.

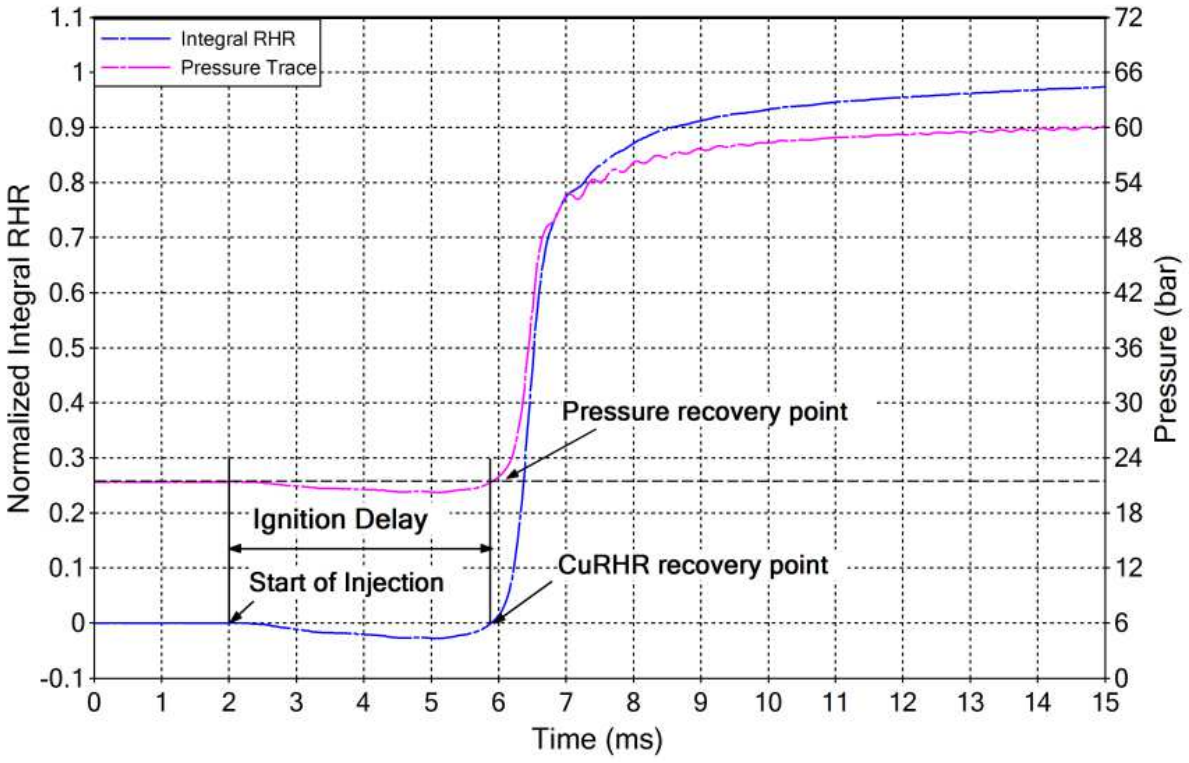

Figure 5.3: ID method used for IQT based on recovery point

5.3 Comparison between Ignition Delay Definitions

A comparison between different ignition delay definitions has been made to see the closeness of each definition to an approximate pressure rise delay. The ID definitions used for comparison are the most widely used definitions and the new definition based on recovery point for CuRHR curve. They are as follows:

1. ID_P = delay between SOI and a detectable start of pressure rise.

2. ID_R = delay between SOI and RHR curve crossing zero.

3. ID_{CA5} = delay between SOI and 5% of CuRHR curve.

4. ID_{CA10} = delay between SOI and 10% of CuRHR curve.

5. ID_{RP} = delay between SOI and CuRHR curve crossing zero.

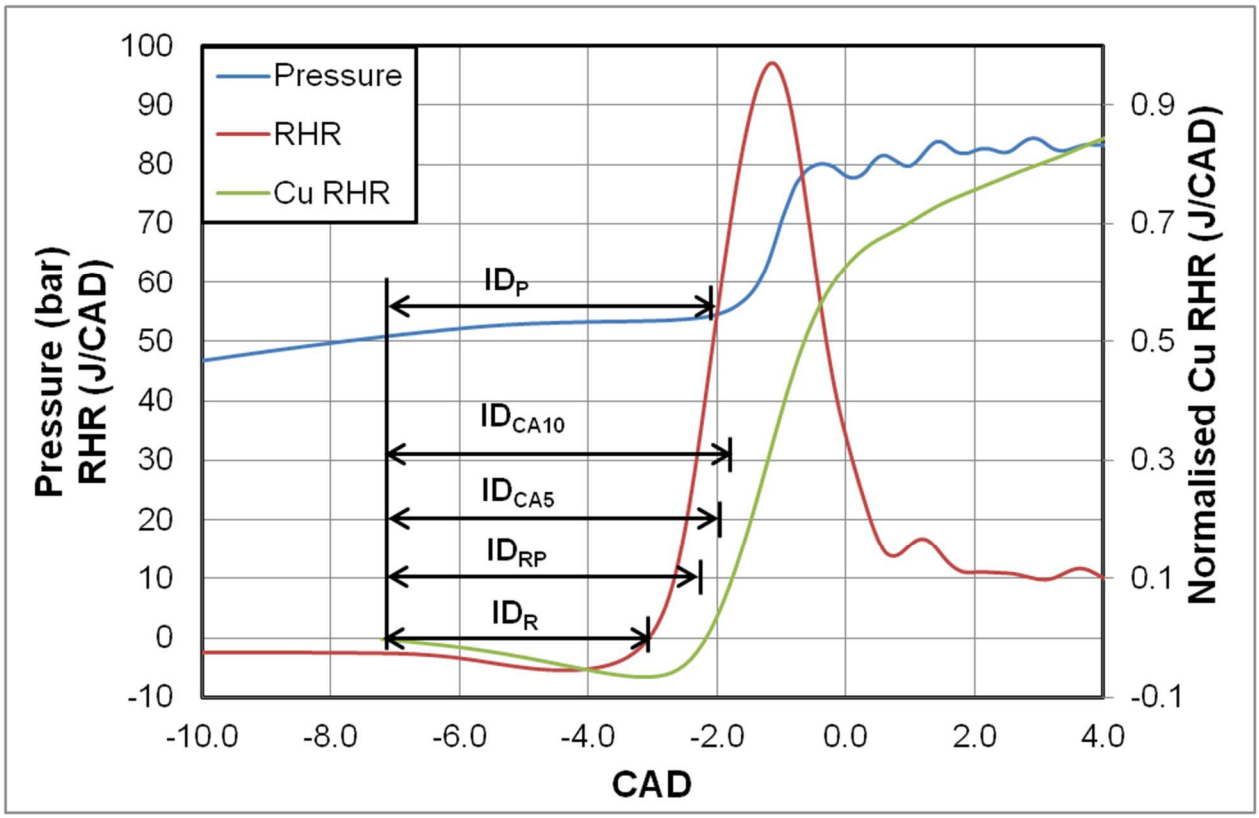

Figure 5.4: A comparison of different ID definitions for a conventional CI case

In the first case, ULSD, a high CN fuel is injected early in the compression stroke so that the pressure rise takes place before TDC (Fig. 5). As a result, ignition delay is very short and there is absence of observable pressure dip before the peak of pressure. A comparison between the various ignition delay definitions reveals ID_R gives the smallest value of the ignition delay period, and has the biggest offset to the start of pressure rise. On the other hand, ID_{CA10} has the longest delay period compared to other definitions; also, it ends very close to the peak of RHR curve which signifies combustion

has already started and is reaching its highest rate. ID_{CA5} and ID_{RP} gives ignition delay value close to the ID_P.

In the next case, Sasol IPK, a high volatility, low ignition quality fuel of 25 CN; which exhibits two-stage combustion, is injected at the same SOI as the previous case. In this instance, except for ID_R, rest of the definitions includes the cool flame in the ignition delay period. Again we see that the SOC for ID_{CA10} occurs closer to the peak of RHR curve, compared to the other definitions. Even in this case, ID_{CA5} and ID_{RP} give ignition delay values closer to the ID_P.

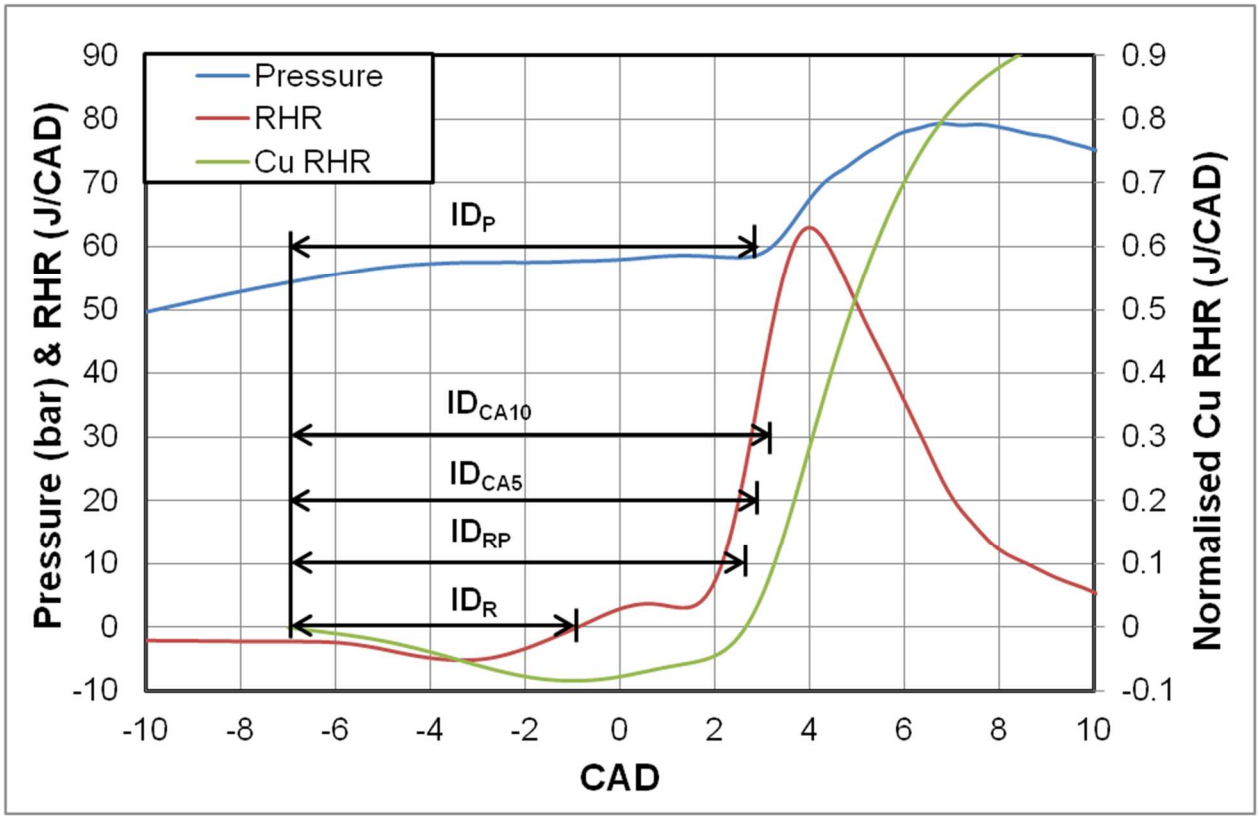

Figure 5.5: A comparison of ID definitions for Sasol IPK which shows two-stage combustion

5.3.1 Dependence of Activation Energy on the definition of the end of ID period (SOC)

There is a need to study and compare between the different ignition delay definitions, because ID values are used in Arrhenius plots to calculate the global activation energy of the auto-ignition reactions of the fuel based on Eq. (5.1). Any change in ignition delay value would cause variation in the global activation energy value. Therefore, a detailed comparison of Arrhenius plots is done, in which natural logarithm of ignition delay values are plotted against the reciprocal of the mean absolute temperature during the ignition delay period. In these data sets, the engine intake air temperature was varied while the air mass (density) and SOI timing were kept as constant.

The SOI definition is based on the needle lift signal and comparison would be done between the SOC definitions discussed in the previous section i.e. ID_{RP}, ID_{R}, ID_{CA5} and ID_{CA10}.

Table 5.1: Activation energy values for ULSD

Definition	E_a/R_u (K)	E_a (KJ/kg mole)	Variation (%)
ID_{CA10}	1069	8888	0
ID_{CA5}	1095	9104	2.43
ID_{R}	1167	9702	9.17
ID_{RP}	1247	10368	16.65

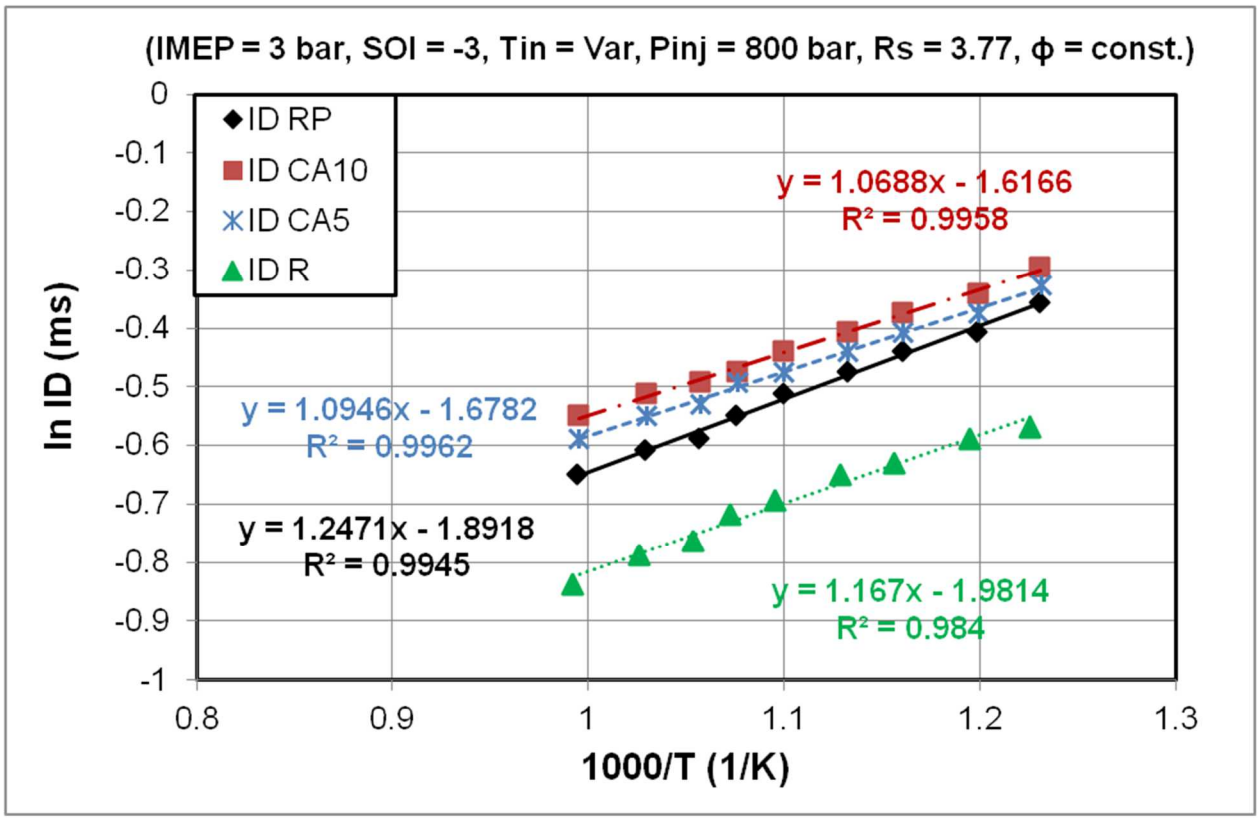

Figure 5.6: A comparison of activation energy using different ID definition for ULSD fuel

For ULSD, the E_a/R_u value represented by the slope of the lines, are very close for all ignition delay definitions showing a variation of 16.65 % between the highest and lowest values, as shown in (Table 5.1). The ignition delay values obtained using ID_R as SOC definition is smaller compared to values obtained using the other three definitions. However, the data does not show any specific trend for the global activation energy values.

On the other hand, for Sasol IPK, the E_a/R_u values are close for three ID definitions while quite different for ID_R (Table 5.2). In this case the difference between the maximum and minimum E_a/R_u value is 144 %. This large difference in the activation

energy using ID_R definition is due to its lack of including the cool flame. Thus, it is clear that ID_R is not a suitable definition of ignition delay for fuels that exhibit two-stage combustion.

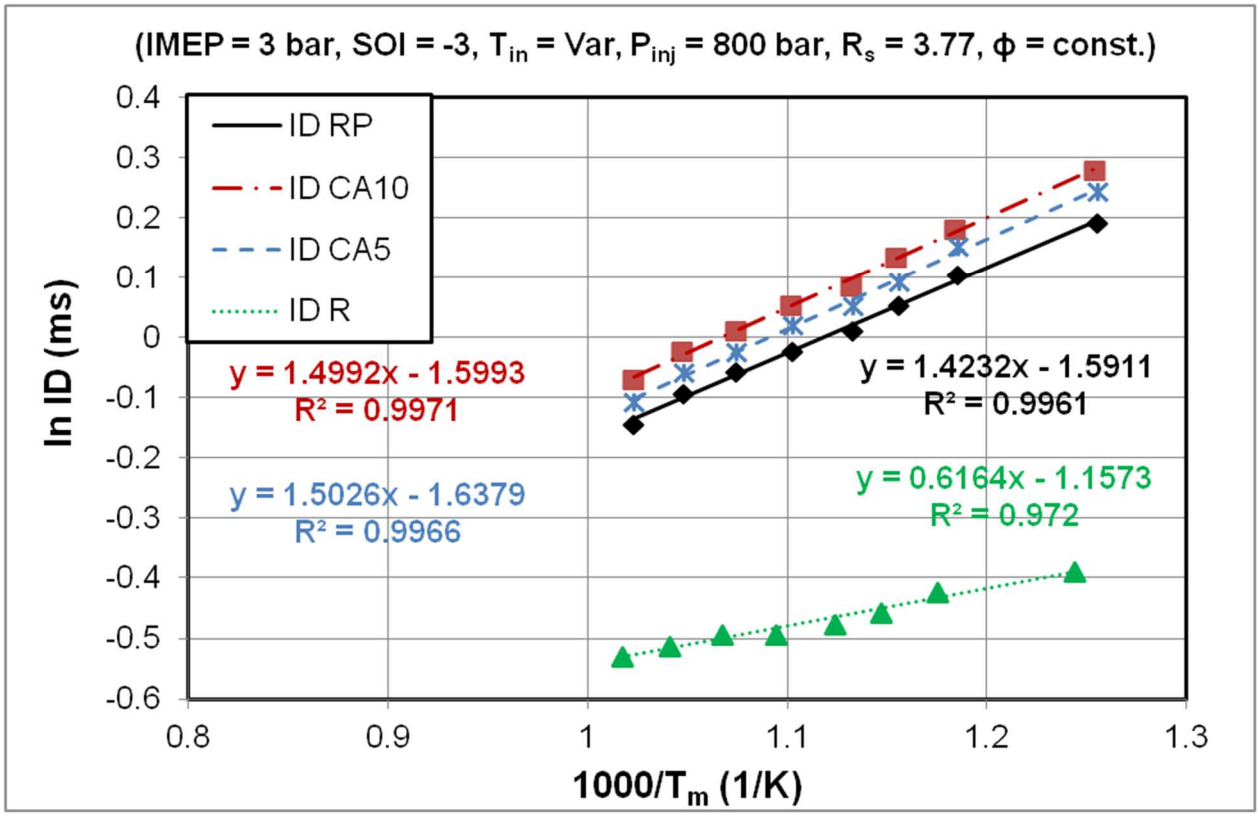

Figure 5.7: A comparison of Arrhenius plots using different ID definitions for Sasol IPK

Table 5.2: Activation energy values for Sasol IPK

Definition	E_a/R_u (K)	E_a (KJ/kg mole)	Variation (%)
ID_R	616	5121	0
ID_{RP}	1423	11831	131
ID_{CA10}	1499	12463	143.34
ID_{CA5}	1503	12496	144

5.3.2 Dependence of Activation Energy on the definition of the start of ID period (SOI)

As stated earlier, the ID value can also change depending on the definition of its starting point, usually considered to be the SOI. In order to study this dependence, two definitions of SOI were used: first determined from the needle lift (NL) signal and second from the fuel pressure (FP) signal. The SOC definition was kept same as 5% of CuRHR trace in this analysis.

The SOI from the fuel pressure trace is taken as the point after injection where it shows a considerable drop in the pressure trace, which is around -0.8 CAD, as shown in Fig 5.8. However, the fuel pressure transducer is upstream of the injector and there is a small delay in the pressure wave reaching the transducer. This delay has been measured during instrumentation and calibration, which was found to be 1.7 CAD, thus shifting the actual SOI to -2.5 CAD. The needle lift sensor doesn't have a lag and gives instantaneous values. The SOI is determined as the point where the needle lift signal crosses value 2. This value is determined by the bounce back obtained during the downward movement of the needle signifying the needle has reached its seat. Thus the needle's minimum lift is 2, the lower values being noise in the signal, based on this fact the SOI value using needle lift signal is at -3 CAD. Thus the difference between the two SOI definitions is a constant value of 0.5 CAD.

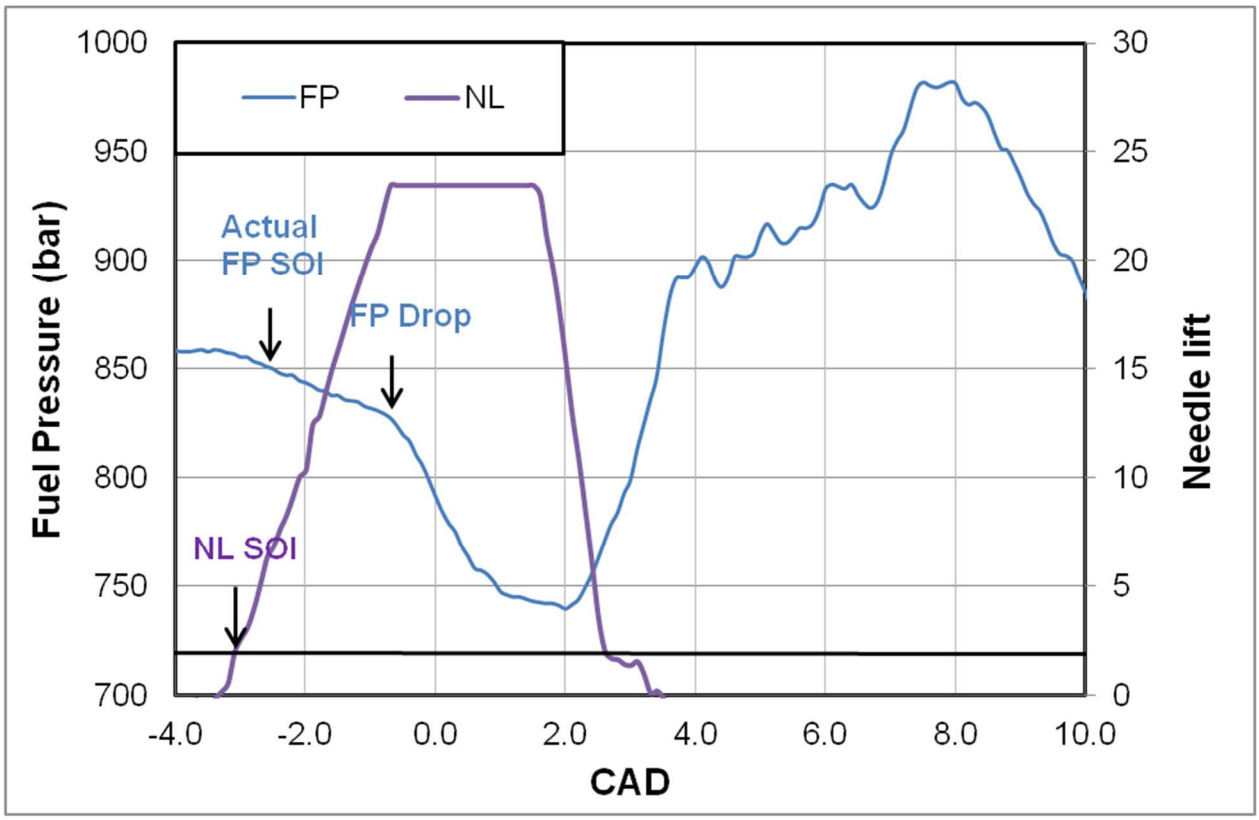

Figure 5.8: Start of ignition defined by needle lift and fuel pressure drop

Figure 5.9 shows Arrhenius plots based on the ID values obtained using the above mentioned SOI definitions, for both ULSD and Sasol IPK. The results show that E_a/R_u values are fairly close with a variation of 7.54 % and 4.89 % for ULSD and Sasol IPK, respectively. Since the two SOI definitions have a constant difference of 0.5 CAD between them, it would result in a constant deviation of 0.5 CAD in the ID values. However, the lines in Arrhenius plot are not parallel as the y-axis is based on logarithmic values. It is interesting to note that the variation is smaller for Sasol IPK than ULSD. A change of 0.5 CAD will reflect as a bigger percentage for a smaller value than a larger value, therefore ULSD will show a bigger change (8.12 %) than Sasol IPK which shows much lower (5.18 %). Thus the effect of SOI on global activation energy is very less, but it can be significant for those fuels which have small ID periods.

Table 5.2: Activation energy values for ULSD and Sasol IPK

Definition	E_a/R_u (K)	E_a (KJ/kg mole)	Variation (%)
ULSD NL	1095	9104	0
ULSD FP	1184	9844	8.12
Sasol NL	1506	12521	0
Sasol IPK	1584	13169	5.18

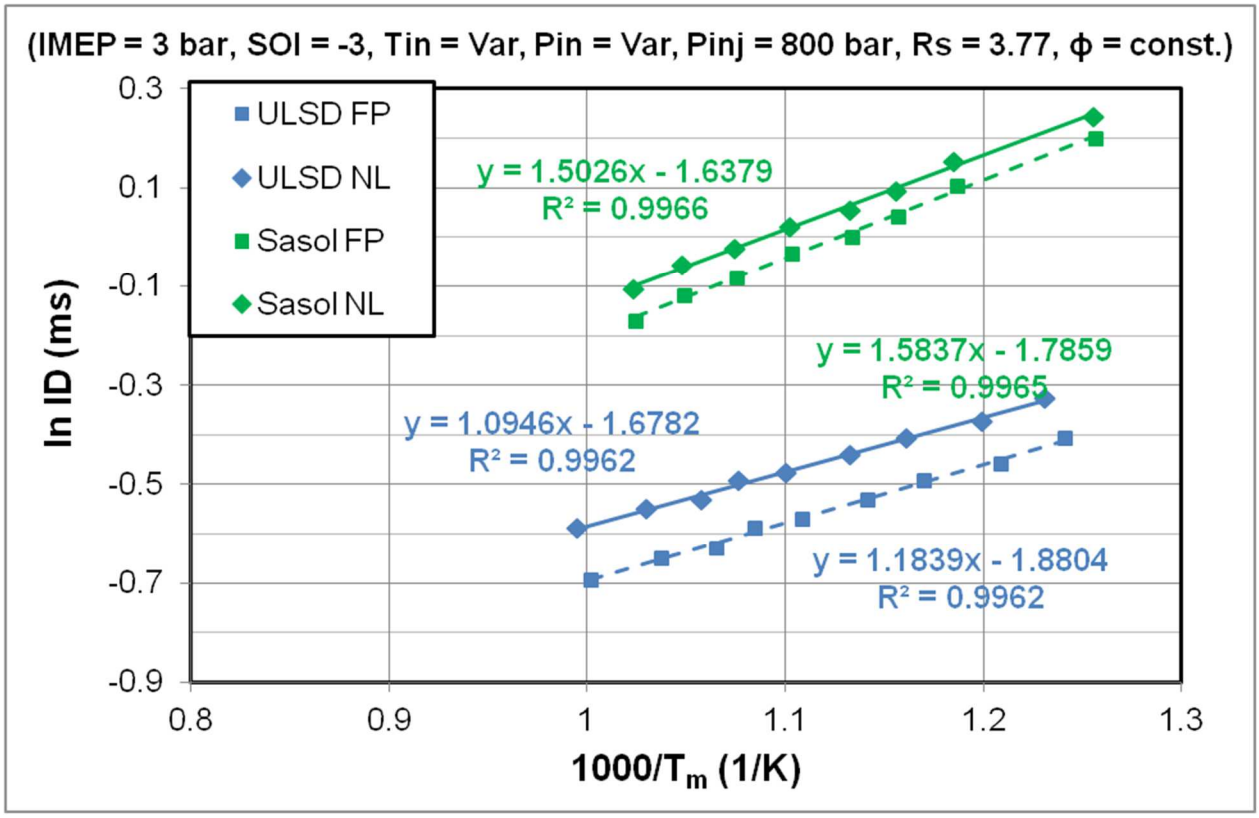

Figure 5.9: A comparison of Arrhenius plots for ULSD and Sasol IPK using two different SOI definitions

5.4 Conclusions

- ID_R is not a suitable ignition delay definition for the cases where the fuel shows two-stage combustion. It does not include cool flame and NTC; thus, leads to smaller value for global activation energy.
- ID_{CA10} does include cool flame and NTC regime in the ignition delay time; however, its proximity to peak of ARHR is debatable.
- ID_{RP} and ID_{CA5} have given values closest to the ID_P definition; and therefore, are suitable for activation energy calculations.
- ID_{RP} can be used as a common yardstick between constant volume instruments and diesel engines to study auto-ignition characteristics of fuels.
- A change in SOI definition brings about smaller change in ID time compared to SOC definition. Also, its effect on activation energy is less than SOC definition, but for fuels which have shorter ID time the effect of SOI can be more significant.
- Since, SOI definition does not affects global activation energy significantly, needle lift signal is used to define SOI and location of 5% of CuRHR being the closest to the pressure rise delay point, ID_{CA5} is used as the ID definition for the rest of the dissertation.

CHAPTER 6

EFFECT OF CYLINDER GAS TEMPERATURE DEFINITIONS

6.1 Introduction

The global activation energy of combustion is calculated from the Arrhenius plot that has ID on the Y-axis and inverse of temperature on the X-axis; therefore its value is directly affected by ID and temperature values used. In shock tubes, rapid compression machines, homogeneously charged constant volume reactors and engines there is no physical delay part; and if there is any, it's not as dominant compared to heterogeneous combustion. As a result there is no drop in temperature due to evaporation and the temperature variation in the chamber is very less. In such cases it is feasible to use initial temperature in ID correlations and in turn to calculate global activation energy. However, for heterogeneous combustion an effective temperature is used, which would provide as the best representation for the data. The effect of different ID definitions on global activation energy was discussed in the previous chapter, and in this chapter we will discuss effect of different effective temperature methods on it.

6.2 Literature Review

Previously researchers have used temperature at start of injection [5], start of pressure rise delay [6], peak of compression [7], mean temperature during ignition delay

period [20, 106], and average of SOI and SOC temperature [8] in the correlation for ignition delay data.

The most popular methods have been temperature at SOI, mean temperature during ignition delay period and temperature average for SOI and SOC. In this chapter the main focus has been to do comparison between these three methods and study their effect on global activation energy calculations. The ID definitions used for these calculations are the two most popular methods used by researchers nowadays, ID_{CA5} and ID_{CA10}.

6.3 Effective Temperature for a High CN fuel (ULSD)

6.3.1 Early Injection

A high CN fuel shows a typical combustion behavior of short ID time and single stage combustion. In conventional diesel engine combustion, injection takes place early in the compression stroke that leads to auto-ignition before or around TDC (Fig. 6.1). In such cases, after injection the temperature initially keeps rising due to compression. But soon the evaporation and endothermic reactions catch up and the temperature starts falling until the exothermic reactions take over finally, leading to combustion. When we compare the temperatures at SOI and the SOC points, defined by CA5 and CA10, they are very close with a difference of 3 K and 4 K respectively. In this case the T_{SOI}, T_{AVE} and T_M will be very close with a difference of ≤ 7 K. It is likely that an Arrhenius plot using any of them would show almost similar representation. The data set was limited to just one point at this setting due to high rates of pressure rise with further increase in

intake temperature and pressure, leading to concern for engine safety. As a result, the data was not sufficient to develop Arrhenius plots.

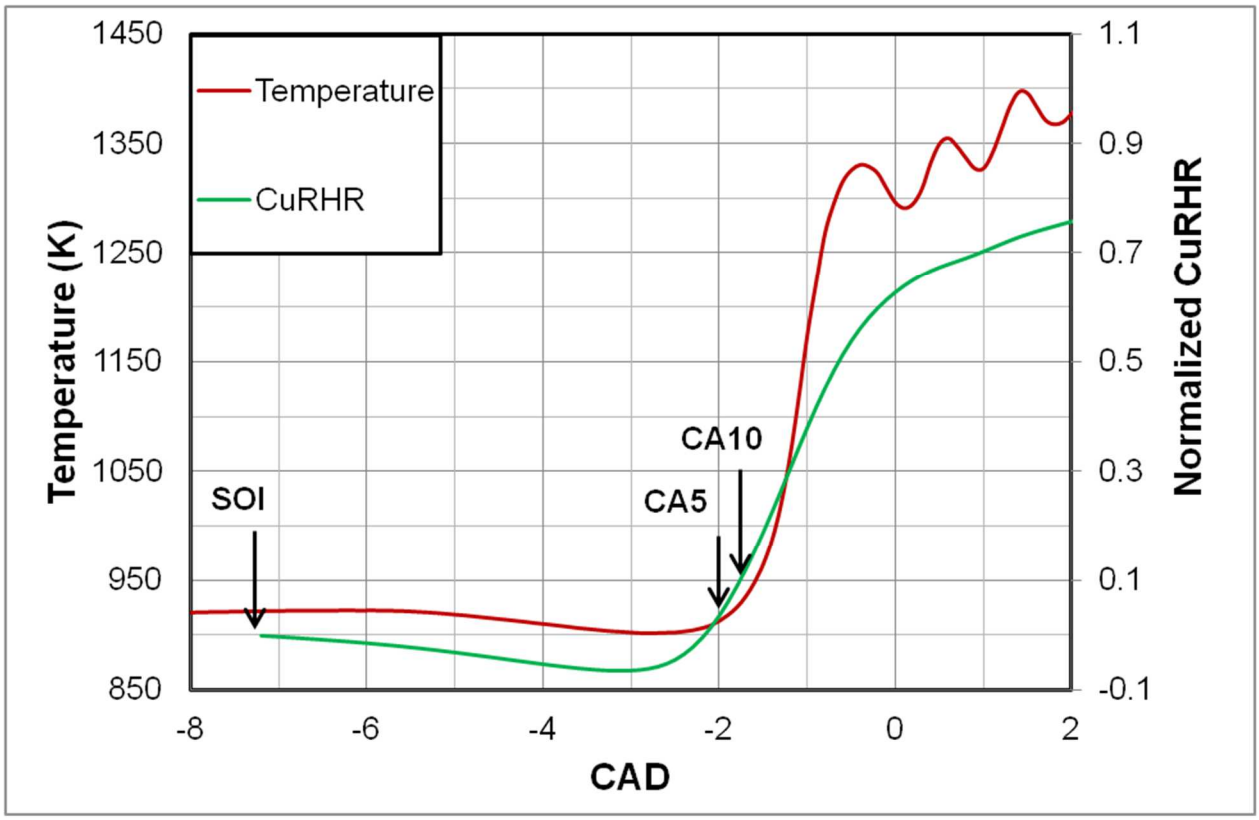

Figure 6.1: Temperature and cumulative heat release for an early injection diesel combustion

6.3.2 Near TDC Injection

The location of peak compression temperature is always a few CAD before the TDC, and it starts to fall as the piston advances to TDC due to heat losses. An injection event near TDC would lead to further fall in temperatures with onset of evaporation and endothermic reactions (Fig. 6.2). Finally, when the exothermic reactions overtake the collective effort of the cooling phenomenon the temperature starts rising again, leading to combustion. A comparison between temperatures at SOI and the SOC points, CA5

and CA10, show that the difference has increased to 20 K and 9 K respectively. This would result in values for T_{SOI}, T_{AVE} and T_M with a difference of ≤ 16 K, which is still small but noticeable on the Arrhenius plot. A detailed discussion on the effect of different effective temperature methods on apparent activation energy is discussed in next section.

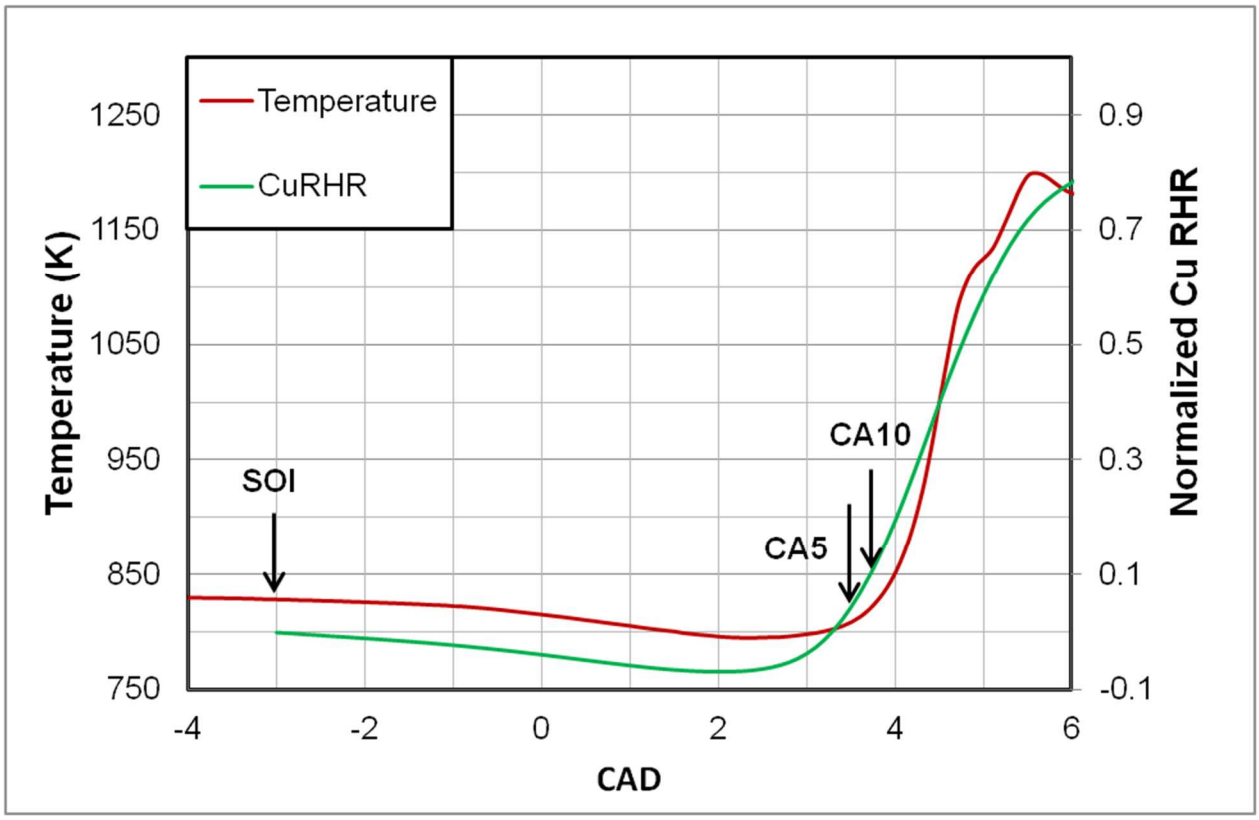

Figure 6.2: Temperature and cumulative heat release for near TDC diesel injection

6.3.2.1 Effect on Global Activation Energy

Figures 6.3 (a) and (b) shows Arrhenius plots for the same data set with two different ID definitions, ID_{CA5} and ID_{CA10} respectively. The test points have the same SOI, swirl ratio and injection pressure, but incremental intake temperature (30-110°C) at same charge density, speed and load of 3 bar IMEP.

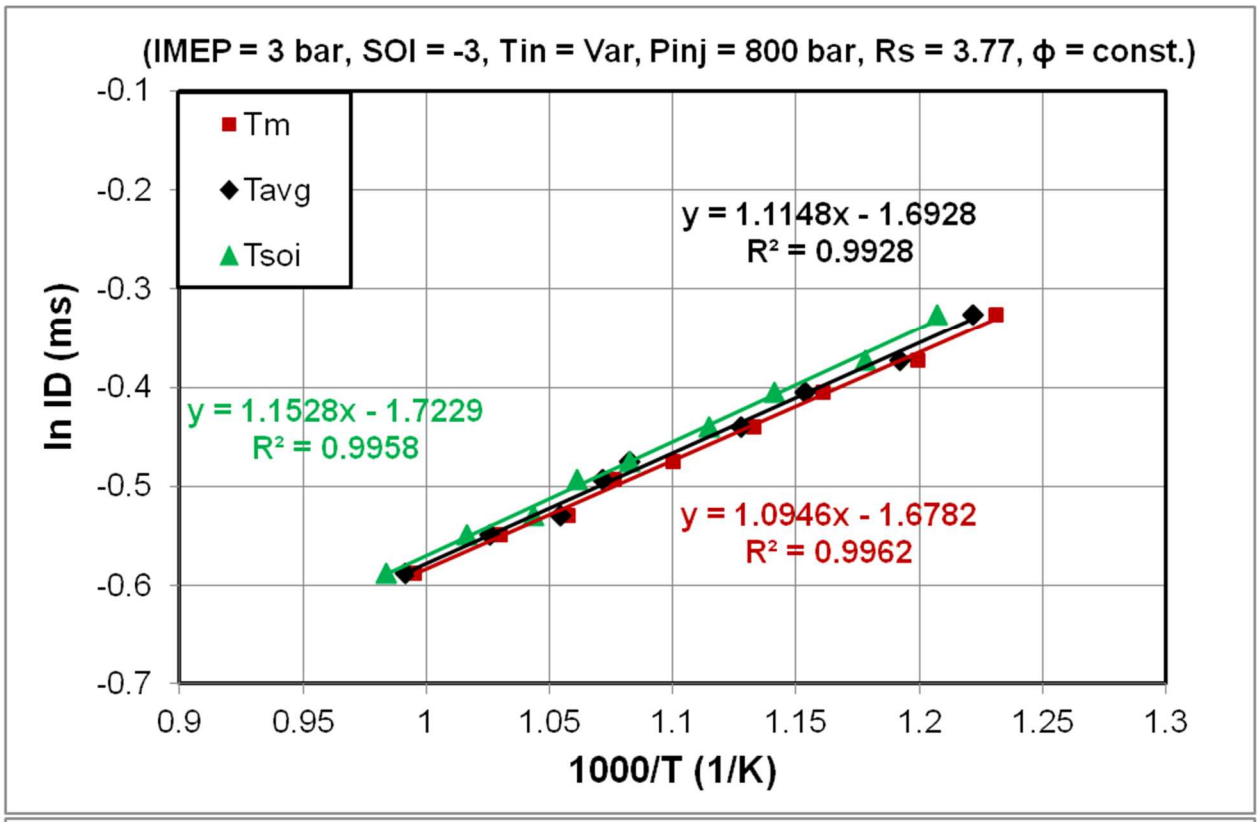

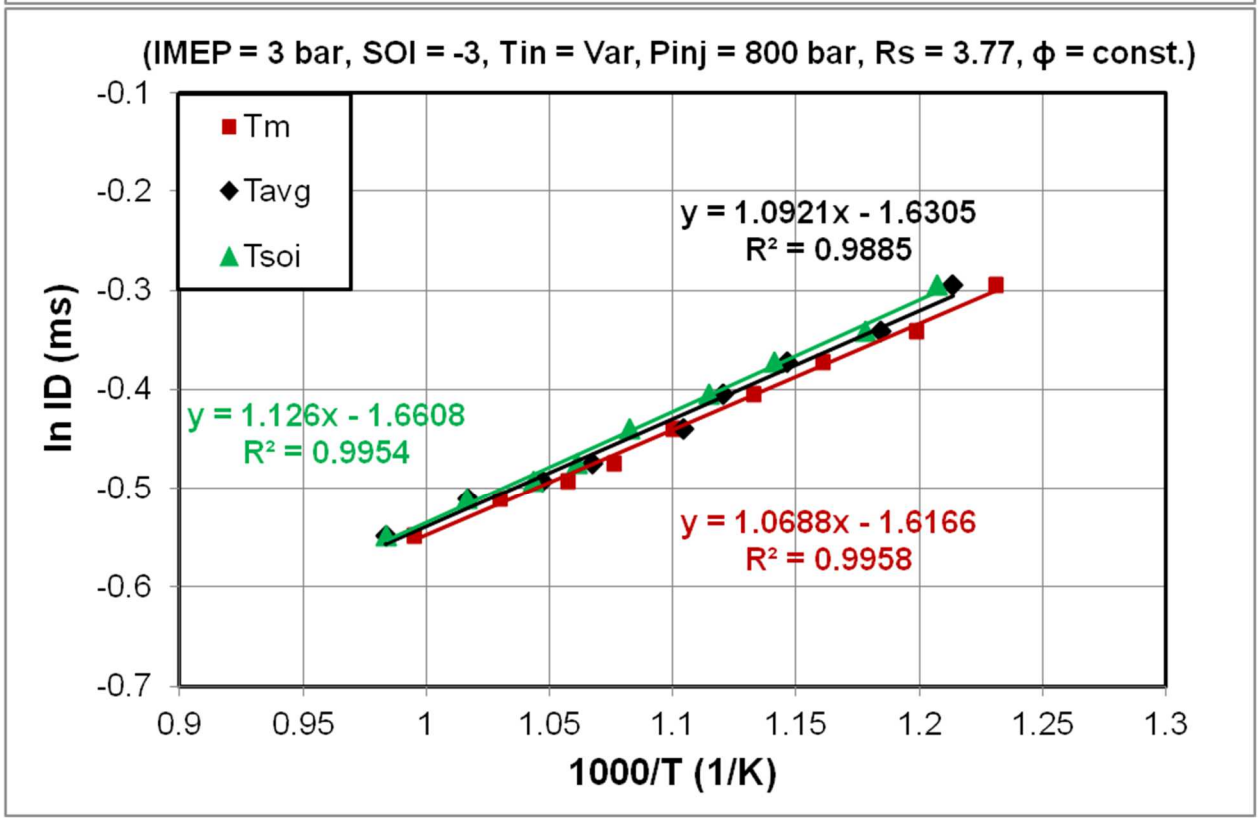

Figure 6.3: Arrhenius plots using (a-top) ID_{CA5} definition (b-lower) ID_{CA10} definition

In Fig. 6.3(a) the global activation energy values obtained using the three different temperature measurement methods are pretty close (Table 6.1) with a max variation of 5.29 % between the highest and lowest value. The temperature values obtained for T_{AVE} lie in between those of T_M and T_{SOI}, with T_M being the lower boundary and T_{SOI} being the upper boundary. As T_M is the mean of all temperatures after injection it will always be lower than the other two temperatures. T_{AVE} values are close to the T_M values and with the increase in intake temperature are getting closer. In fact, the difference between all of them tends to be decreasing with the increase in intake temperature. It can be attributed to the reduction in ID time with rising intake temperatures which would result in combustion happening closer to TDC. We have observed in early injection case that when combustion happens near TDC the difference between T_{SOI}, T_{AVE} and T_M is less. Also, it is interesting to note that the R^2 value is maximum using T_M and least using T_{AVE} as effective temperature, which means T_M provides the best fit for the data points statistically.

Table 6.1: Activation energy values for ULSD at SOI -3 using ID_{CA5}

Definition	E_a/R_u (K)	E_a (KJ/kg mole)	Variation (%)
T_M	1095	9104	0
T_{AVE}	1115	9270	1.82
T_{SOI}	1153	9586	5.29

Again in Fig. 6.3(b) the apparent activation energy values obtained are very close with a variation of 5.33 % between the maximum and minimum value (Table 6.2). It should be noted that T_{SOI} values don't change with ID definition, and even in this case

T_M is the lower boundary and T_{SOI} the upper boundary, while T_{AVE} lies in between them. However, T_{AVE} values are closer to T_{SOI} in here and at higher intake temperatures they completely overlap each other. Considering 5% more mass of fuel is burnt at the location of CA10 than CA5 the temperature achieved will be higher as well; hence, resulting in higher T_{AVE} values which are more close to T_{SOI} than observed in Fig. 6.3(a). Nonetheless, the overall trend is they all are getting closer with further increase in intake temperature. Even in this case using T_M shows highest R^2 value and T_{AVE} the least, indicating T_{AVE} doesn't provide statistical best fit to the data.

Table 6.2: Activation energy values for ULSD at SOI -3 using ID_{CA10}

Definition	E_a/R_u (K)	E_a (KJ/kg mole)	Variation (%)
T_M	1069	8888	0
T_{AVE}	1092	9079	2.15
T_{SOI}	1126	9362	5.33

6.3.3 Late Injection

In the expansion stroke the mass average temperatures are already falling due to expansion. In fact, for the low intake temperatures the engine combustion was unstable with peak combustion pressures lower than the motoring pressure. As a result, the intake temperatures had to be ≥ 70°C to sustain a load of 3 bar IMEP. An injection event in such a situation would further add to the reduction in temperature. This trend will continue until the exothermic reactions arrest the fall in temperature and starts producing heat leading to combustion. In this case the difference in temperature between SOI and SOC points is huge. The temperatures at CA5 point is 38 K lower and at CA10 point is 19 K lower (Fig. 6.4). This would result in values for T_{SOI}, T_{AVE} and T_M

with a difference of ≤ 33 K which would reflect as a substantial difference in the Arrhenius plots. These effects will be discussed in detail in the next section.

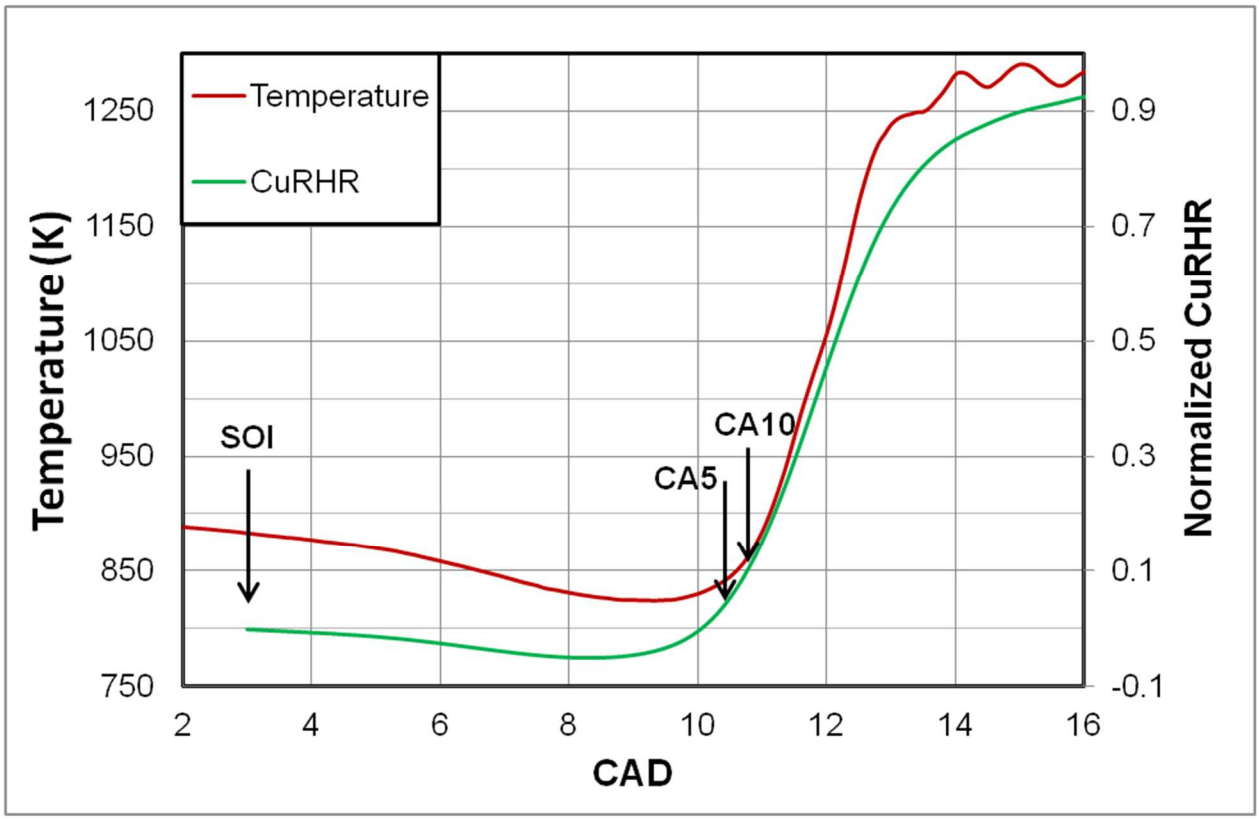

Figure 6.4: Temperature and cumulative heat release for a late injection diesel case

6.3.3.1 Effect on Global Activation Energy

These tests were also done using the same strategy of fixed SOI, swirl ratio and injection pressure with an incremental intake temperature and pressure. This data set includes five test points only, in the temperature range 70-110°C, as the combustion was unstable for temperatures lower than these. Fig 6.5 (a) and (b) shows Arrhenius plot using the definitions of ID_{CA5} and ID_{CA10} respectively. It was interesting to observe that the apparent activation energy value for these late injection test points is higher than near TDC injection cases and will be discussed in detail in the following chapter.

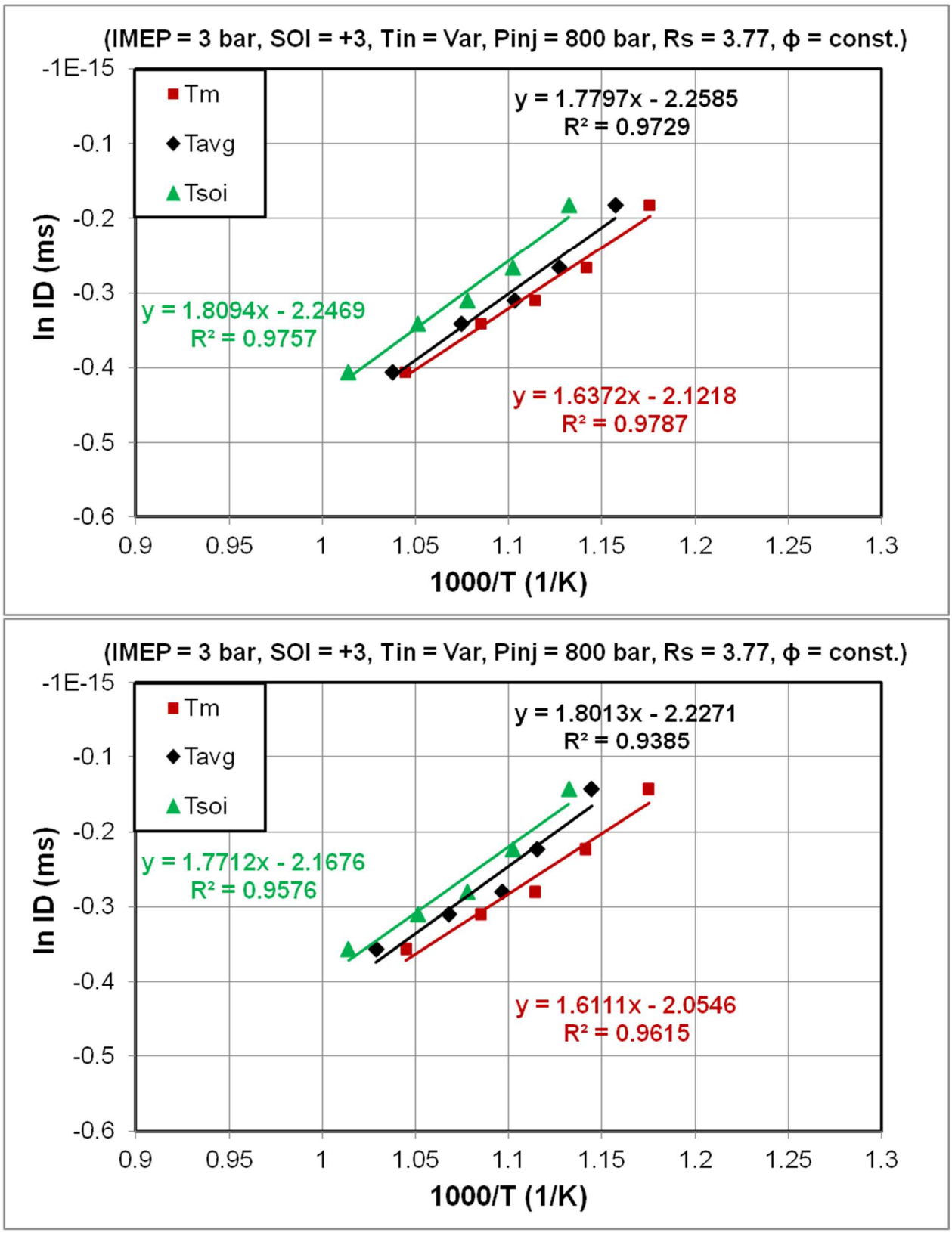

Figure 6.5: Arrhenius plots using (a-top) ID_{CA5} definition (b-lower) ID_{CA10} definition

The apparent activation energy values obtained using ID_{CA5} definition (Table 6.3) show an increased difference of 9.5 % between the highest and lowest values. The T_{AVE} values show similar closeness to T_M values, and are in between T_{SOI} and T_M, as shown in Fig. 6.5(a). Also, at higher intake temperatures the three effective temperatures are converging however the effect is less considering combustion is still taking place far from the TDC. The R^2 value, which is indicator of best fit in the data, has decreased in comparison to near TDC injection case; but the trend remains unaltered with lower value for T_{AVE} and higher for T_M method of effective temperature.

Table 6.3: Activation energy values for ULSD at SOI 3 using ID_{CA5}

Definition	E_a/R_u (K)	E_a (KJ/kg mole)	Variation (%)
T_M	1637	13610	0
T_{AVE}	1780	14799	8.73
T_{SOI}	1809	15040	9.5

Table 6.4: Activation energy values for ULSD at SOI 3 using ID_{CA10}

Definition	E_a/R_u (K)	E_a (KJ/kg mole)	Variation (%)
T_M	1611	13394	0
T_{AVE}	1801	14974	11.79
T_{SOI}	1771	14724	9.93

Similar, to ID_{CA5} the difference between highest and lowest global activation energy values has increased to 10.79 % with ID_{CA10} definition (Table 6.6), in the late

injection case. The increase in variation is larger for ID_{CA10} than it was for ID_{CA5} method. The closeness of T_{AVE} values to T_{SOI} is also evident here, shown in Fig. 6.5(b), with T_M being the lower boundary. Again the three effective temperatures do seem to be converging; however, the effect is minimized due to combustion happening far away from the TDC. Even with different ID definition the trend for R^2 remains same and T_{AVE} remains as the least fit method for determining effective temperature for ULSD.

6.4 Effective Temperature for a Low CN fuel (Sasol IPK)

6.4.1 Early Injection

Sasol IPK, a low CN fuel, shows a typical combustion behavior of long ID time and two stage combustion. Although injection takes place at same SOI (-7 CAD) in the compression stroke for this fuel, but unlike conventional diesel engine combustion the auto-ignition happens after TDC (Fig. 6.6). In this case, after injection the temperature initially keeps rising due to compression. But soon the evaporation and endothermic reactions catch up and the temperature starts falling until the exothermic reactions take over, leading to a cool flame. However, the temperature falls once more resulting in a negative temperature coefficient (NTC) regime, before finally rising to high temperature combustion. When we compare the temperatures at SOI and the SOC points, defined by CA5 and CA10, they have a big difference of 13 K and 29 K respectively. The interesting thing to note is that the temperatures at SOC point are higher compared to SOI. Despite the big difference in temperature between SOI and SOC points, the T_{SOI}, T_{AVE} and T_M values are close with a difference of ≤ 12 K. However, it would still have some effect on apparent activation energy values.

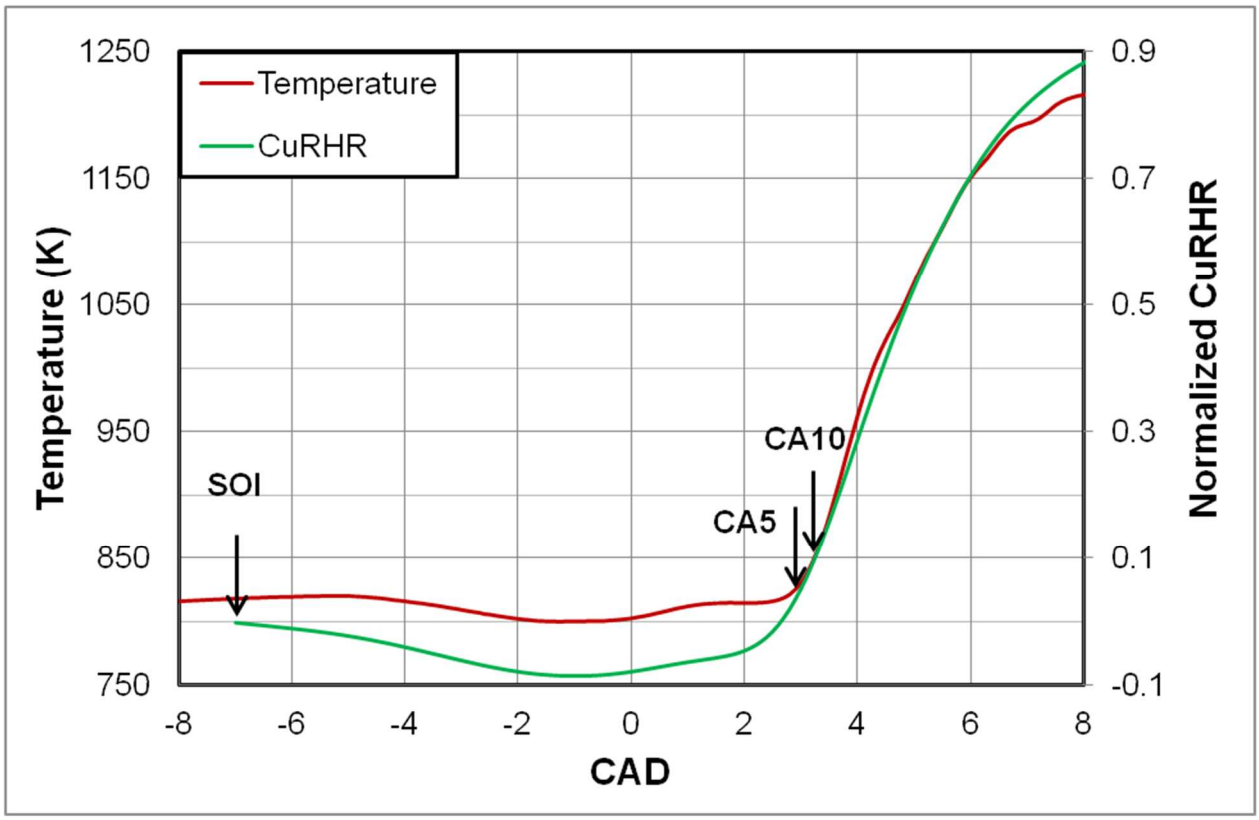

Figure 6.6: Temperature and cumulative heat release for an early injection case of Sasol IPK

6.4.1.1 Effect on Global Activation Energy

Figures 6.7 (a) and (b) shows Arrhenius plots for the same data set with the two ID definitions, ID_{CA5} and ID_{CA10} respectively. The test conditions are similar to the ones used for ULSD; however, due to the high peak pressures and pressure rise rates attained at higher intake temperatures the tests were not conducted beyond 70°C intake temperature. The tests were performed at a constant speed and a light load of 3 bar IMEP.

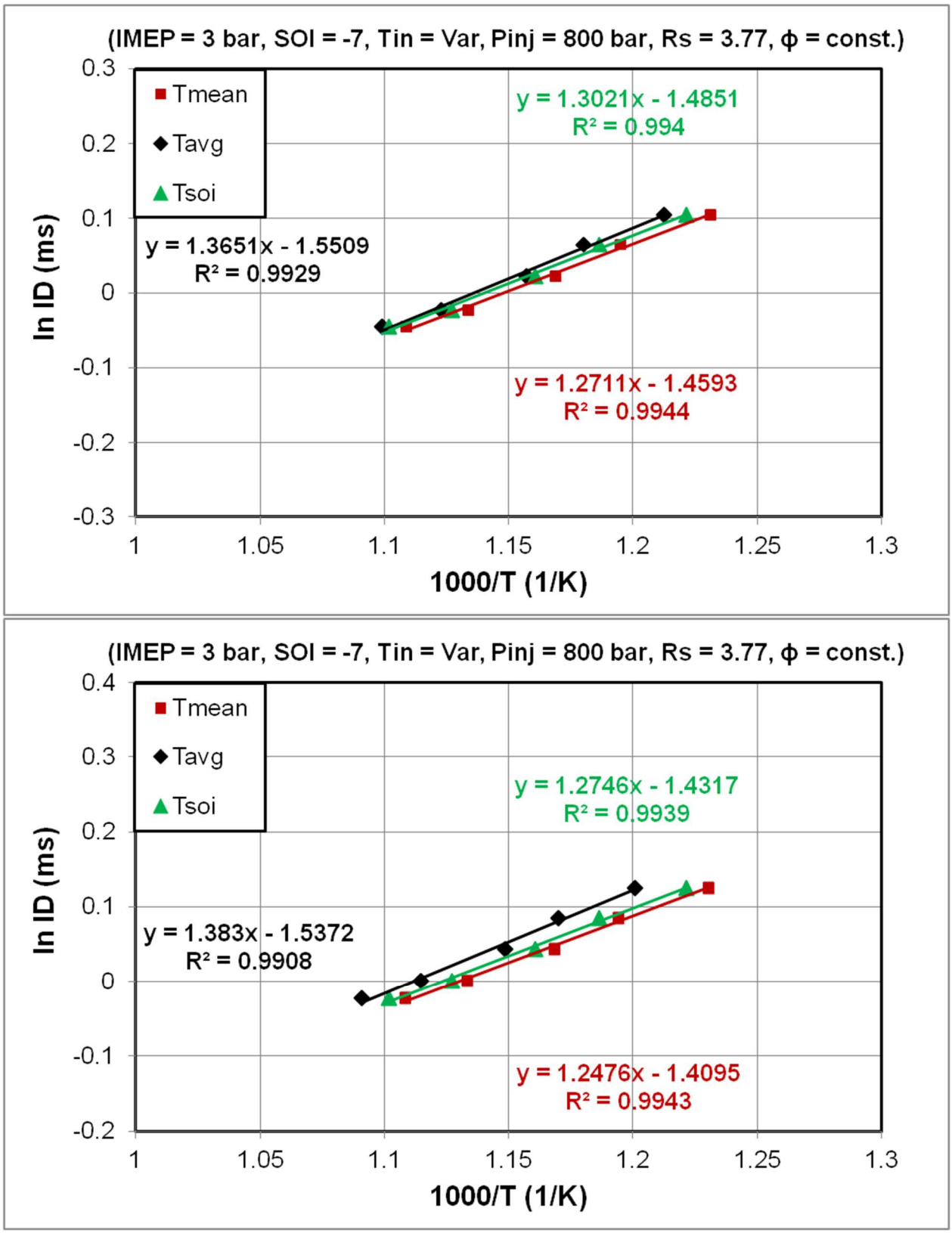

Figure 6.7: Arrhenius plots using (a-top) ID_{CA5} definition (b-lower) ID_{CA10} definition

In Fig. 6.7(a) the global activation energy values obtained using the three different temperature measurement methods are pretty close (Table 6.5) with a max variation of 7.39 % between the highest and lowest value. In this case, the temperature values obtained for T_{AVE} don't lie in between those of T_M and $T_{SOI.}$ Although T_M still remains the lower boundary, T_{AVE} is the new upper boundary. As the SOC points, CA5 and CA10, had temperatures higher than the SOI temperature T_{AVE} would be higher than T_{SOI}. Also, T_{SOI} and T_M values are almost parallel. The difference between all of them tends to be decreasing with the increase in intake temperature as before. It can be again attributed to the reduction in ID time resulting in combustion happening closer to TDC and when combustion happens near TDC the difference between T_{SOI}, T_{AVE} and T_M is less. The R^2 value is still maximum using T_M and least using T_{AVE} as effective temperature, which means T_M provides the best fit for the data points statistically.

Table 6.5: Activation energy values for Sasol IPK at SOI -7 using ID_{CA5}

Definition	E_a/R_u (K)	E_a (KJ/kg mole)	Variation (%)
T_M	1271	10567	0
T_{AVE}	1365	11349	7.39
T_{SOI}	1302	10825	2.43

In Fig. 6.7(b) the apparent activation energy values obtained are not that close with a variation of 10.81 % between the maximum and minimum value (Table 6.6), and it is also higher than observed when using ID_{CA5} definition. Even in this case T_M is the lower boundary and T_{AVE} the upper boundary, while T_{SOI} lies in between them. Although, T_{AVE} values are moving away from T_{SOI} it is in consistence with ULSD trends,

when for ID_{CA10} the T_{AVE} would move closer towards T_{SOI} i.e. shifting towards higher temperatures. The 5% more mass of fuel burnt at the location of CA10 results in higher temperature at CA10 than CA5, shifting the T_{AVE} values to the left. Nonetheless, the overall trend is they all are getting closer with further increase in intake temperature. Even in this case using T_M shows highest R^2 value and T_{AVE} the least, indicating T_{AVE} doesn't provide statistical best fit to the data.

Table 6.6: Activation energy values for Sasol IPK at SOI -7 using ID_{CA10}

Definition	E_a/R_u (K)	E_a (KJ/kg mole)	Variation (%)
T_M	1248	10376	0
T_{AVE}	1383	11498	10.81
T_{SOI}	1275	10600	2.16

6.4.2 Near TDC Injection

The lower CN for Sasol IPK results in longer ID time; as a result, the near TDC injection for Sasol IPK produces results similar to diesel late injection case. Similar to ULSD, for the low intake temperatures the engine combustion was unstable with peak combustion pressures lower than the motoring pressure. In order to fix this, the intake temperatures had to be ≥ 80°C to sustain a load of 3 bar IMEP. The mass average temperatures are already falling due to expansion, an injection event in such a situation would further add to the reduction in temperature. The exothermic reactions would arrest the fall in temperature until it leads to cool flame and NTC regime, after which once more exothermic reactions pick up to lead to combustion. In this case the temperature at SOI is 28 K higher than CA5 point and only 3 K higher than CA10 point

(Fig. 6.4). This would result in values for T_{SOI}, T_{AVE} and T_M with a difference of ≤ 33 K which would have some effect on the Arrhenius plots. These effects will be discussed in detail in the next section.

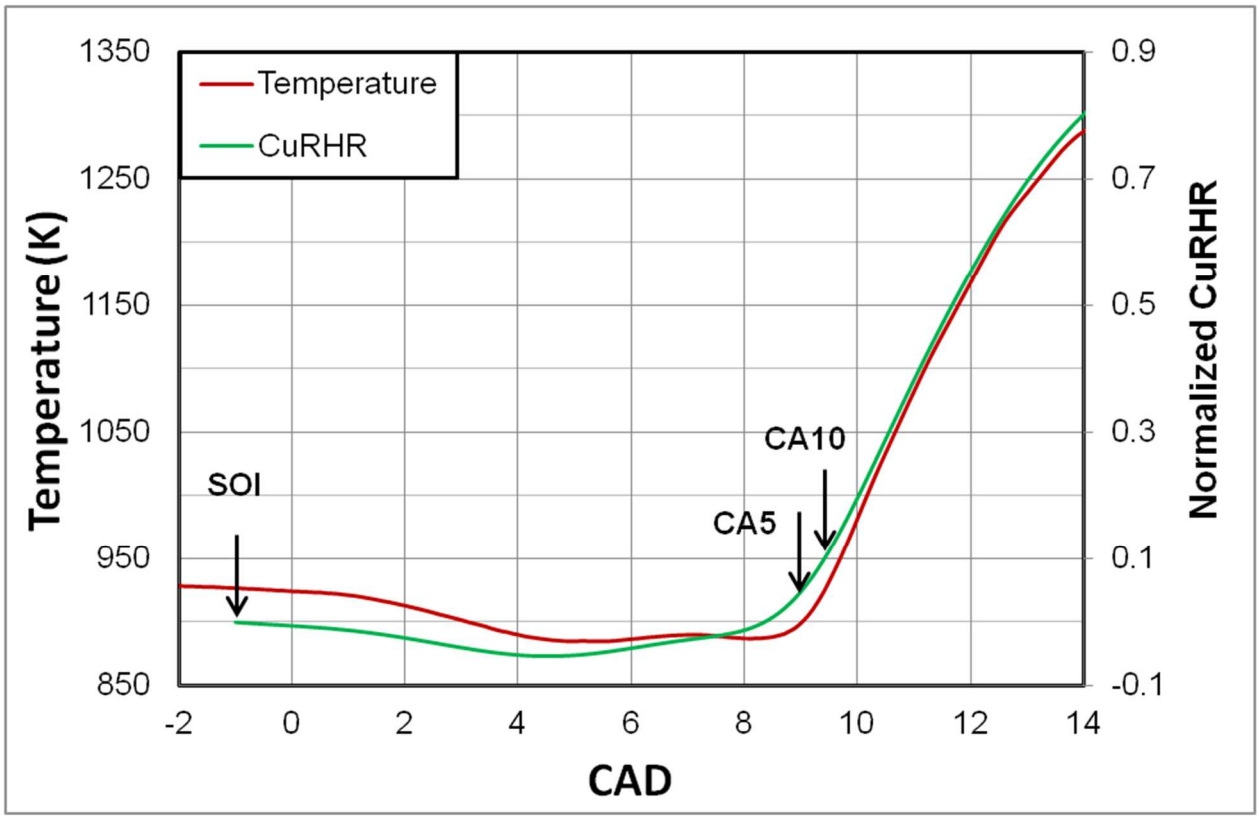

Figure 6.8: Temperature and cumulative heat release for near TDC injection case of Sasol IPK

6.4.2.1 Effect on Global Activation Energy

The test strategy remains same: fixed SOI, swirl ratio and injection pressure with an incremental intake temperature and pressure. This data set includes four test points only, in the temperature range 80-110°C, as combustion was unstable for the range 30-70°C. Fig 6.9 (a) and (b) shows Arrhenius plot using the definitions of ID_{CA5} and ID_{CA10}, respectively. Again it was observed that the apparent activation energy value for these

late injection test points is higher than near TDC injection cases, which will be discussed in detail in following chapters.

The apparent activation energy values obtained using ID_{CA5} definition (Table 6.7) show an increased difference of 8.97 % between the highest and lowest values. In this case the T_{AVE} values are neither close to T_{SOI} nor to T_M and are equidistant from both, as shown in Fig. 6.9(a). Also, at higher intake temperatures the three effective temperatures are converging however the effect is unnoticeable considering combustion is still taking place far from the TDC. The R^2 value, which is indicator of best fit in the data, has decreased in comparison to near TDC injection case; but the trend remains unaltered with lower value for T_{AVE} and higher for T_M method of effective temperature.

Table 6.7: Activation energy values for Sasol IPK at SOI -1 using ID_{CA5}

Definition	E_a/R_u (K)	E_a (KJ/kg mole)	Variation (%)
T_M	1918	15946	0
T_{AVE}	2066	17177	7.71
T_{SOI}	2090	17376	8.97

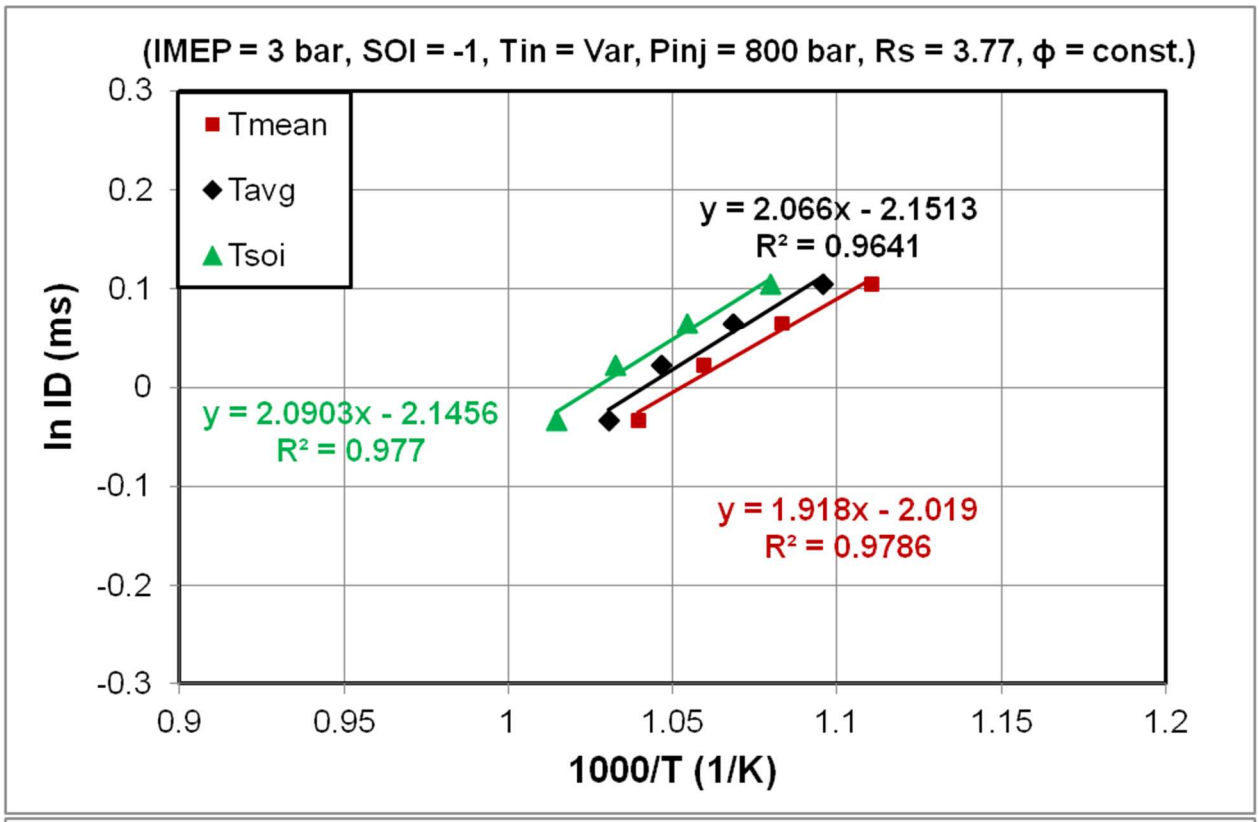

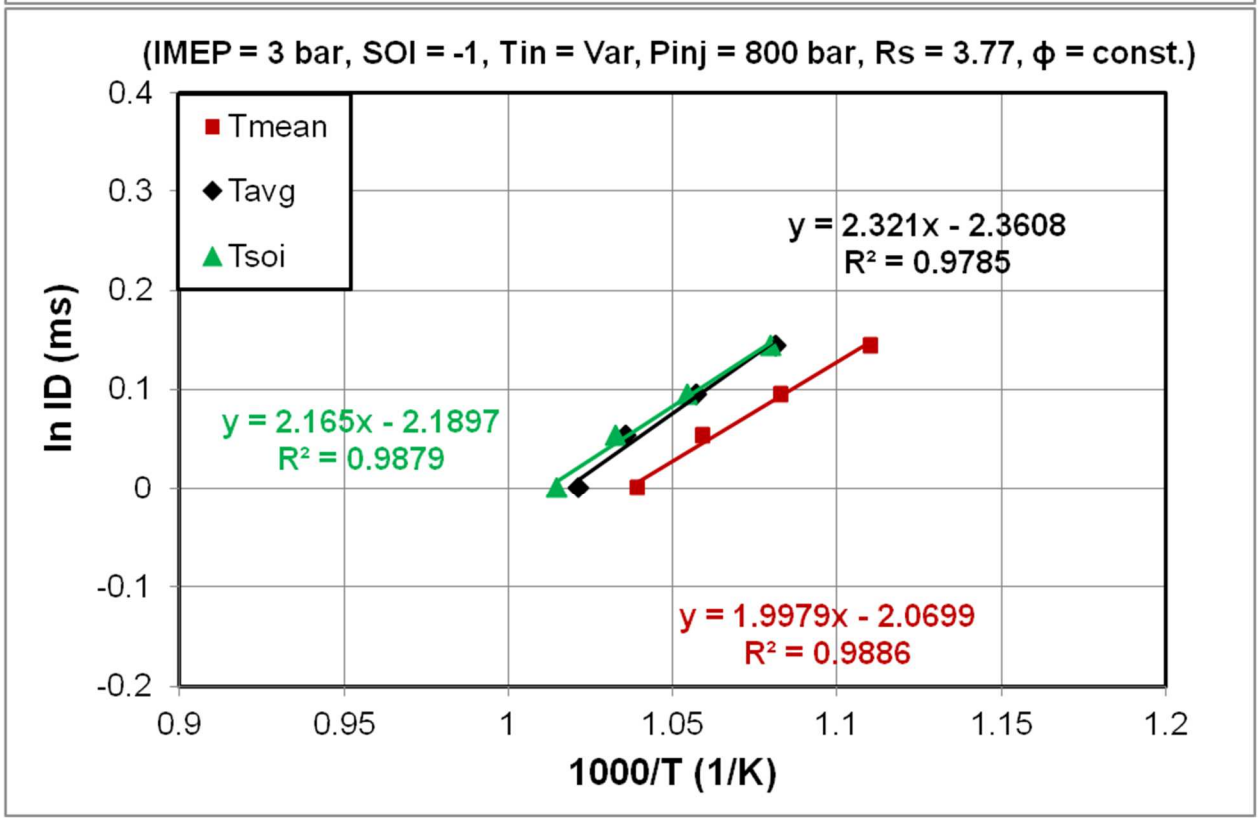

Figure 6.9: Arrhenius plots using (a-top) ID_{CA5} definition (b-lower) ID_{CA10} definition

Table 6.8: Activation energy values for Sasol IPK at SOI -1 using ID_{CA10}

Definition	E_a/R_u (K)	E_a (KJ/kg mole)	Variation (%)
T_M	1998	16611	0
T_{AVE}	2321	19297	16.17
T_{SOI}	2165	18000	8.36

Similar, to ID_{CA5} the difference between highest and lowest global activation energy values has increased to 16.17 % with ID_{CA10} definition (Table 6.8), in the late injection case. The increase in variation is larger for ID_{CA10} than it was for ID_{CA5} method. Since, T_{SOI} does not change with ID definition it is evident that T_{AVE} has shifted towards T_{SOI}, shown in Fig. 6.9(b), with T_M values still maintaining a fair distance. Again the three effective temperatures do seem to be converging; however, the effect is minimized due to combustion happening far away from the TDC. The overall trend has been that R^2 values reduce for combustion happening late in the expansion stroke, which is the case here also. Also we observe T_{AVE} remains as the least fit method for determining effective temperature for Sasol IPK as well.

6.5 Conclusions

ULSD a high CN, petroleum based fuel and Sasol IPK a low CN, coal to liquid (CTL), high volatility, jet fuel are tested in a single cylinder engine. A variable intake temperature test was conducted for the fuels at two combustion phasing: (1) near TDC and (2) late in expansion stroke. Two popular ID definitions were used in this analysis, ID_{CA5} and ID_{CA10}. The effective temperature methods discussed are T_{SOI} – temperature

at SOI, T_{AVE} – average of temperature at SOI and SOC, and T_M – integrated mean of all temperatures between SOI and SOC. The data was analyzed for apparent activation energy trends and the effective temperature during ID time.

- In conventional diesel combustion i.e. combustion phasing before TDC, there is not much difference between T_{SOI}, T_{AVE} and T_M.
- As the combustion shifts into the expansion stroke the difference between the three effective temperatures increases for both ULSD and Sasol IPK.
- The variation in apparent activation energy calculated based on different effective temperatures, for both the fuels, is less near TDC and increases as combustion goes into expansion stroke. Also, it is less while using ID_{CA5} than ID_{CA10} as ID definition.
- The T_{AVE} values are affected a lot by ID definition and shows huge shift. On the other hand, T_M values show miniscule changes with ID definition.
- T_{SOI} values don't change with ID definition, until and unless if the SOI definition is changed.
- The R^2 value, an indicator of best fit data points, is max for data sets using T_M as effective temperature and least for T_{AVE}, thus suggesting T_M is the best approach for effective temperature.

CHAPTER 7

EFFECT OF SOI AND INTAKE TEMPERATURE

7.1 Introduction

In a constant volume chamber the charge temperature can be changed only by varying the intake air temperature. On the other hand, in an engine besides the intake air temperature, piston movement can also affect the in-cylinder charge temperature. In order to study the sensitivity of ID to temperature in engines, researchers have the option either to keep the SOI constant and change the intake air temperature [91],or keep the intake temperature constant and change the fuel injection timing [8],. As a result, the mean temperature during the ignition delay period changes with variations in SOI and/or the engine intake air temperature. Therefore, a series of experiments were conducted to determine the sensitivity of activation energy to these changes. In addition, 3-D CFD simulation and 0-D simulation has also been performed to provide better understanding of the processes taking place during auto-ignition period.

7.2 Simulation Models

7.2.1 Converge 3D-CFD Simulation

CONVERGE package consisting of a 3D CFD code coupled with SAGE, a chemical kinetic solver, is used to simulate the behavior of spray injection and auto-ignition in the engine. The model parameters of fuel injection, droplet formation,

atomization, combustion model etc. are defined using the CONVERGE Studio. The mechanism used by SAGE to perform calculations is the reduced n-heptane mechanism developed by Chalmers, which consists of 42 species and 168 reactions.

Unlike other CFD software which rely on the user to create mesh or grid, CONVERGE generates a real time grid while running the CFD simulation. This innovative method recreates the mesh at each step for simulations with moving boundaries or changing embedding according to base cell sizes defined in the CONVERGE Studio. The adjustments taking place in the grid is a combination of the following grid refinement methods.

- Fixed Embedding: This feature of the code allows user to specify where and when refinement needs to be done using fixed embedding. The regions where refinement needs to be done can exist at certain specified locations in the grid, or along specified boundaries. This helps in providing special emphasis to areas which require additional resolution, such as injection event.
- Adaptive Mesh Refinement (AMR): This feature allows adjustment in the mesh size while the simulation is running to better accommodate for flow variables of interest, as specified by the user. CONVERGE has the ability to automatically modify the grid based on user choices to improve the accuracy.
- Grid Scaling: The software also gives the user flexibility to change the base grid size during simulation. This feature is helpful specially in reducing run-times of non-critical simulation by increasing the mesh size.

The base grid size for the simulation is 2 mm with further mesh refinements at critical areas using fixed embedding and AMR. For example, fixed embedding keeps the mesh size to 0.5 mm at the injector tip area; and AMR reduces the mesh size to 0.5 mm at places where reactions occur, and 1 mm at the boundary.

The software also takes into consideration droplet trajectories, break-up, collision and coalescence, evaporation, and turbulent dispersion; and wall interaction and heat transfer. The Converge code uses the following models for simulating the above droplet and spray behaviors.

1. Kelvin-Helmholtz/Rayleigh-Taylor (KH-RT) [107] breakup model to predict spray behavior. The KH model simulates the primary aerodynamic instabilities breakup and the RT model calculates the secondary breakup due to deceleration instabilities.
2. Chiang [107] model to simulate droplet evaporation.
3. No Time Counter (NTC) collision model along with the wall film [107] model are used for droplet-wall interaction, including droplets adhesion, spread, rebound, and splash.
4. O'Rourke & Amsden [107] model to simulate wall heat transfer.
5. RNG k-ε [107] model, a kind of Reynolds Averaged Navier-Storkes (RANS) model, is used for turbulence calculations.

7.2.2 DARS-Basic 0-D Simulation

In diesel engines it is difficult to separate the effects of equivalence ratio, temperature and pressure on ignition delay. A 0-D constant volume model was used to

simulate homogeneous charge conditions in order to understand the effect of temperature, pressure and equivalence ratio on ignition delay time, separately. The 0-D analysis was done with DARS-basic using the detailed PRF (Primary Reference Fuel) mechanism from Lawrence Livermore National Lab (LLNL). This mechanism consists of 545 number of species and 2635 reactions, and is based on previous mechanism developed by Curran et al [108]. This mechanism has been validated numerically and experimentally in the initial pressure range of 3 to 50 atm, the temperature range of 650 to 1200 K, and equivalence ratios from 0.3 to 1.0.

7.3 Results

The experiments were conducted on ULSD, Sasol IPK, JP-8 and a Surrogate (S2) for JP8. Surrogate S2 was developed at Center for Automotive Research at Wayne State University to emulate the physical and chemical properties of JP8 fuel [92, 109]. It consists of the following two type of molecular class components: n-alkanes (60 % dodecane) and aromatics (40% 1,2,4-trimethyl benzene). All of these fuels have different physical and chemical properties and are listed in Appendix 1.

The mean temperature during the ignition delay period changes with variations in SOI and/or the engine intake air temperature. Therefore, a series of experiments were conducted to determine the sensitivity of activation energy to these changes. In these experiments, the engine intake temperature was varied from 30˚C to 110˚C in steps of 10˚C at a given SOI, while maintaining the same charge density. This is achieved by increasing the intake air pressure at the higher intake temperatures. This whole process

is then repeated at different SOI timings. It should be noted that air density, pressure and temperature are different at different injection timings (Fig. 7.1). The change in density due to piston movement is symmetrical around the TDC; however, pressure and temperature reach their maximum a few degrees before the TDC.

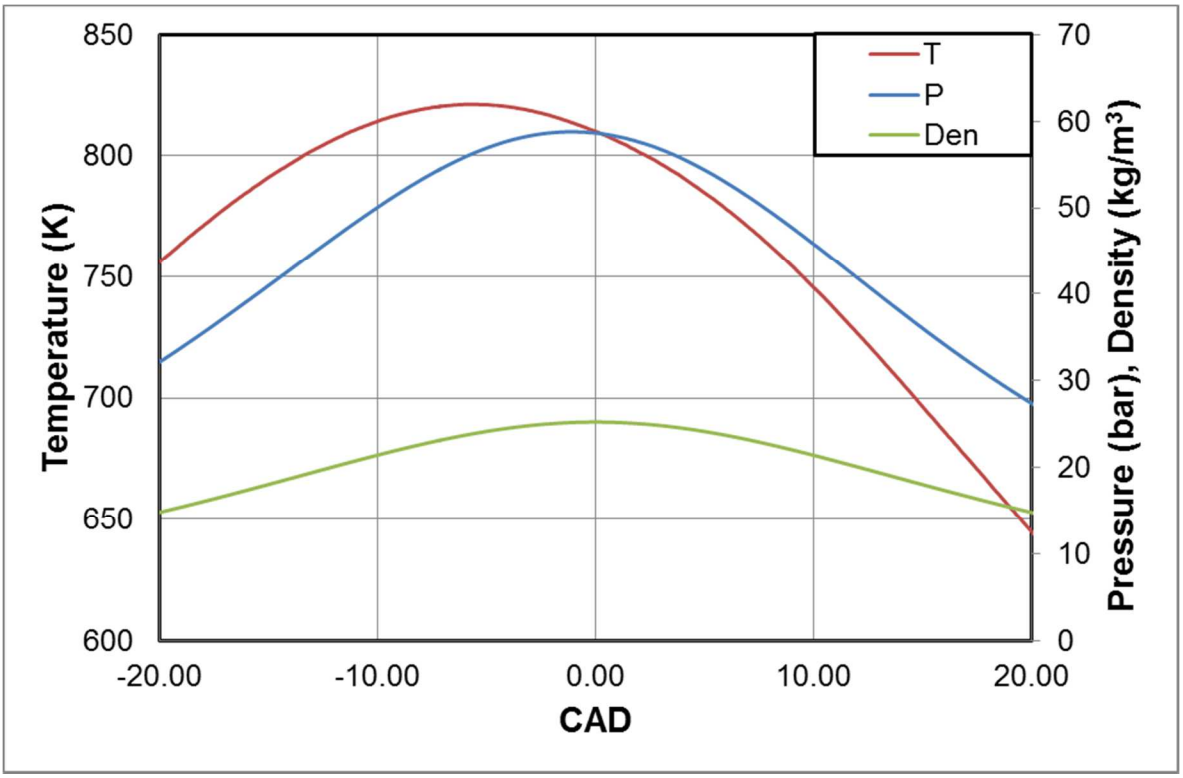

Figure 7.1: Temperature, pressure and density changes in an engine during motoring

Figure 7.2 and 7.3 shows the Arrhenius plots for all the tested fuels in such a way that each color represents a fixed SOI case. At each SOI the intake temperature was increased from 30˚C to 110˚C in steps of 10˚C keeping constant density. For Sasol IPK at SOI -1 CAD and ULSD at SOI 3 CAD the intake temperature range was from 80˚C to 110˚C and 70˚C to 110˚C respectively, as the engine misfired at the lower intake temperatures. It can be observed for all fuels the data points lie in the same temperature range of 750-1000 K. Also, as the SOI retards and combustion shifts more

into the expansion stroke the slopes of the Arrhenius plots are increasing. The global activation energy values derived in Fig. 7.2 show very small change at SOI's before the TDC, especially before -1 CAD. During the testing for JP8 and Surrogate S2 due to an error in the needle lift sensor the SOI was retarded by 0.7 CAD. As a result, the real SOI during testing were -2.3, -0.3 and 1.7 instead of the target -3, -1 and 1 respectively. This small shift however resulted in a large change in the apparent activation energy for JP8 and Surrogate S2 in comparison to the values obtained for ULSD. For ULSD, the global activation energy values obtained at SOI -3 and -1 are very close. However, for JP8 and Surrogate S2 the global activation values at SOI -2.3 and -0.3 have large gap (Fig. 7.3). The activation energy increased more by changing SOI from -2.3 to -0.3 CAD in comparison to changing SOI from -3 to -1 CAD. So, a small shift in SOI from -1 to -0.3 CAD resulted in a huge change in apparent activation energy value.

It can be noted from Fig. 7.1 that the in-cylinder charge temperature peaks at around -5.7 CAD and starts dropping as the piston approaches TDC. As activation energy is sensitive to changes in temperature, it will fluctuate more with changes in temperature. When the temperature starts dropping in an engine the global activation energy value starts increasing and this effect might become more substantial after -1 CAD. It is not possible to eliminate the temperature variations in an engine, but if they can be limited to minimum it will be beneficial for global activation energy calculation in engines. For activation energy calculations we can therefore set -1 CAD as the limit to which SOI can be retarded before drastically affecting global activation energy calculations.

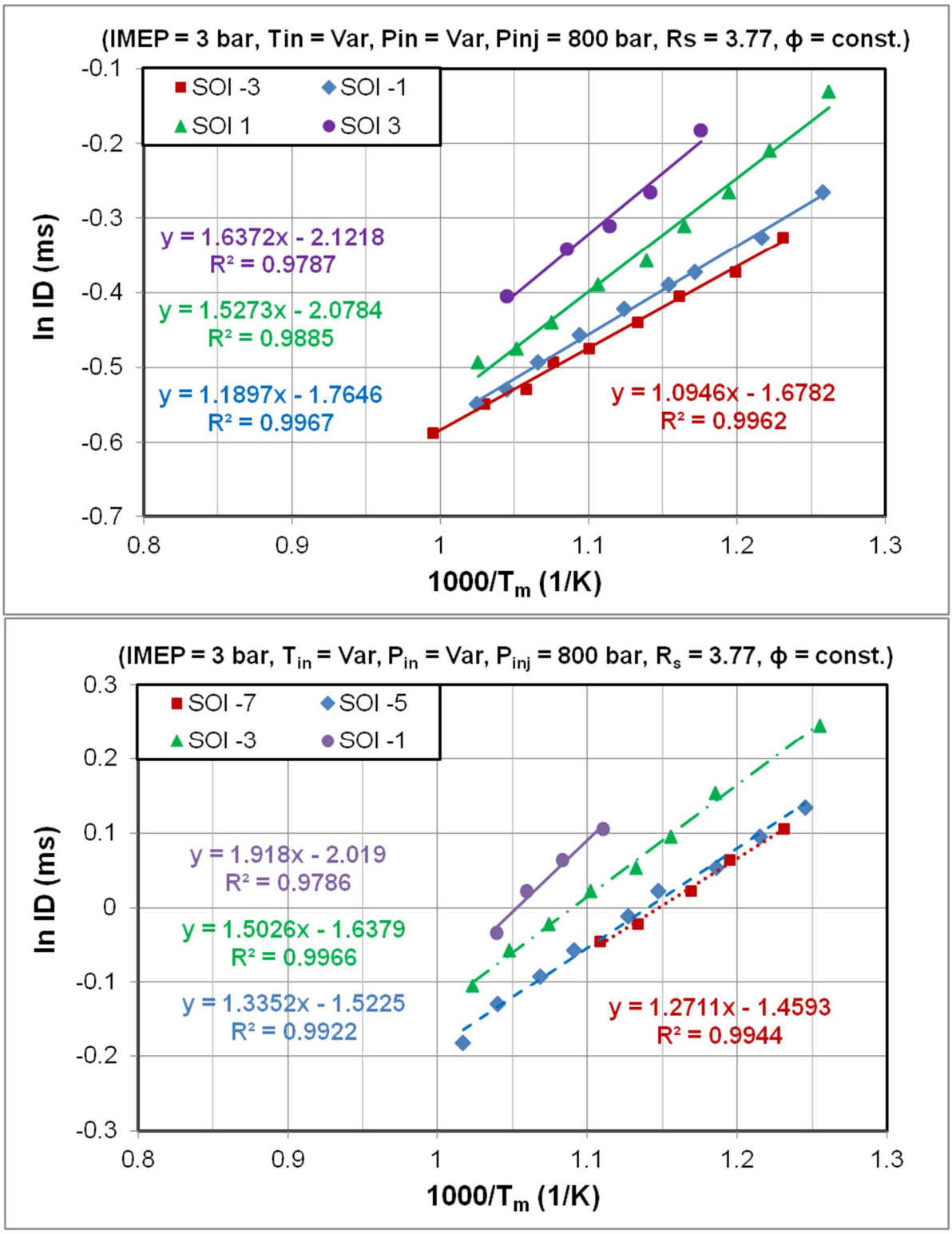

Figure 7.2: Arrhenius plot at fixed SOI using ID_{CA5} for a) ULSD b) Sasol IPK

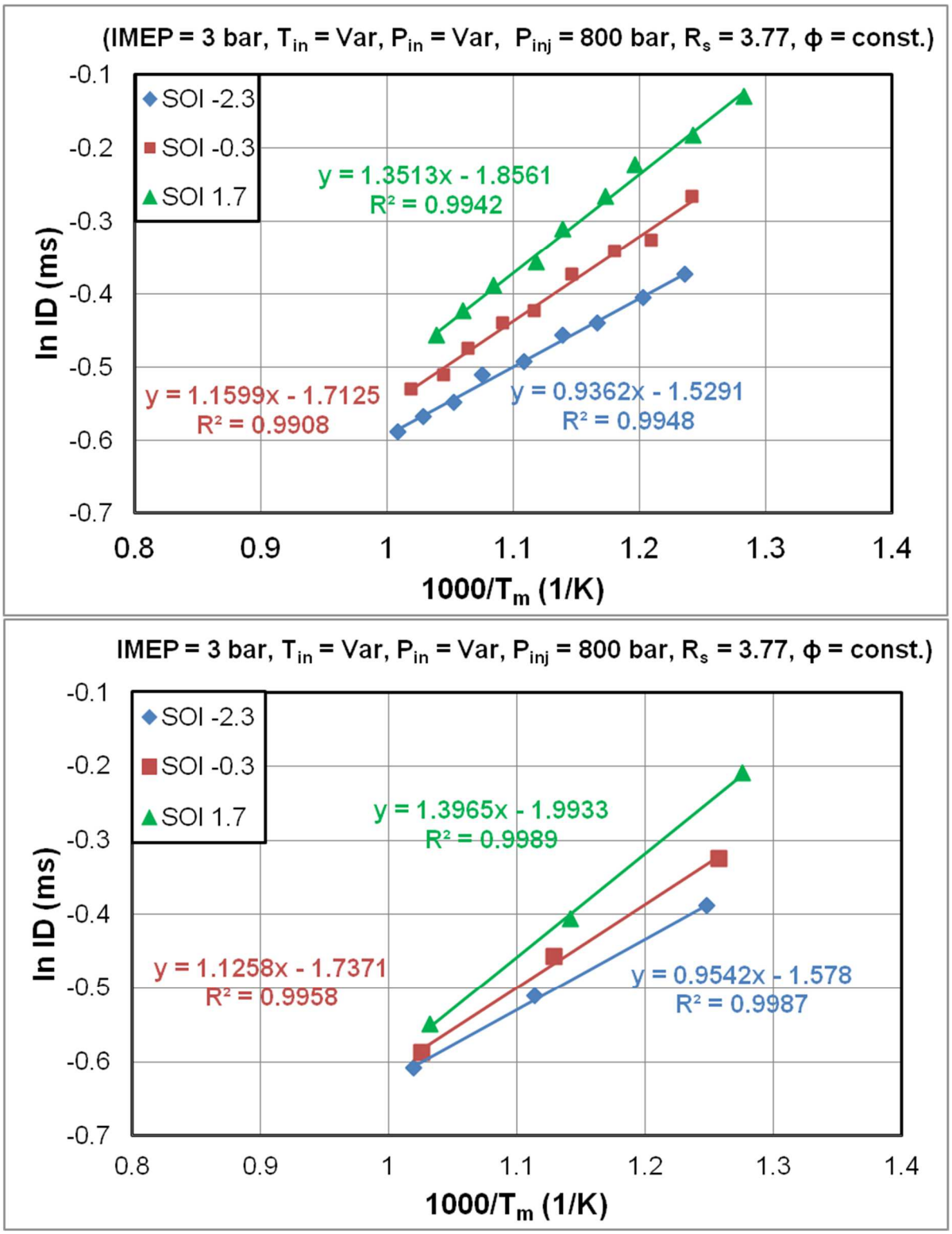

Figure 7.3: Arrhenius plot at fixed SOI using ID_{CA5} for a) JP8 b) Surrogate S2

In Fig. 7.4 and 7.5 each color represents a fixed intake temperature and pressure condition at different SOIs. Therefore, we will see the effect of SOI on global activation at fixed intake conditions. In these graphs (Fig. 7.4 and 7.5) the slopes are higher than those in Fig. 7.2 and 7.3, signifying a small change in temperature resulting in a large change in ignition delay. In fact the slopes are higher compared to variable intake temperature case at all intake conditions and for all fuels. The values obtained are almost three times higher than the ones obtained in the previous method. Thus it can be said that the global activation energy is more sensitive to the change in SOI.

This huge disparity in the two methods used to quantify the auto-ignition behavior of fuels in engine can be explained by studying the effect of parameters like equivalence ratio, pressure and density on auto-ignition, especially in the intermediate temperature regime (850-1000 K). The following section will give a detailed explanation of these behaviors.

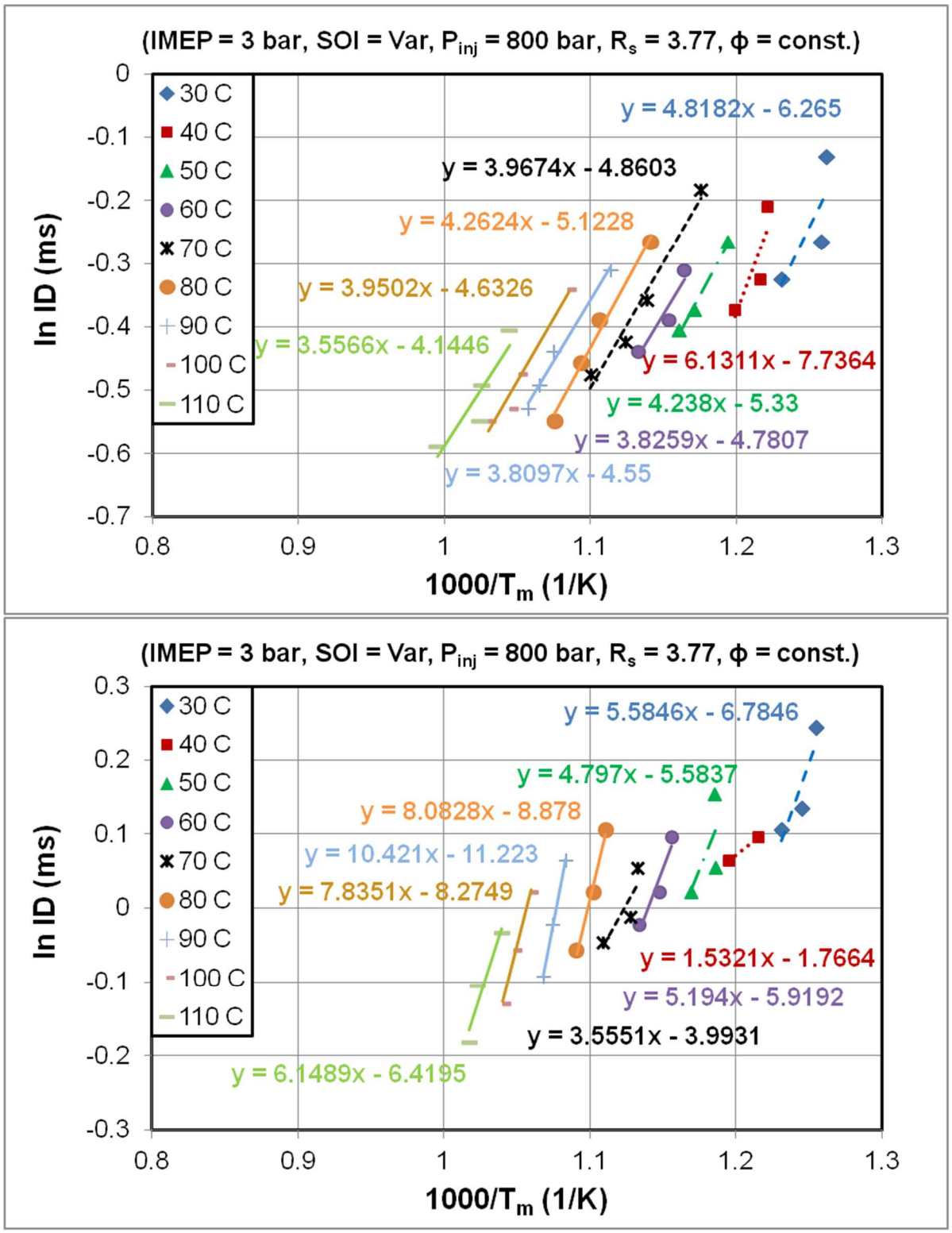

Figure 7.4: Arrhenius plot at fixed intake conditions using ID_{CA5} for a) ULSD b) Sasol IPK

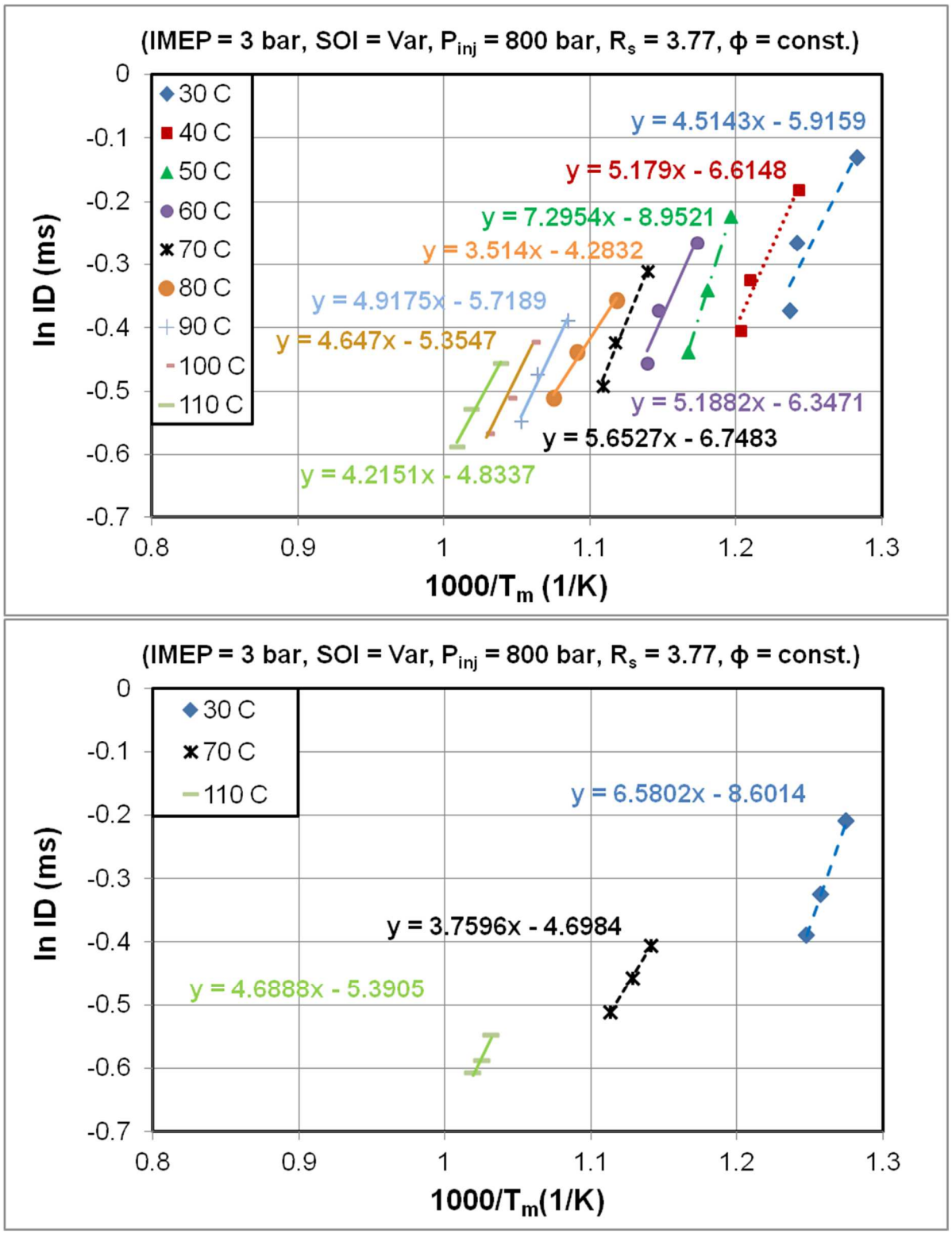

Figure 7.5: Arrhenius plot at fixed intake conditions using ID_{CA5} for a) JP8 b) Surrogate S2

7.4 Discussions

In an internal combustion engine due to the piston movement the volume of the chamber is always changing. As a result the charge temperature and pressure, effectively the charge density, can continuously vary during the ignition delay period. Such changes become more severe if auto-ignition occurs far from TDC where the auto-ignition process is affected by the change in density, in addition to the change in temperature. This is the reason behind the higher slopes obtained in Fig. 7.4 and 7.5, where changes in SOI caused changes in temperature and density.

The mean pressure (P_{mean}) and the mean temperature (T_{mean}) during the ID period for ULSD, are shown in Fig. 7.6. Both variable intake temperature and variable SOI data was used in these plots. Figure 7.6a indicates that as combustion shifts into the expansion stroke the P_{mean} increases faster with increasing T_{mean} compared to early SOI timings. The slopes of these lines would represent changes in the mean density of the charge in the combustion chamber during the ID period. So it would indicate the change in mean charge density is higher in the expansion stroke.

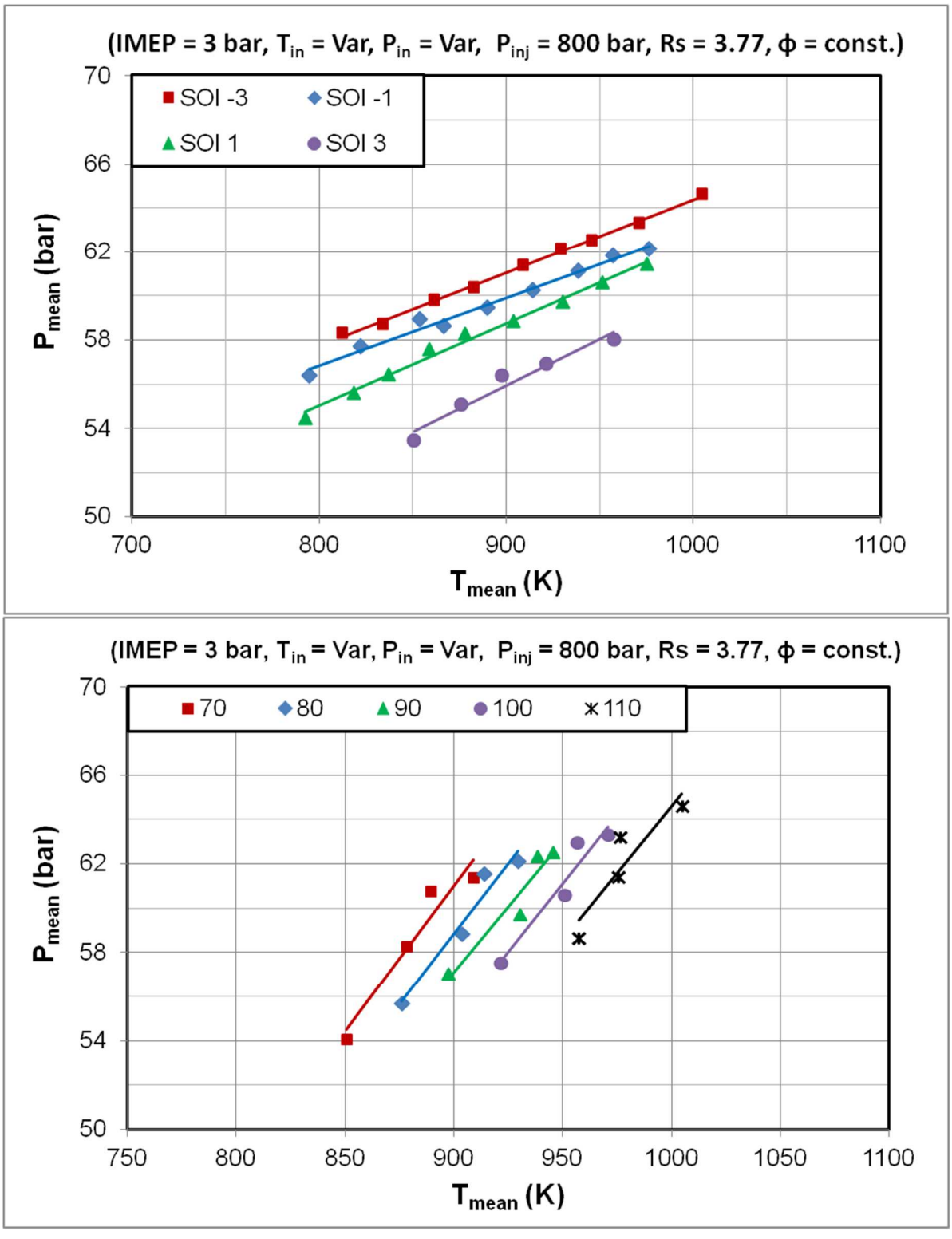

Figure 7.6: P_{mean} vs T_{mean} during ID period a) variable intake temperature test b) variable SOI test

Variable intake temperature as a control parameter compared to variable SOI has smaller changes in P_{mean} with respect to T_{mean} (Fig 7.6b). Therefore, the variable intake temperature test results in smaller changes in the mean charge density during ID period compared to the variable SOI test. Based on these comparisons the mean charge density will have a higher impact on the slopes of the Arrhenius plots in the expansion stroke and variable SOI tests. Therefore we recommend the variable intake temperature test instead of the variable SOI test. Also, it would be beneficial to obtain ID values near TDC where the variation in temperature and density is minimum.

In order to further understand the combustion behavior of fuels in the engine, the effect of various combustion parameters on ignition delay of a homogenous mixture needs to be understood. Minagawa et al [110] suggested that the ID of fuels in the NTC regime i.e. 850-1000 K is greatly affected by equivalence ratio and pressure. In this range any increase in temperature would result in an increase in ID, unlike the trends in the low and high temperature regimes. However, an increase in equivalence ratio can negate this effect of temperature and result in reduction of ID. Thus equivalence ratio becomes the dominant factor for ignition in the intermediate temperature range.

Results for 0-D simulation for n-heptane using DARS-basic are shown in Fig. 7.7 to elaborate the above point. In the temperature range 850-1000 K (1-1.2 on the x-axis) the ID value increase with increase in temperature, thus showing a NTC behavior. In Fig. 7.7a the charge pressure is kept constant at 50 bar and the equivalence ratio is varied. With increase in equivalence ratio the ID value decreases even in the NTC regime. In addition, further reduction in ID is possible by increasing the pressure at a given equivalence ratio, as shown in Fig. 7.7b. In heterogeneous combustion

environments there are zones of different equivalence ratio, and in the intermediate temperature (850-1000 K) range each zone will have an effect on auto-ignition. In addition, in engines due to the motion of the piston there are changes in the cylinder pressure resulting in changes in density, which can again have significant effect on ignition delay in the intermediate temperature range. Therefore, in this temperature range the global activation energy in engines will be sensitive to combined changes in equivalence ratio and density.

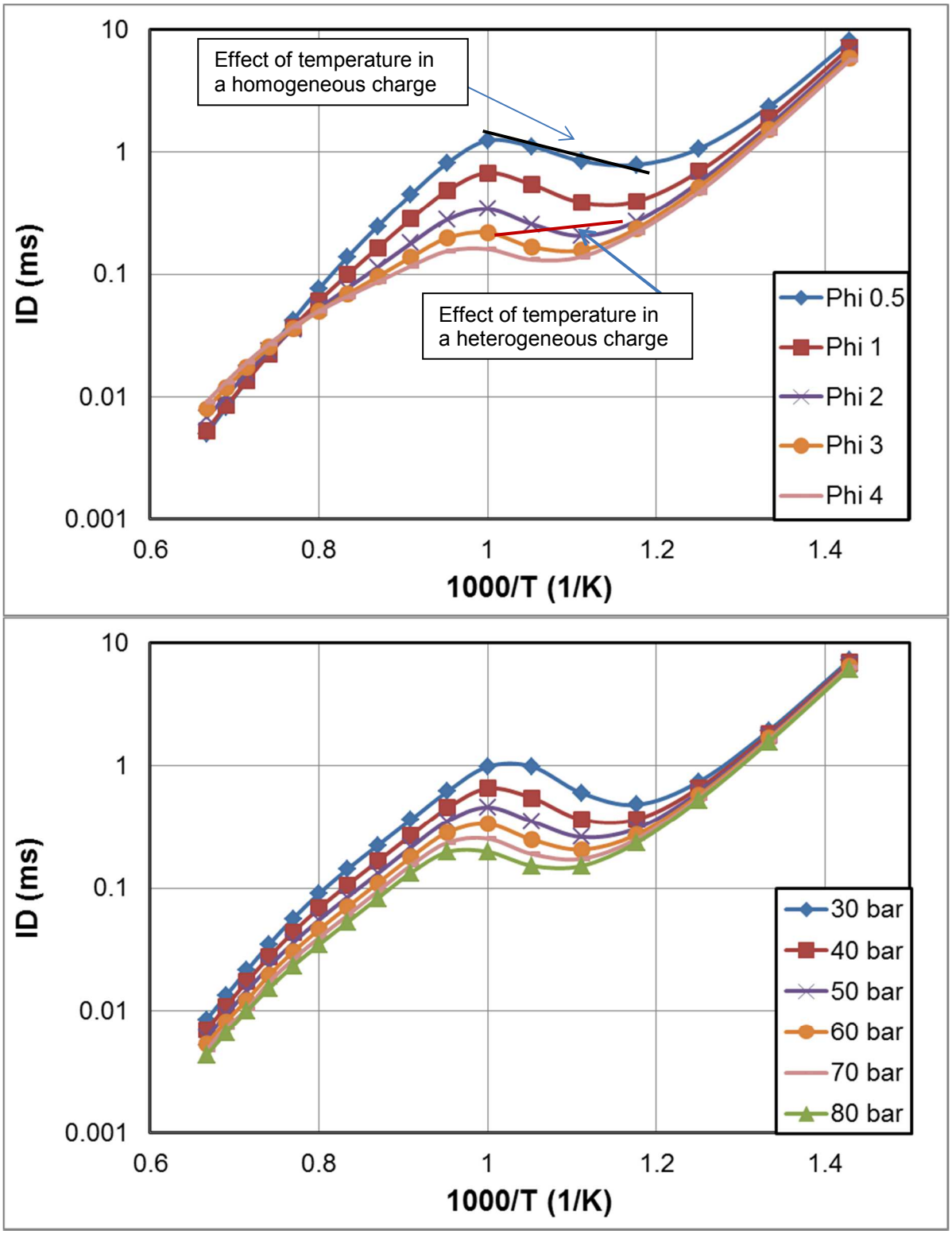

Figure 7.7: Arrhenius plots for n-heptane for a homogeneous constant volume chamber at a) fixed pressure of 50 bar b) fixed equivalence ratio of 1.5

In heterogeneous flames, in order to compensate for the lower sensitivity of ignition to temperature in NTC regime, ignition shifts towards zones of higher equivalence ratio [110]. The findings from this study are based on simulation of transient free fuel sprays. It needs to be confirmed whether the combustion behavior of fuel jets in an engine follows a similar trend or not. CFD simulation of the spray behavior inside the PNGV engine was used to corroborate this finding at two injection pressures of 800 bar and 400 bar, and is discussed in the next sections.

7.4.1 CFD Simulation for 800 bar injection pressure

In CFD simulation instead of simulating the entire combustion bowl, it is divided into equal sectors based on the number of nozzle holes (in this case 6) to reduce simulation time. There was an anti-clockwise swirl motion in the combustion chamber when observed from the top view. The simulation was done using n-heptane fuel and was based on intake parameters from the experimental data set for ULSD. The test points under consideration are at intake temperatures of 30 °C, 70 °C and 110 °C. An additional data point was added by extrapolation at an intake temperature of 10 °C to widen the temperature range. The results are shown in Fig. 7.8 - Fig. 7.13.

Figure 7.8 - 7.9 shows the isometric view of a sector of the combustion bowl with two planes passing through the first site of auto-ignition. One plane is vertical and is parallel to the z-axis and the other plane is an arbitrary plane chosen to cut through the spray (not shown in the diagram) axis along with the first site of auto-ignition. It is to be noted that the vertical plane does not pass through the center of the spray axis and is located to the left or right of it depending on where the first site of auto-ignition is located. Also the temperature distribution on the two planes is similar, but due to a

difference in the viewing angle they have different shades of the same color. The white dot represents the first site of auto-ignition through which the two planes pass. The temperature and equivalence ratio at this location at both SOI and SOC are also given. The temperature at SOI is indicative of the entire combustion bowl chamber temperature, with a ±20 K variation in the extremities. With the increase in intake temperature, the temperature of the first site of combustion increases, but the equivalence ratio remains zero as the fuel spray hasn't arrived at this location yet. As the spray progresses downstream of the nozzle, chemical reactions start raising its temperature; and by the time the fuel spray arrives at this location the temperatures are high enough to start combustion.

The SOC location also coincides with the sudden rise in pressure in the combustion chamber. A temperature of 1500 K was chosen as an indicator of start of auto-ignition. However, at SOC the rate of change of temperature was so high that sometimes with a small change in time step the temperature would increase by 400-600 K, especially at higher intake temperatures. As a result a temperature window of ±200 K around 1500 K was used as an indicator of SOC.

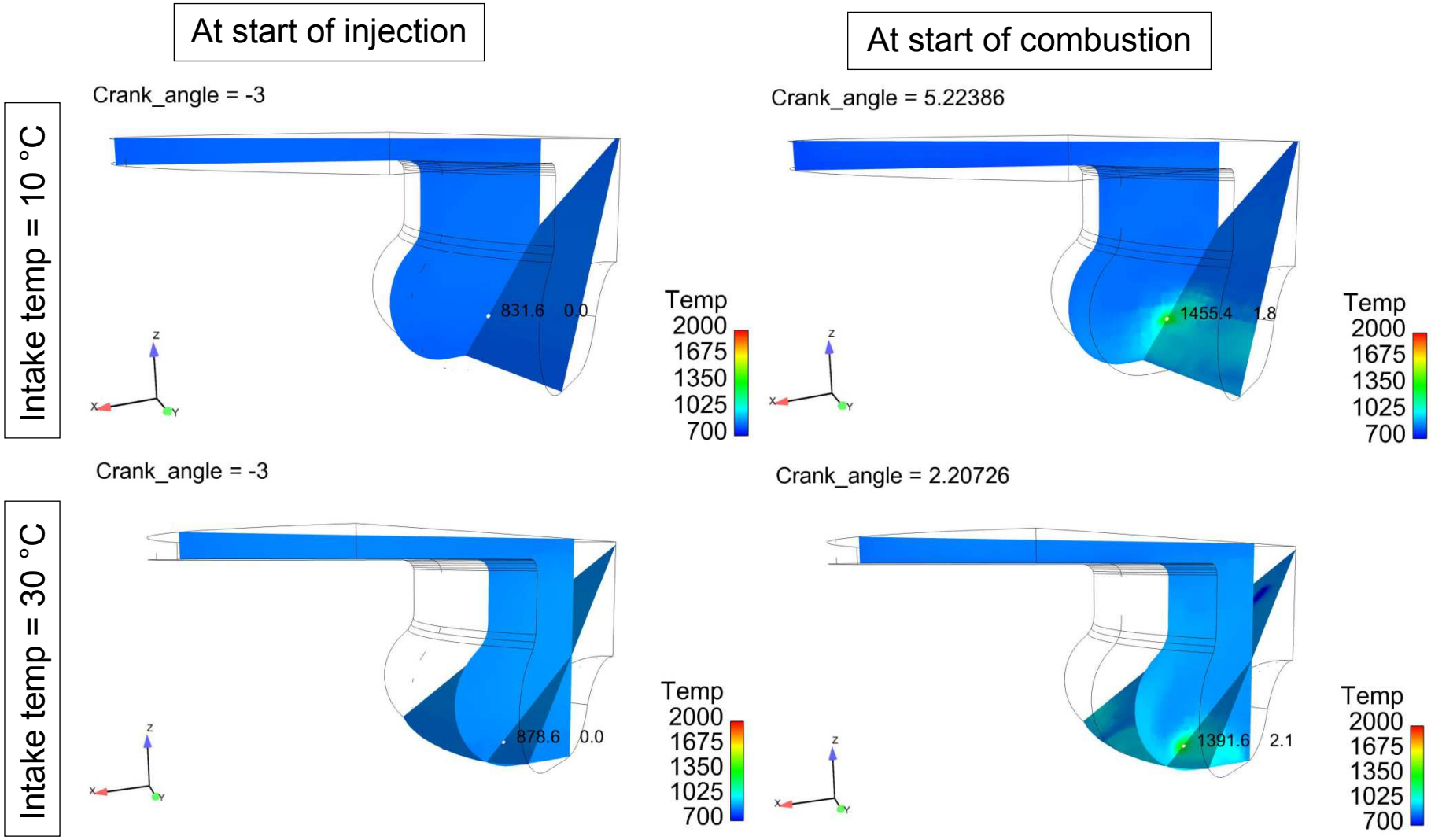

Figure 7.9: Temperature distribution in the combustion chamber at two different inlet air temperatures and at two planes : top row for 10 °C and bottom row for 30 °C. The left column is at SOI and right column at SOC.

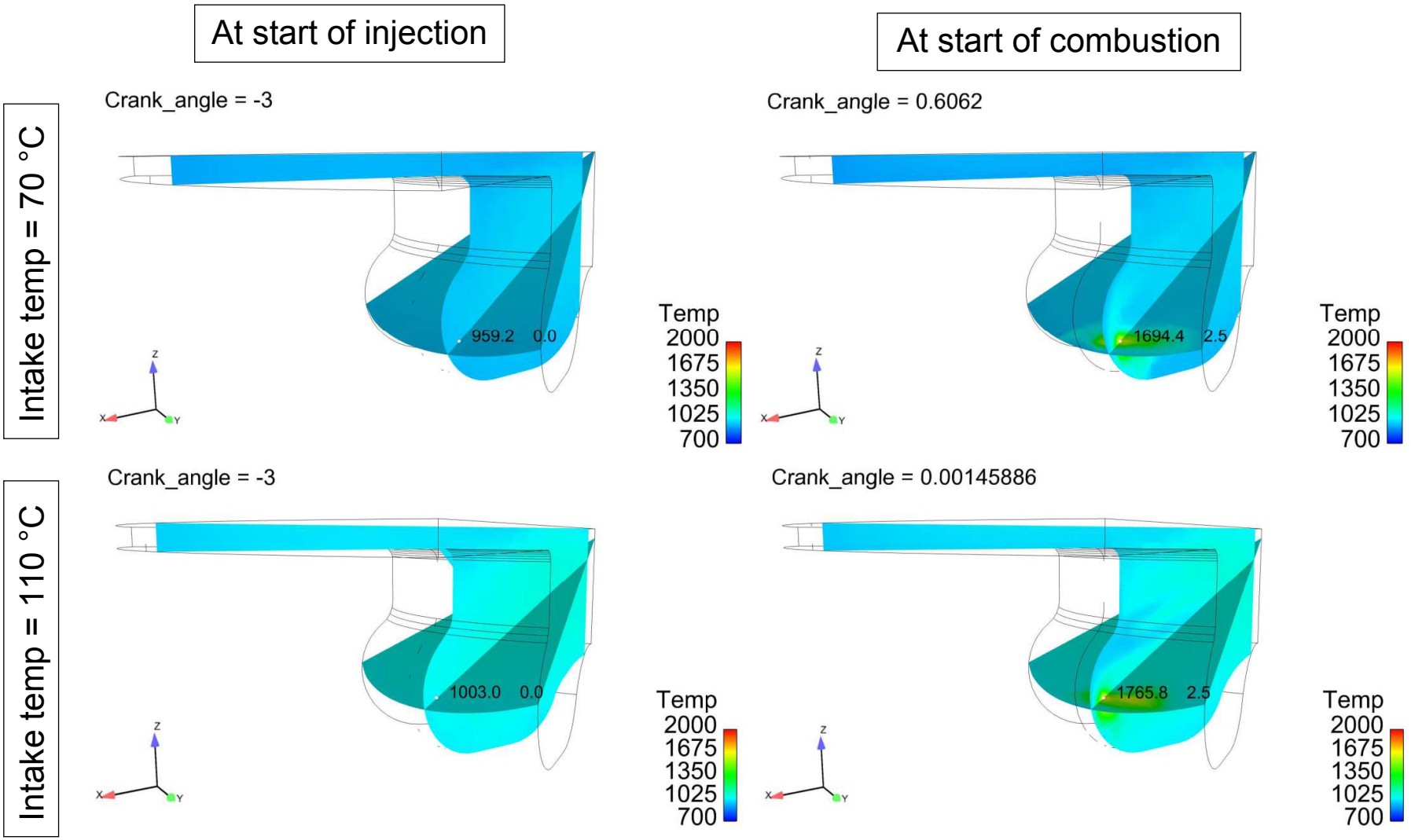

Figure 7.10: Temperature distribution in the combustion chamber at two different inlet air temperatures and at two planes: top row for 70 °C and bottom row for 110 °C. The left column is at SOI and right column at SOC.

Figures 7.10 - 7.11 shows the detailed temperature distribution at SOC in the two planes discussed above. For 10 °C intake temperature it can be observed that the auto-ignition site is at the bottom of the combustion bowl, and from the top view it is evident it is located towards the left of center. The swirl motion is in the anti-clockwise direction, and therefore the fuel spray would move towards the right side. The location of the auto-ignition site at the left of center would mean that combustion is happening in the fuel spray coming from the adjacent sector in left. In other words, the spray from this sector would ignite in the adjacent sector towards right. The low intake temperature results in a longer ignition delay time and hence by the time auto-ignition starts the spray has moved to the bottom of the combustion bowl in the next sector. As a result we see the first site of auto-ignition at the bottom of the combustion bowl.

With the increase in intake temperatures to 30 °C, 70 °C and 110 °C the ignition delay decreases progressively. As a result at SOC, due to the shorter time available the fuel spray advancement in the combustion chamber reduces. This can be confirmed by comparing the top and side views of the combustion chamber temperature and equivalence ratio distributions (Fig. 7.10 - 7.13). There is a visible clockwise shift in combustion sites in the top view with the increase in intake temperatures. Also the side view shows the upward movement of the combustion sites as well. This shift is more prominent at the lower intake temperatures compared to higher intake temperatures.

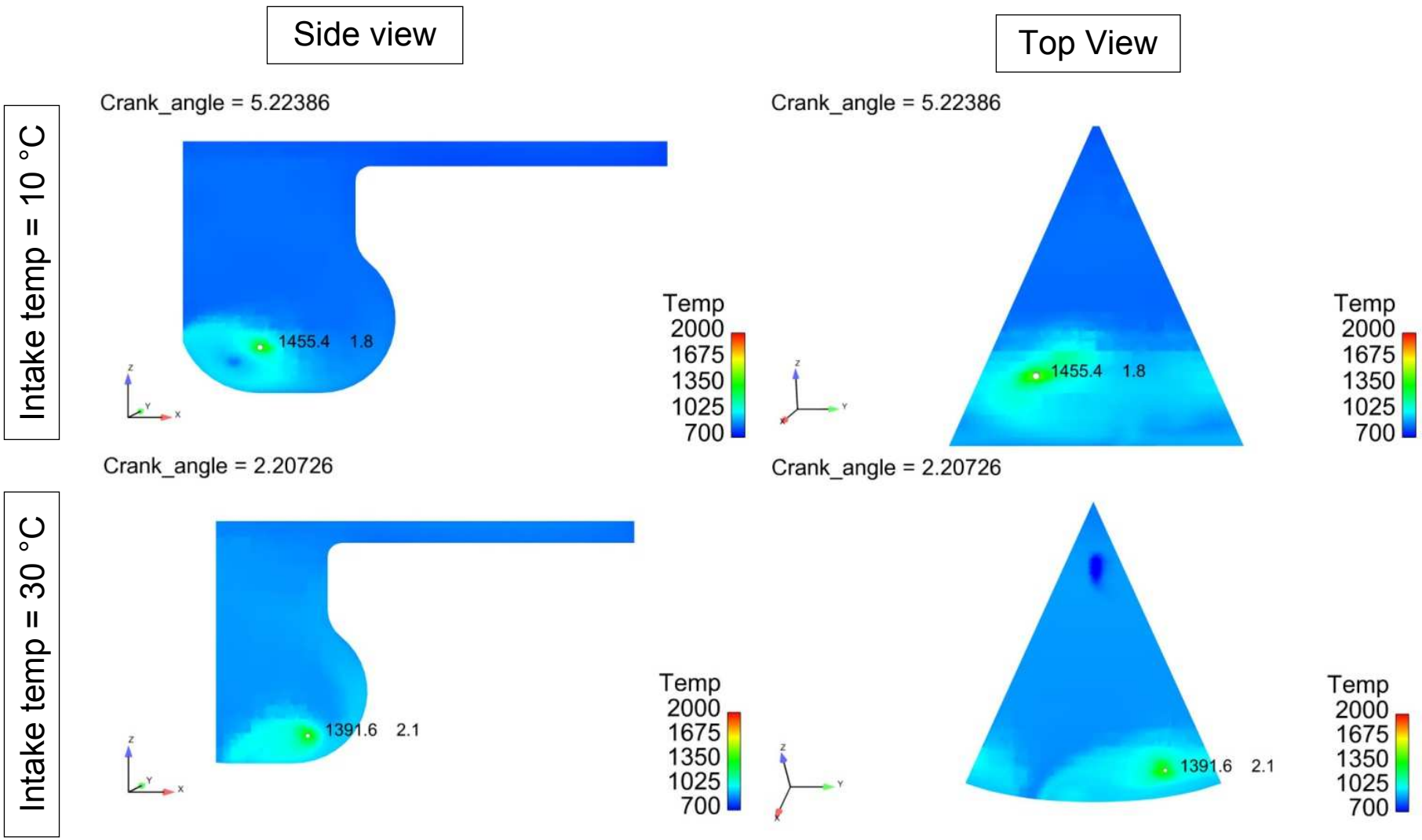

Figure 7.10: Temperature distribution in the combustion chamber at two different inlet air temperatures: top row for 10 °C and bottom row for 30 °C. The left column shows the side view and right column shows the top view.

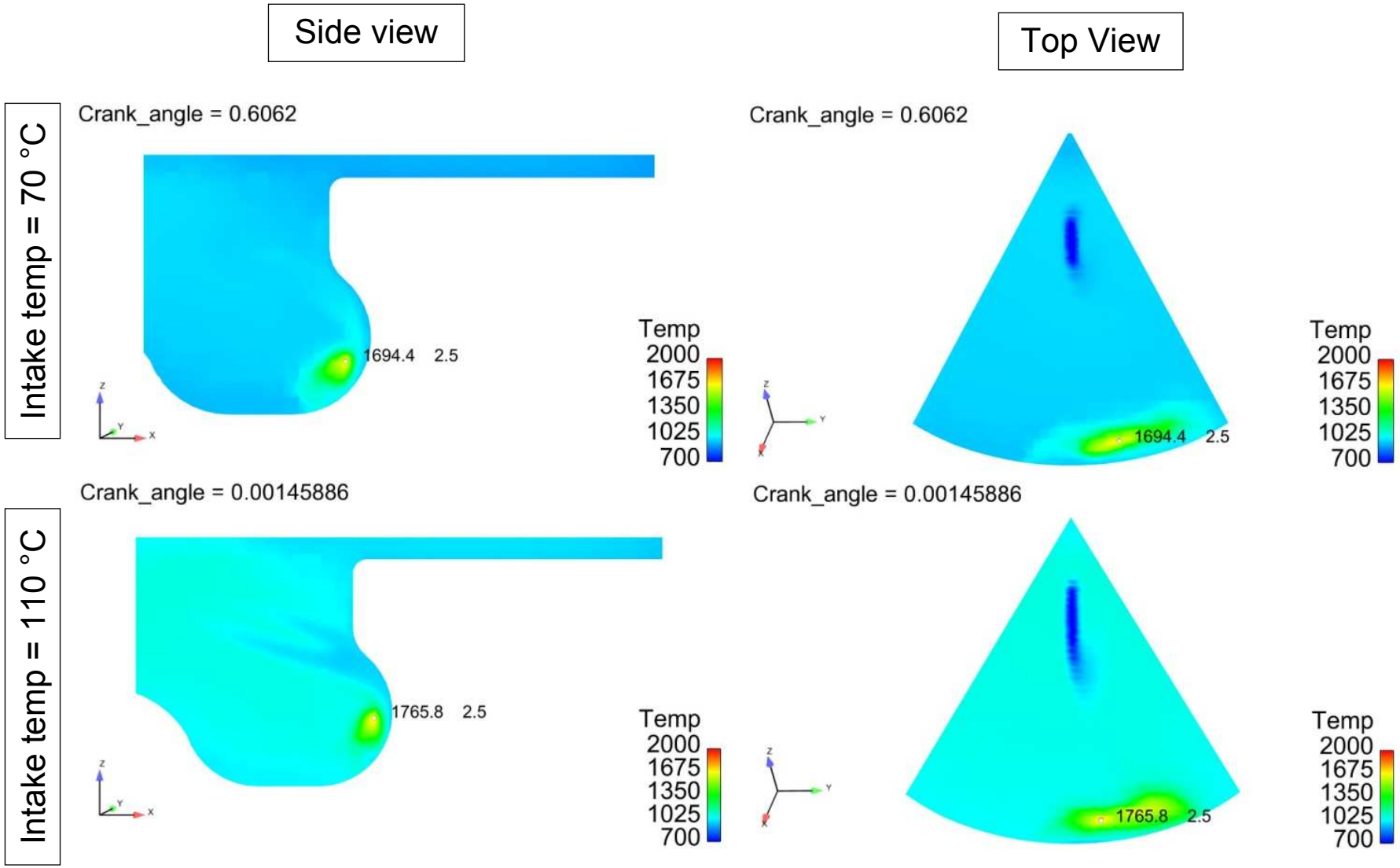

Figure 7.11: Temperature distribution in the combustion chamber at two different inlet air temperatures: top row for 70 °C and bottom row for 110 °C. The left column shows the side view and right column shows the top view.

Figure 7.12 - 7.13 shows the side and top view of the equivalence ratio distribution in the combustion bowl chamber at SOC. As the intake temperature increases and the ID decreases, combustion shifts to zones of higher equivalence ratio. As shown in increase from 1.8 at 10 °*C* to 2.5 at 70 °C (Fig. 7.12 - 7.13). This results in the first site of auto-ignition site moving closer to the inner core of the spray where the high equivalence ratio zones exist. However, there is not much change in equivalence ratio between 70 °C and 110 °C intake temperature. It is to be noted that the temperature at SOI for 70 °C intake air is 959 K and for 110 °C intake air is 1003 K, which is at the upper boundary of the intermediate temperature range (850-1000 K). Looks like as the temperatures approaches the upper boundary of the intermediate temperature range the equivalence ratio at the first site of auto-ignition attains its maximum value and remains constant. The increase in equivalence ratio leads to smaller ID period in the intermediate temperature range; as a result, the NTC behavior observed in homogeneous mixtures is not seen. Around 1000 K an increase in gas temperature results in a decrease in ID value; therefore, temperature becomes the dominant parameter which affects auto-ignition and as a result no further change in equivalence ratio is observed.

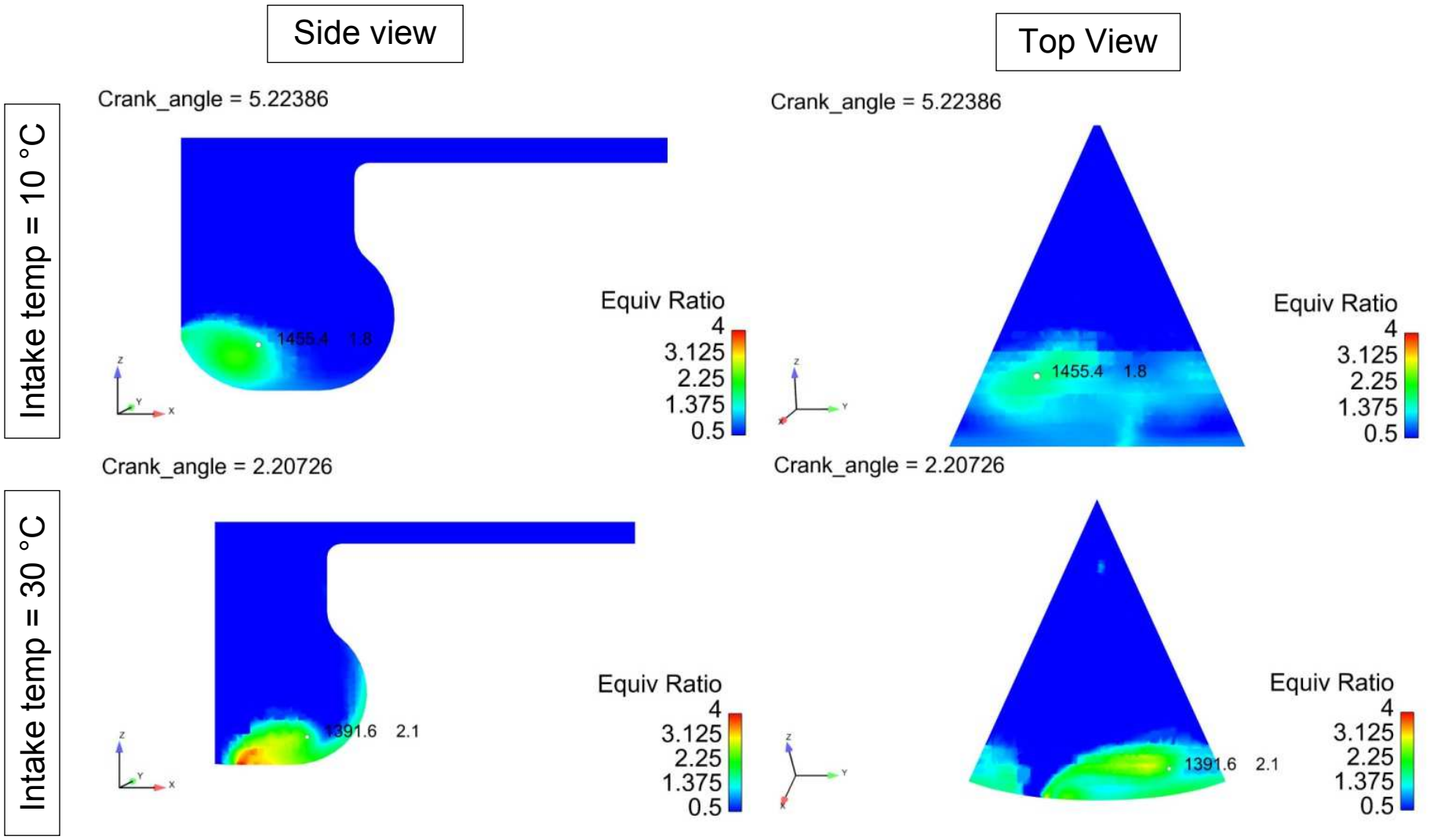

Figure 7.12: Equivalence ratio distribution in the combustion chamber at two different inlet air temperatures: top row for 10 °C and bottom row for 30 °C. The left column shows the side view and right column shows the top view.

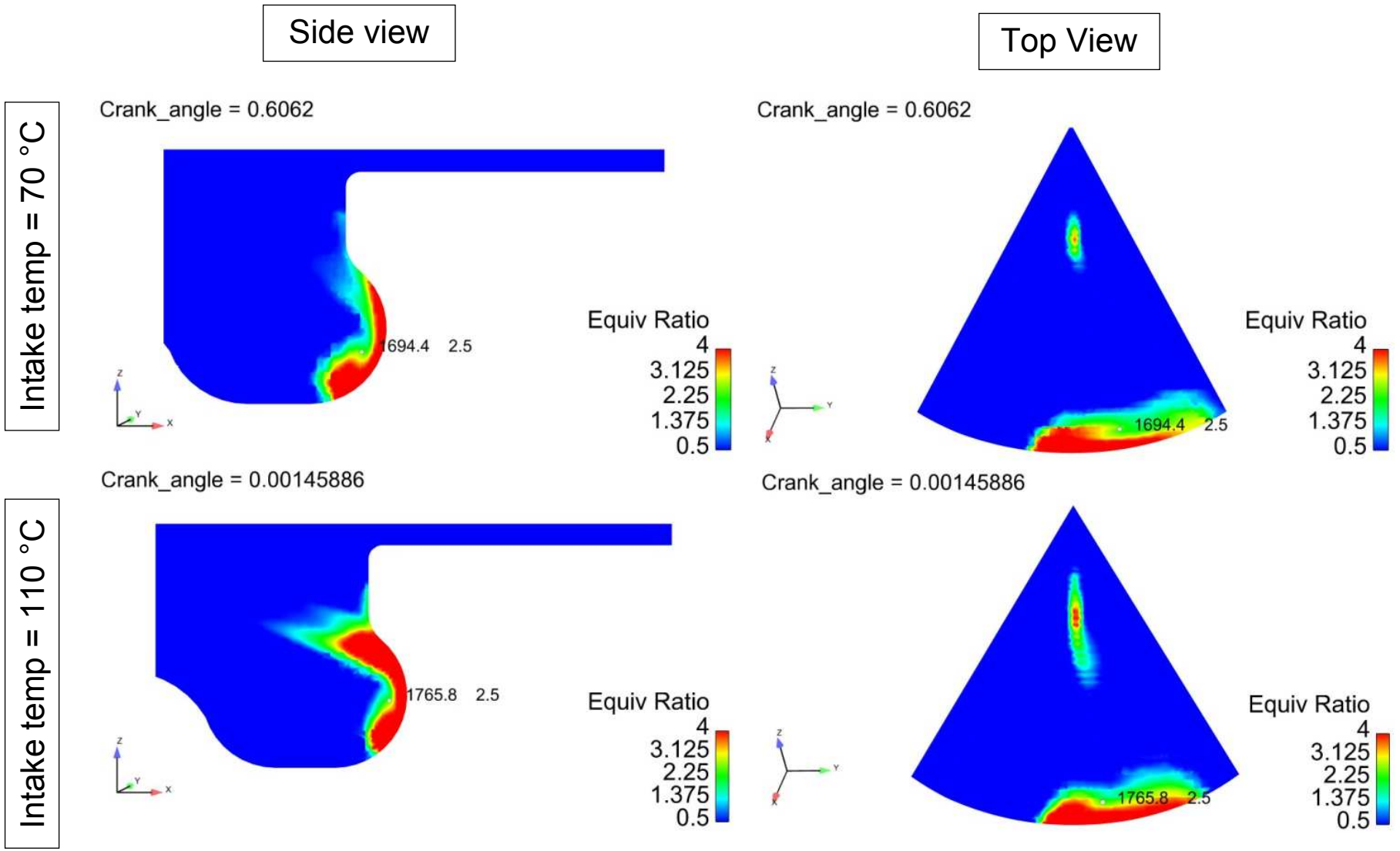

Figure 7.13: Equivalence ratio distribution in the combustion chamber at two different inlet air temperatures: top row for 70 °C and bottom row for 110 °C. The left column shows the side view and right column shows the top view.

7.4.2 CFD Simulation for 400 bar injection pressure

The same test conditions were simulated at a lower injection pressure of 400 bar, and the temperature and equivalence ratio distributions were observed. The idea was to see how injection behavior affects the equivalence ratio at the first site of combustion. Figure 7.14 - 7.15 shows the isometric views of the sector of the combustion bowl with two planes passing through the first site of auto-ignition marked by the white dot. One of the planes is parallel to the z-axis, and the second plane is arbitrary chosen to pass through SOC point and closer to the axis of the spray (not shown in the figure). The temperature and equivalence ratio values at both SOI and SOC are also given. The SOI temperature is indicative of the combustion bowl chamber with a ±20 K variation at places closer to the wall and in the squish zone.

In comparison to the 800 bar cases, the ID time for the 400 bar cases are longer (Fig. 7.14 - 7.19). As a result, the first site of auto-ignition is further downstream in the fuel spray in comparison to that at similar intake temperature at 800 bar injection pressure. A decrease in injection pressure will result in less atomization of the fuel spray thus affecting evaporation and increasing physical delay time. However, the equivalence ratio values obtained at the first site of auto-ignition are very close to the values obtained at 800 bar. The longer ignition delay time does not have an effect on the equivalence ratio at which combustion will start. Also, with increase in intake temperature, auto-ignition starts at higher equivalence ratio,_which agrees with the findings reported by Minagawa et al [110].

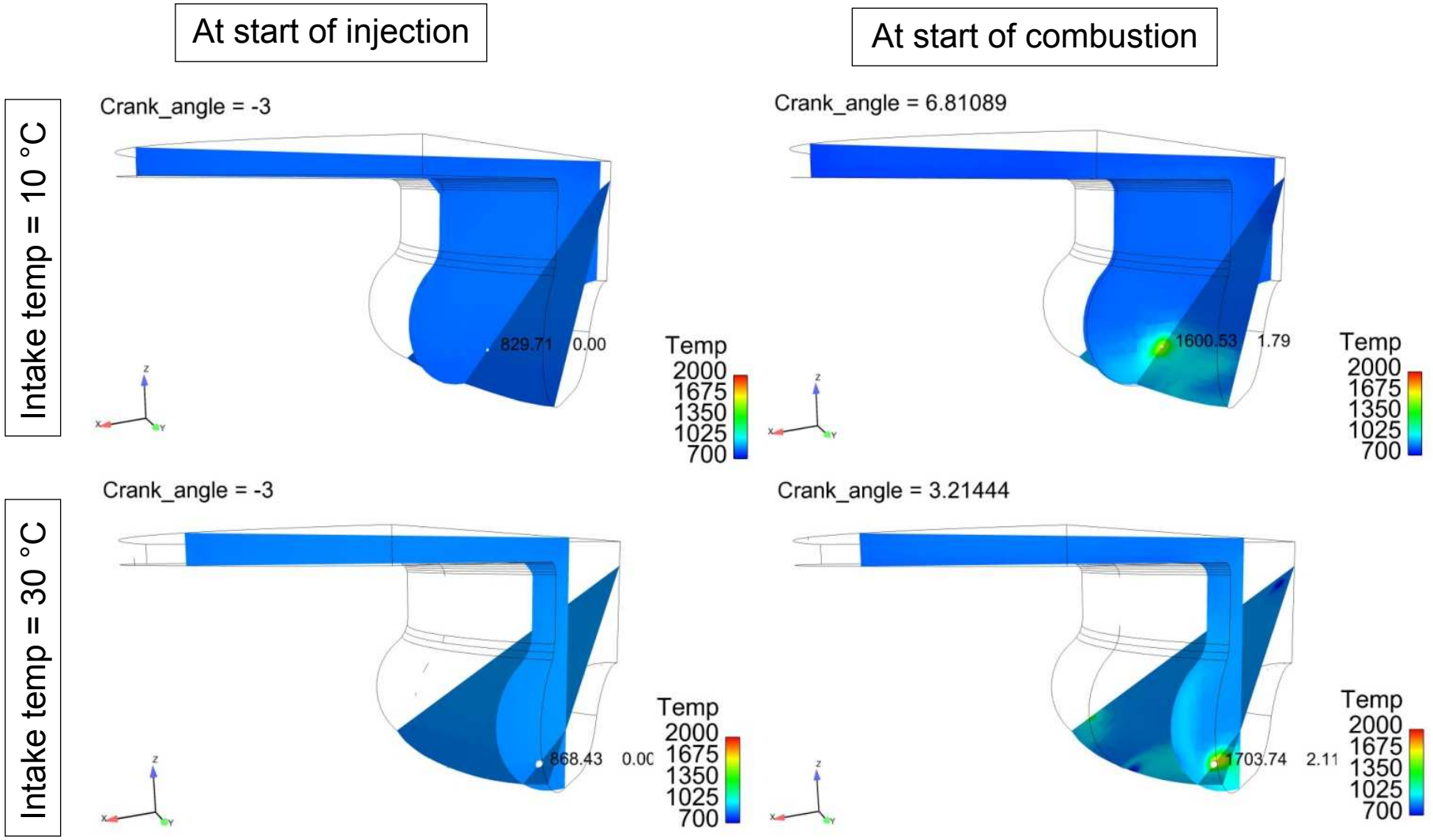

Figure 7.14: Temperature distribution in the combustion chamber at two different inlet air temperatures and at two planes : top row for 10 °C and bottom row for 30 °C. The left column is at SOI and right column at SOC.

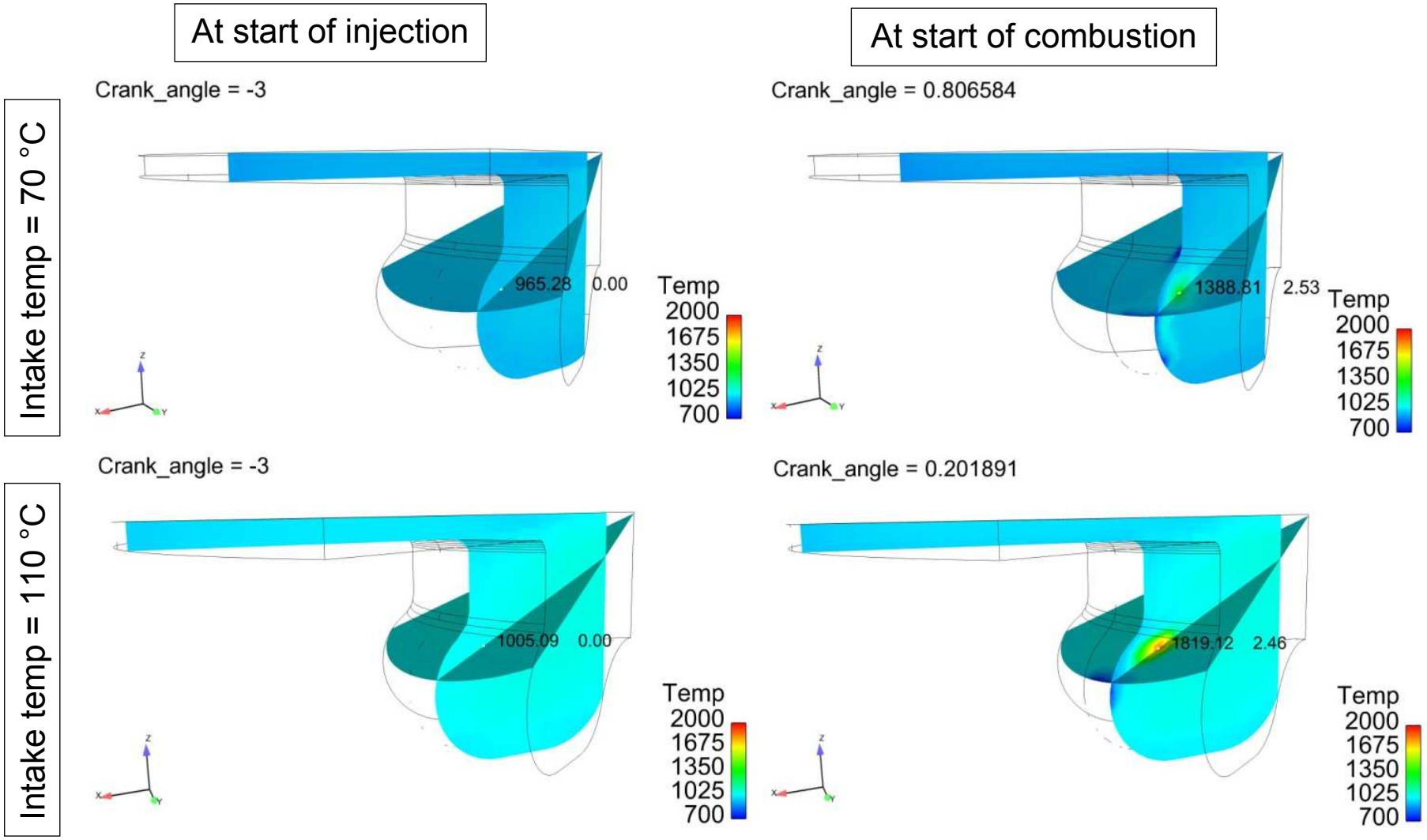

Figure 7.15: Temperature distribution in the combustion chamber at two different inlet air temperatures and at two planes : top row for 70 °C and bottom row for 110 °C. The left column is at SOI and right column at SOC.

The detailed temperature distribution at SOC with the side and top view of the combustion chamber is shown in Figure 7.16 - 7.17. Similar to 10 °C intake temperature case for 800 bar injection pressure, it can be observed that the auto-ignition site at 400 bar injection pressure is at the bottom of the combustion bowl. However, in the top view its location is almost at the center of the combustion chamber. This collaborates with the longer ID time observed in this case, which will result in the fuel spray moving further downstream in the combustion chamber. As discussed before longer ID time gives ample time for the fuel sprays to move to the adjacent sectors rightwards. With the anti-clockwise swirl motion the fuel spray would further move towards the right side and ignite at the center of the combustion chamber.

With the increase in intake temperatures to 30 °C, 70 °C and 110 °C the ignition delay reduces progressively. As a result at SOC, due to the shorter time available the fuel spray advancement in the combustion chamber reduces. This can be confirmed by comparing the top and side views of the combustion chamber temperature and equivalence ratio distributions (Fig. 7.16 - 7.19). There is a visible clockwise shift in combustion sites in the top view with the increase in intake temperatures. Also the side view shows the upward movement of the combustion sites as well. This shift is more prominent at the lower intake temperatures compared to higher intake temperatures.

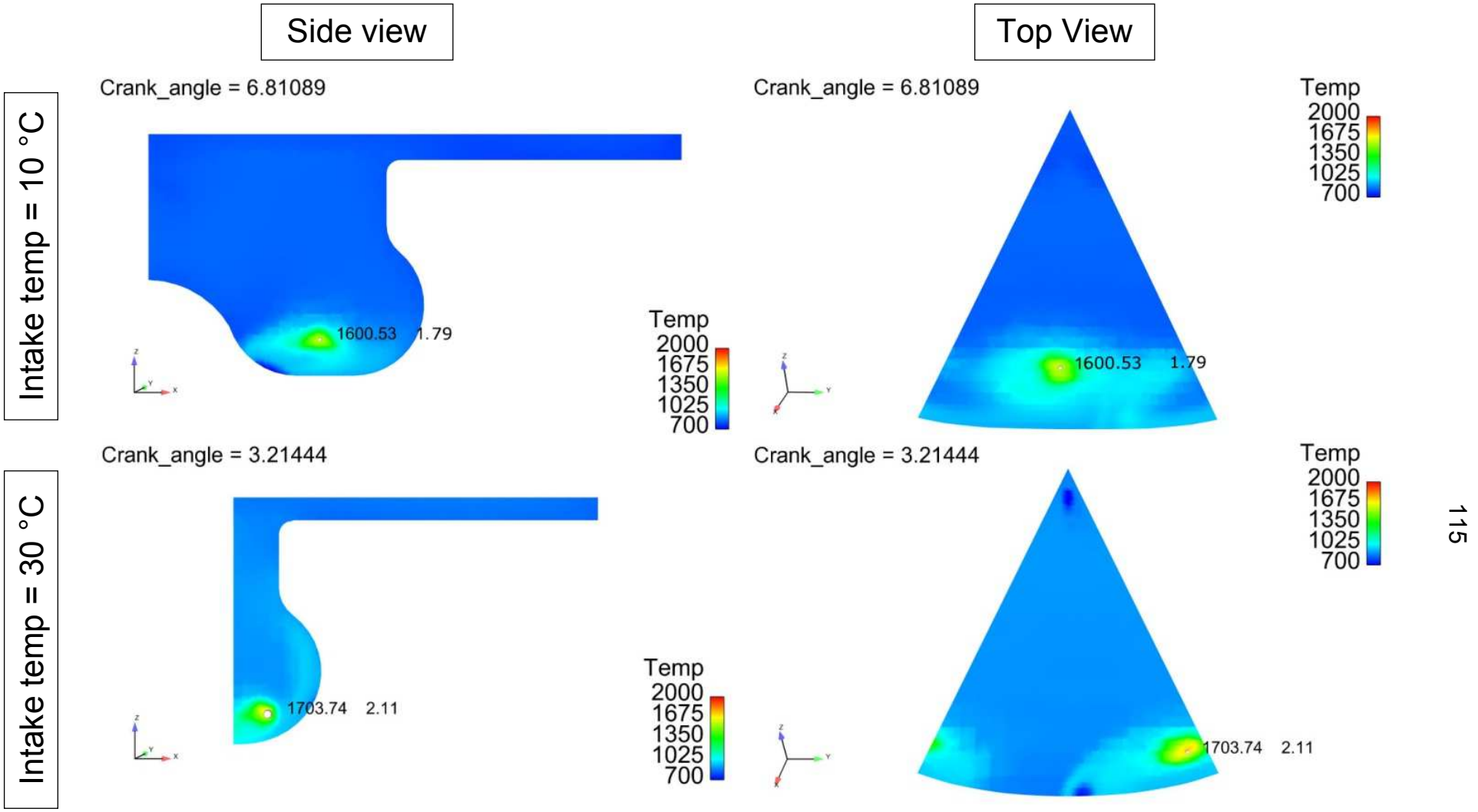

Figure 7.16: Temperature distribution in the combustion chamber at two different inlet air temperatures: top row for 10 °C and bottom row for 30 °C. The left column shows the side view and right column shows the top view.

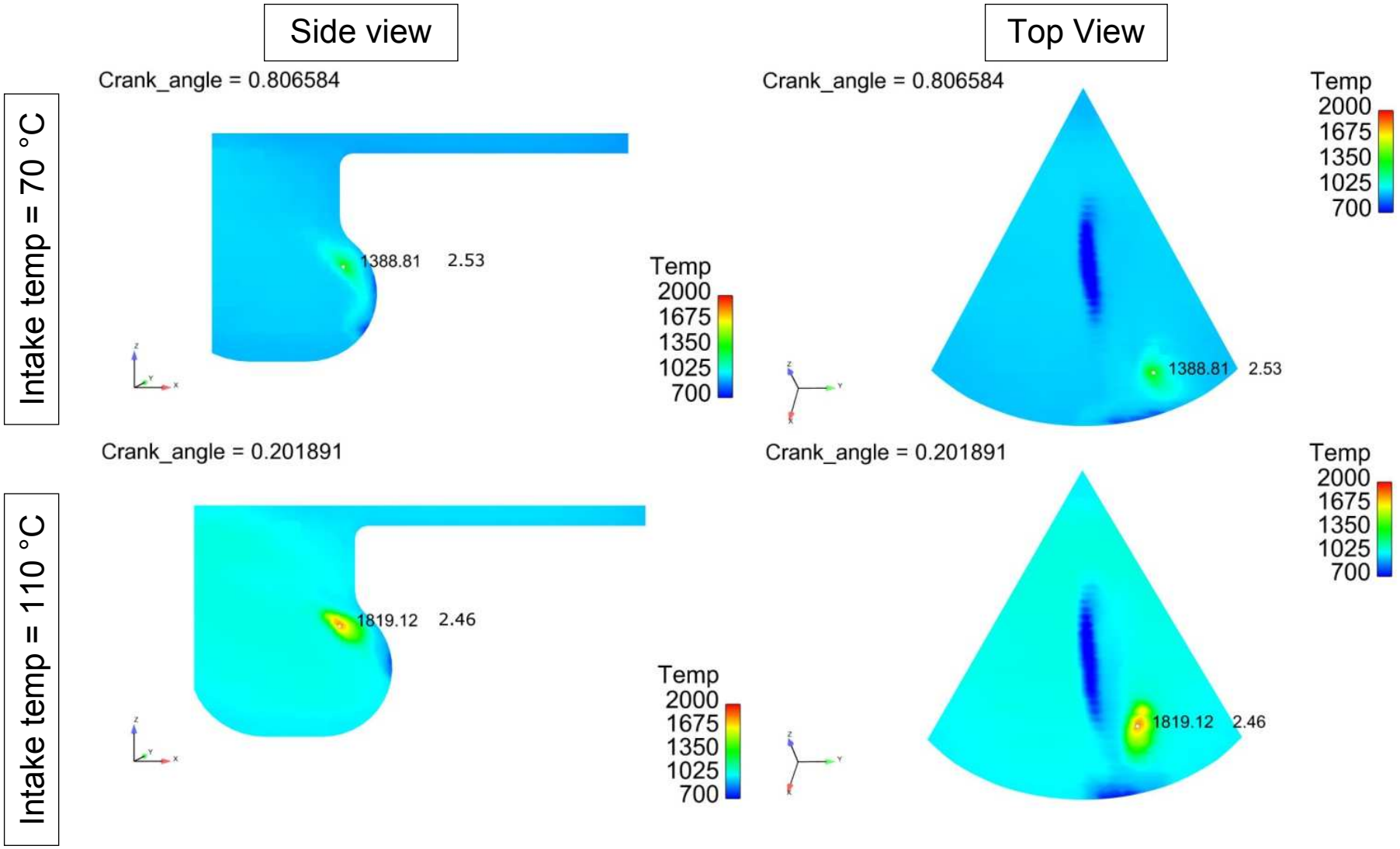

Figure 7.17: Temperature distribution in the combustion chamber at two different inlet air temperatures: top row for 70 °C and bottom row for 110 °C. The left column shows the side view and right column shows the top view.

Figure 7.18 - 7.19 shows the side and top views of the equivalence ratio distribution in the combustion bowl chamber at SOC. The lower injection pressure does affect the spray pattern and the wall impingement behavior, which in turn affects the equivalence ratio distribution. Compared to the 800 bar injection case at 110 °C intake temperature, we observe that the air-fuel distribution along the wall has less spread at 400 bar injection pressure. Although, the ID time is longer at 400 bar still there is higher concentration of air-fuel at SOC than the 800 bar injection pressure. This is due to the lesser entrainment of air at lower injection pressures which results in a less dispersed spray. Also lower injection pressure results in bigger SMD (Sauter Mean Diameter) of fuel droplet, which take longer time to evaporate. A combined effect of these two phenomena will result in highly concentrated zones of air-fuel which take longer time to disperse.

Even at lower injection pressure of 400 bar, with an increase in the intake temperature, the ID time decreases and auto-ignition happens at higher equivalence ratio, which shows an increase from 1.79 at 10 °C to 2.5 at 70 °C (Fig. 7.18 - 7.19). This shifts the first site of auto-ignition closer to the inner core of the spray. Again not much change in equivalence ratio is observed by increasing the intake temperature from 70 °C to 110 °C. The temperatures observed at the first site of auto-ignition at SOI for 70 °C intake air is 965 K and for 110 °C intake air is 1005 K. Since these values are for the gas temperature at the start of injection the temperatures should not change much between the 800 bar and 400 bar injection cases. There will be some variation due to the shift in location of first site of auto-ignition. In this case as well the equivalence ratio becomes consistent at the upper end of the intermediate temperature (850-1000 K)

boundary. The shift in equivalence ratio results in the absence of the NTC behavior observed in homogeneous mixtures. Approaching 1000 K, an increase in temperature reduces the ID period and becomes the dominant parameter which affects auto-ignition. As a result, negligible change in equivalence ratio is observed.

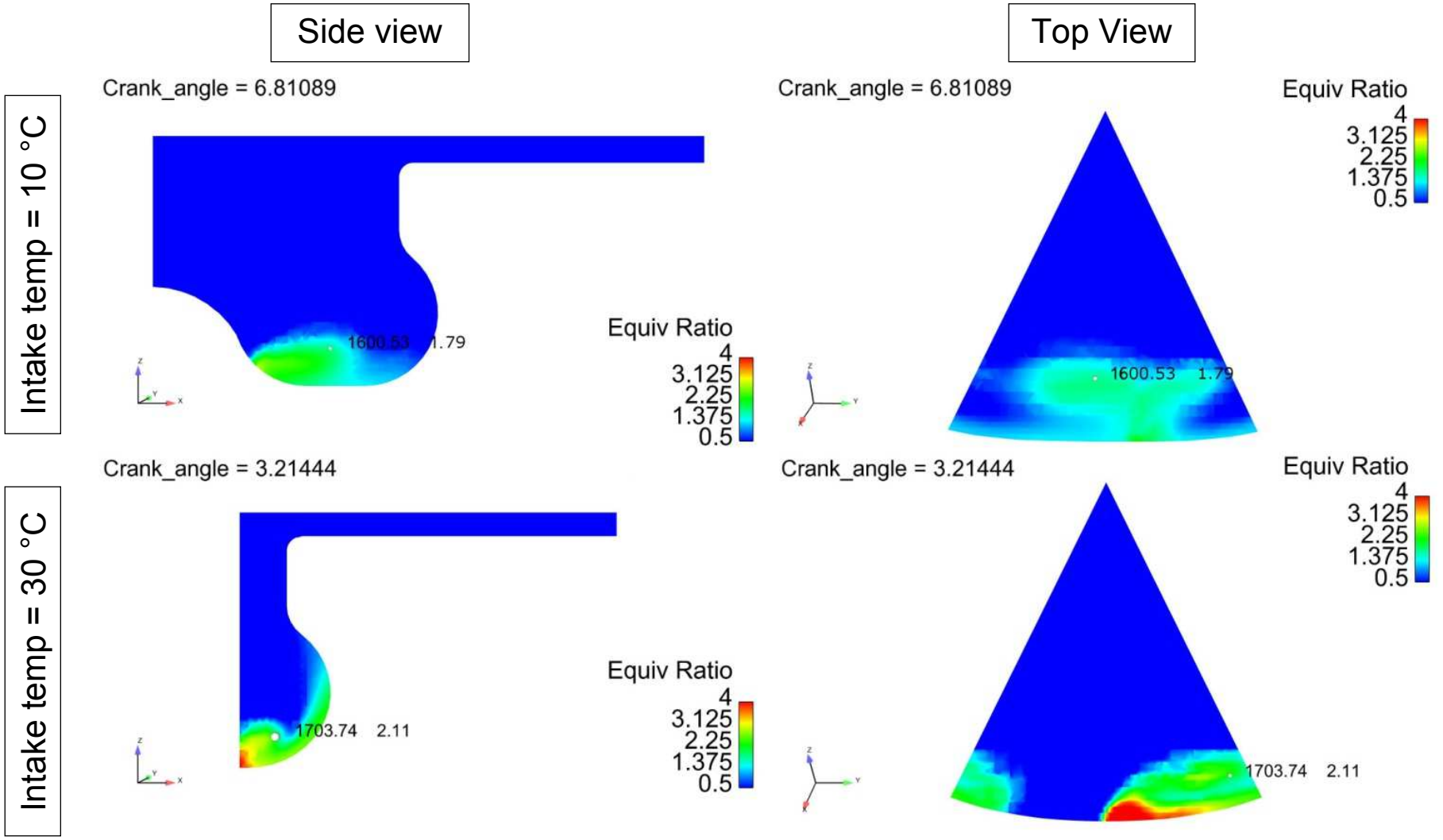

Figure 7.18: Equivalence ratio distribution in the combustion chamber at two different inlet air temperatures: top row for 10 °C and bottom row for 30 °C. The left column shows the side view and right column shows the top view.

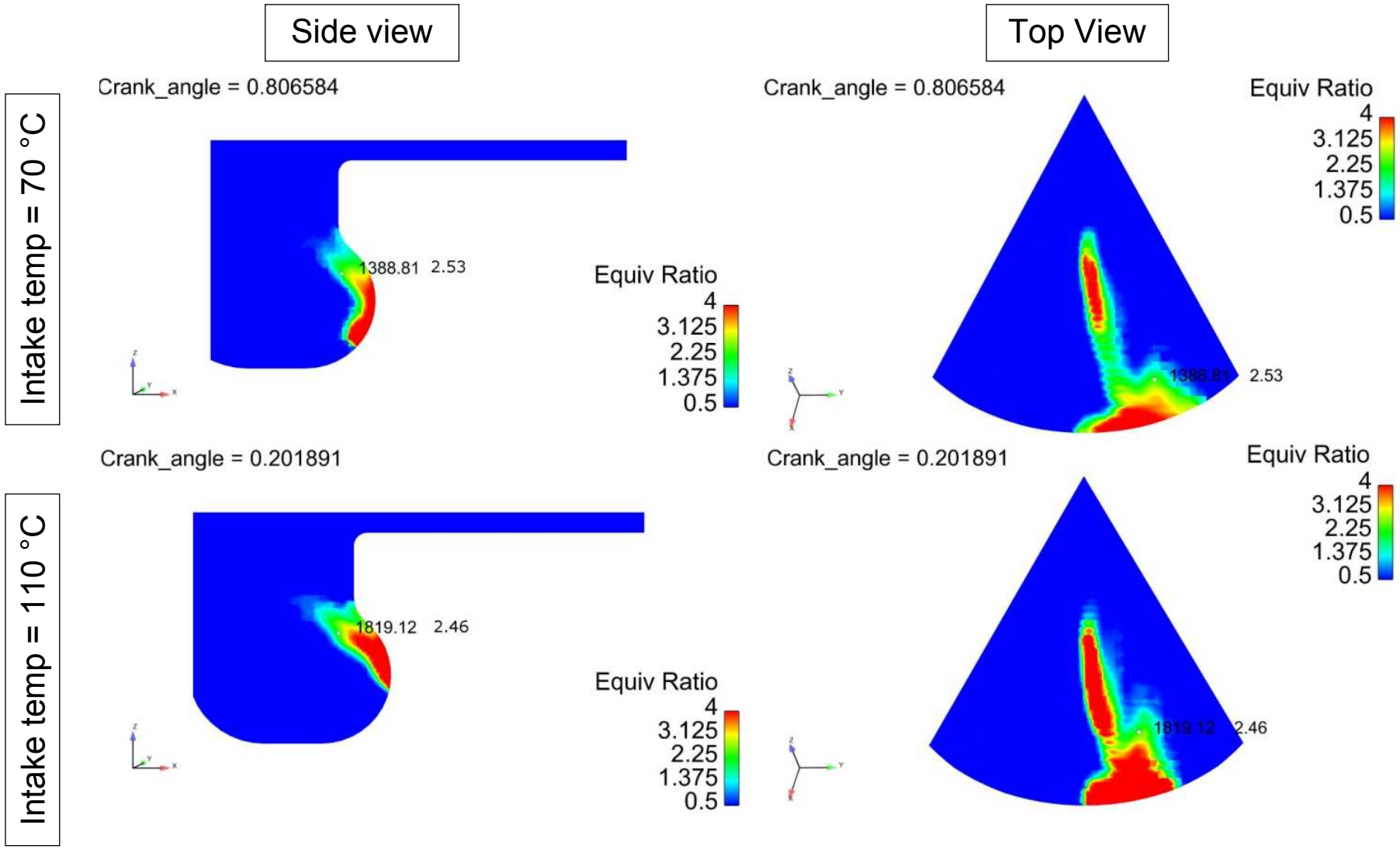

Figure 7.19: Equivalence ratio distribution in the combustion chamber at two different inlet air temperatures: top row for 70 °C and bottom row for 110 °C. The left column shows the side view and right column shows the top view.

The simulation results confirm the observations made by Minagawa et al [110] that in the intermediate temperature range (850-1000 K) with the increase in the gas temperature at SOI the combustion in heterogeneous flames shifts towards zones of higher equivalence ratio. Furthermore, under the given test conditions this finding is applicable at different injection pressures as well (Fig. 7.19).

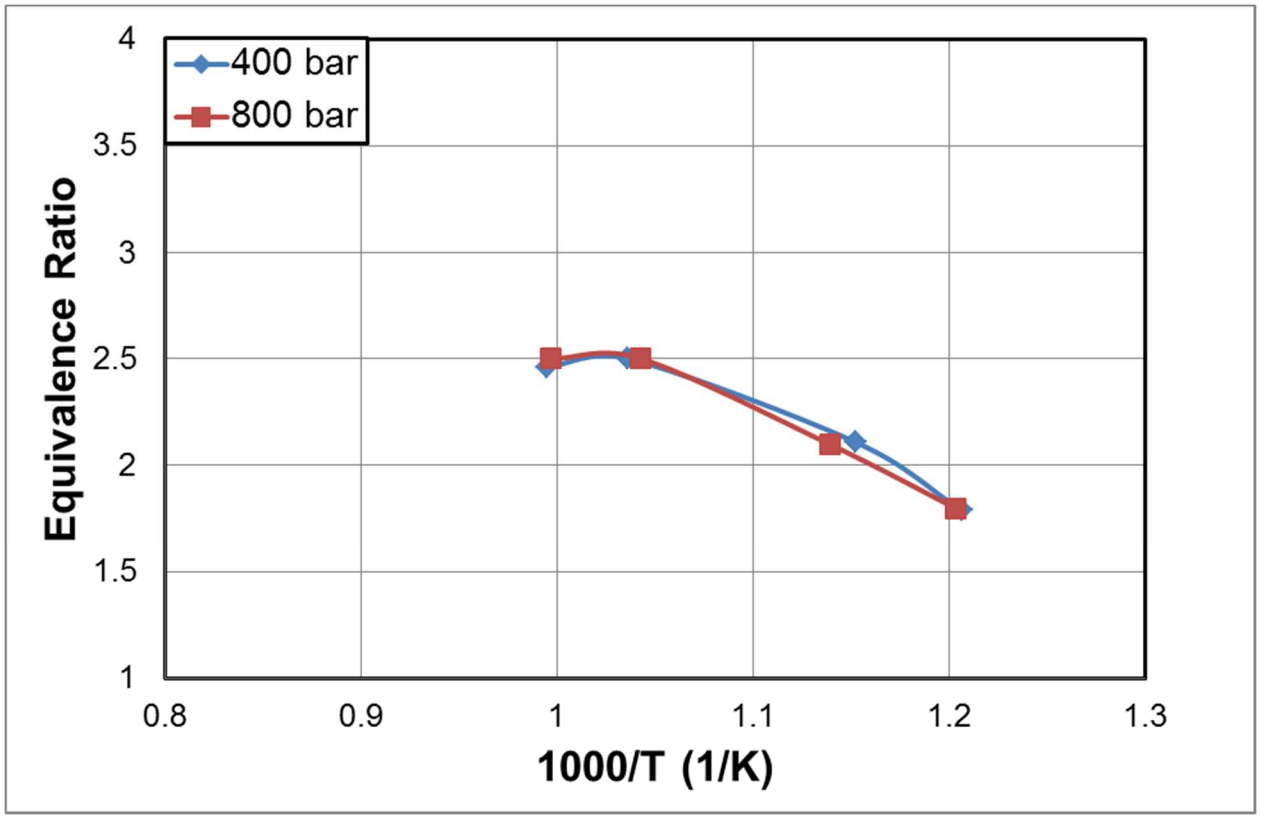

Figure 7.19: Equivalence ratio at the auto-ignition site vs inverse of temperature in intermediate temperature range

The given experimental data lies in the intermediate temperature range, and the large disparity in global activation energy can be fairly attributed to changes in density and equivalence ratio. At a fixed SOI, when the intake air temperature is increased, auto-ignition occurs in the intermediate temperature range, and combustion in the flame

shifts towards higher equivalence ratio. [110]. The rise in charge pressure to maintain same density will further add to this effect. Similar effect will be seen in late injection cases; however, the fall in temperature is aggravated in the expansion stroke leading to sharper changes in ID values. This combined effect of density, temperature and equivalence ratio will become more significant if the data is represented as a variable SOI test.

Changing SOI not only affects the temperature during ID period but also the pressure and density. Hence, there will be three parameters changing at the same time and thus resulting in significant reduction in ID values leading to higher global activation values. On the other hand, an incremental temperature change, while maintaining constant charge density, will only result in change in temperature and pressure. As a result, there will be only two parameters changing at the same time. In engines it is difficult to maintain a constant temperature, pressure and density at the same time. Also, in the late injection cases the drop in temperature is drastic compared to the early injection cases near the location of peak compression temperature. Thus, the large deviation in activation energy in the given data set is due to combined effect of changes in pressure and equivalence ratio dominant in the intermediate temperature range.

7.4.3 Correlation between the Apparent Activation Energy and DCN for Different Fuels

It is important to choose the experimental conditions that would produce a more accurate representation of global activation energy for the different fuels – keeping constant SOI and varying intake air temperature or doing vice versa. In order to get a

more accurate value of global activation energy, it would be better to reduce as many control variables as possible. In diesel combustion the effect of equivalence ratio cannot be avoided, and therefore the density changes should be avoided as much as possible.

A comparison between the SOI -3 and SOI -1 cases for ULSD shows that the activation energy values obtained are close with a deviation of 8.7 % which increases to 39.45 % and 49.49 %, at SOI 1 and 3 aTDC, respectively. With Sasol IPK, due to its longer ignition delay this reliability shifts to early injection case of SOI of -7 and -5 aTDC, in which case the deviation is 5 %. At SOI of -3 and -1 aTDC this variability increases to 18.25 % and 50.90 %, respectively.

Table 7.1 Apparent Activation Energy Values for ULSD

Definition	E_a/R_u (K)	E_a (KJ/kg mole)	Variation (%)
SOI -3	1095	9104	0
SOI -1	1190	9894	8.67
SOI 1	1527	12695	39.45
SOI 3	1637	13610	49.49

Table 7.2 Apparent Activation Energy Values for Sasol IPK

Definition	E_a/R_u (K)	E_a (KJ/kg mole)	Variation (%)
SOI -7	1271	10567	0
SOI -5	1335	11099	5.04
SOI -3	1503	12496	18.25
SOI -1	1918	15946	50.90

The apparent activation energy values for JP8 and Surrogate S2 along with the variations obtained at different SOI are listed in Table 7.3 and 7.4 respectively.

Table 7.3 Apparent Activation Energy Values for JP8

Definition	E_a/R_u (K)	E_a (KJ/kg mole)	Variation (%)
SOI -2.3	936	7782	0
SOI -0.3	1160	9644	23.93
SOI 1.7	1351	11232	44.34

Table 7.3 Apparent Activation Energy Values for Surrogate S2

Definition	E_a/R_u (K)	E_a (KJ/kg mole)	Variation (%)
SOI -2.3	954	7932	0
SOI -0.3	1126	9362	18.06
SOI 1.7	1396	11606	46.33

During the testing for JP8 and Surrogate S2 due to an error in the needle lift sensor the SOI was retarded by 0.7 CAD. As a result, the real SOI during testing were -2.3, -0.3 and 1.7 instead of the target -3, -1 and 1 respectively. The variation in apparent activation energy between -2.3 and -0.3 for JP8 is higher (23.93 %) compared to between -3 and -1 (8.67 %) observed with ULSD. A small shift of 0.7 CAD into the expansion stroke can thus have a noticeable effect on apparent activation energy for SOI later than -1 CAD.

The data above reveals that global activation energy values are more reliable in the cases in which auto-ignition occurs near TDC. Since the global activation energy values between -3 and -1 CAD were very close for ULSD, we can assume the values at -2.3 CAD for JP8 and surrogate S2 would be comparable to the one at -3 CAD for ULSD. Also, for Sasol IPK the global activation energy value at -5 CAD will be comparable to ULSD at -3 CAD due to the longer ignition delay for Sasol.

Table 7.5 Comparable Apparent Activation Energy Values

Fuel	**A**	**E_a/R_u (K)**	**E_a (KJ/kg mole)**	**DCN**
Sasol IPK	0.2213	1335	11099	31.1
ULSD	0.1876	1095	9104	42.1
S2	0.2060	954	7932	49.1
JP8	0.2166	936	7782	50.1

In Figure 7.15, the apparent activation energy values are plotted against the DCNs of the fuels tested. The figure shows that there exists a linear relationship between the apparent activation energy and DCN of the fuel. The DCN is a measure of the ignition quality of a fuel obtained from experimental tests done at standardized conditions in a constant volume chamber. On the other hand, apparent activation energy is a simplified, one-step, kinetic reaction model over an extended range of temperature. Both these parameters are a measure of the ignition quality of a fuel, therefore a correlation between the two can be formulated to understand these parameters better. The equation is:

$$E_a(kJ/mol) = \frac{500}{(DCN + 13.3)}$$

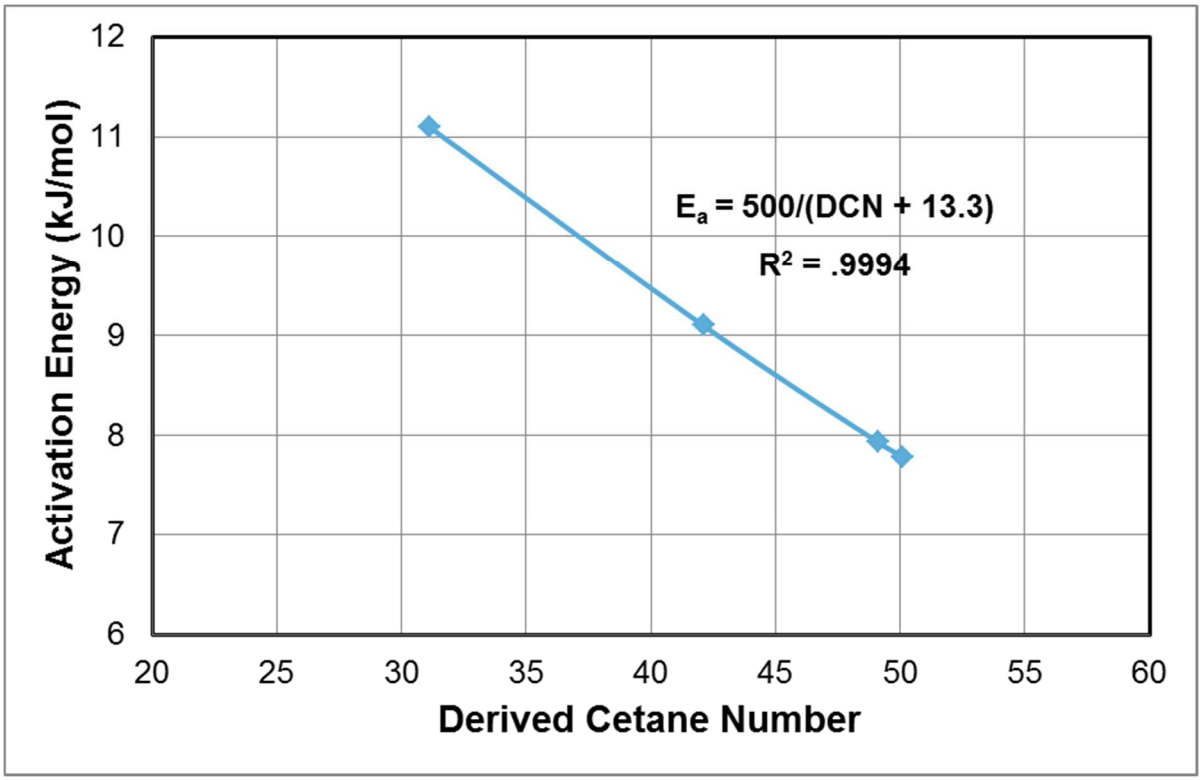

Figure 7.15: Correlation between apparent activation energy and derived cetane number

It is to be noted that these values are much smaller than the ones obtained by previous researchers [3, 8]. As these tests were performed in the intermediate temperature range, effect of the NTC regime produces a slowdown in temperature sensitivity of ID values, as seen in the results of Minagawa et al [110]. As a result, in this temperature range any further increase in temperature will result in a smaller decrease in ID which will be reflected in reduced global activation energy values. However, Sasol IPK has higher activation energy than ULSD, JP8 and Surrogate S2 as it has a low DCN and provides more resistance to auto-ignition.

7.5 Conclusions

1. Quantification of activation energy in engines is based on changes in ID at different charge temperatures, which can be done by controlling the intake air temperature while keeping constant injection timing or by changing the injection timing while keeping the intake temperature constant. The former approach can be achieved while keeping the charge density constant by increasing the charge pressure at the higher intake temperatures. On the other hand, the latter approach results in considerable variations in charge density due to the piston motion. Accordingly, to avoid errors because of changes in the charge density at different injection timings, tests should be conducted using the variable intake temperatures approach.
2. For the variable intake temperature approach, the injection timing should be adjusted to have the ID period around TDC to avoid the effect of rapid change in density during the ID period, associated with the piston motion.
3. The change in the activation energy measured by the slope in the Arrhenius plot can have a positive, zero or a negative value in the intermediate combustion temperature regime (850-1000 K) in auto-ignition of many hydrocarbons in homogeneous environments. This is not the case in the auto-ignition of diesel fuels in heterogeneous combustion mode. The simulation conducted in this investigation indicated that this trend is caused by variations in the equivalence ratio in the auto-ignition of liquid fuel sprays.

4. Cycle simulation showed that under the given test conditions in the intermediate temperature regime, the equivalence ratio at the auto-ignition site in the spray is insensitive to changes in fuel injection pressure.
5. Under the conditions of this investigation, the apparent activation energy is related to the DCN of the fuel according to the following,

$$E_a(kJ/mol) = \frac{500}{(DCN + 13.3)}$$

CHAPTER 8

CONCLUSIONS AND RECOMMENDATIONS

8.1 Conclusions

1. Large variations in the activation energy of fuels with close CN values have been observed in recent research works. These differences can be attributed to variations in:
    - ID Definitions
    - Effective Temperature Definitions
    - Charge Density
    - Temperature Regime
2. In the auto-ignition of homogeneous hydrocarbon fuel-air mixtures, ID decreases with the increase in charge temperature in the low-temperature and high temperature regimes. This is not the case in the intermediate temperature regime (850K-1000K) where ID increases at higher charge temperatures. Accordingly, the activation energy measured by the slope in the Arrhenius plot can have a positive, zero or a negative value. However, in the combustion of diesel fuel sprays, all published data for the activation energy are positive in spite of the fact that the charge temperature lies in the intermediate temperature regime. The simulation conducted in this investigation indicated that this is caused by the

wide variations in the charge pressure and equivalence ratio in the auto-ignition of liquid fuel sprays.

3. The ID values obtained under the conditions of this investigation can be correlated to the apparent activation energy of the fuels in the general form:

$$ID = A \cdot e^{\frac{E_a}{R_u T}}$$

where, the values for A and E_a/R_u for each fuel is listed in the table below.

Fuel	**A**	**E_a/R_u (K)**	**DCN**
Sasol IPK	0.2213	1335	31.1
ULSD	0.1876	1095	42.1
S2	0.2060	954	49.1
JP8	0.2166	936	50.1

4. In addition, under the given test conditions, the apparent activation energy is related to the DCN of the fuel according to the following,

$$E_a(kJ/mol) = \frac{500}{(DCN + 13.3)}$$

8.2 Recommendations for Future Work

- Engine experimental investigation of fuels of different molecular structures in the intermediate temperature regime to get a better understanding of their behavior in actual diesel engines.
- Computer modeling and simulation of the physical and chemical processes in the auto-ignition and combustion of fuels in the intermediate temperature regime.

- Development of a general correlation for the ignition delay in engines in terms of the DCN and the other properties of the fuel.

APPENDIX A

Table A1: Properties for Different Fuels

Fuel	ULSD	Sasol IPK	JP-8	Surrogate S2
D613 CN	42.3	25.4	49	-
D6890 DCN	42.1	31.1	50.1	49.28
Flash point (°C) min	69	42	49.5	-
Density (@15°C) kg/m3	842	755	802	802
Viscosity (cSt @ 40°C)	2.438	1.125	1.367	-
Heating Value (MJ/kg)	41.2	44	43.2	43.2
Aromatic Content (%Mass)	27.8	0.2	16.3	40

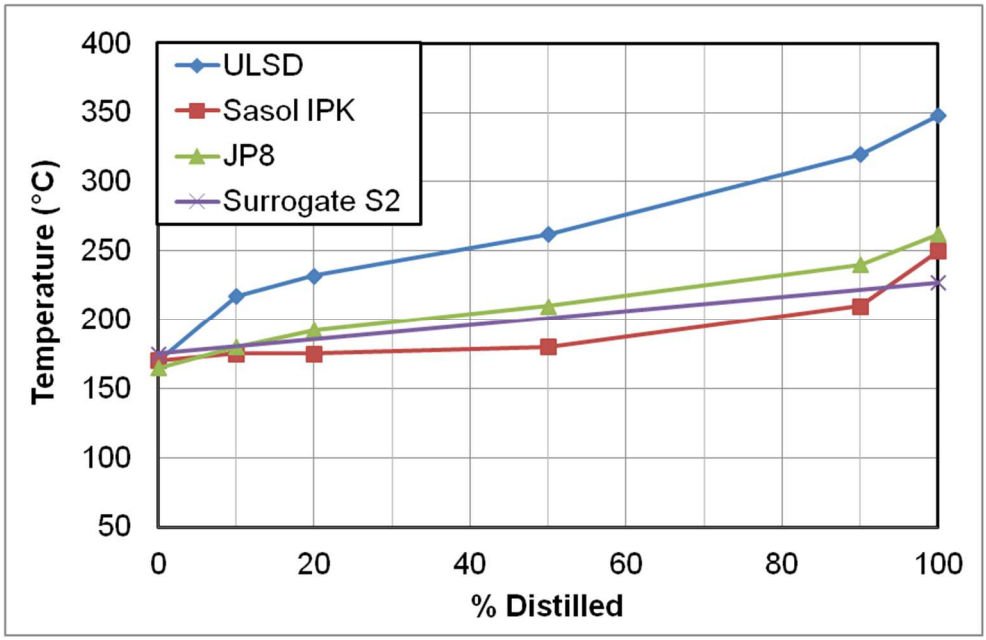

Figure A1: Distillation curves for different fuels

APPENDIX B

Physical Delay in IQT vs Engine

Zheng [3] separated the physical and chemical delay time in Ignition Quality Tester by superimposing the data obtained by injecting fuel in air and later into nitrogen. The point where the two data curves separate marks the end of physical delay time and start of chemical reactions which would lead to auto-ignition and combustion (Fig. B1).

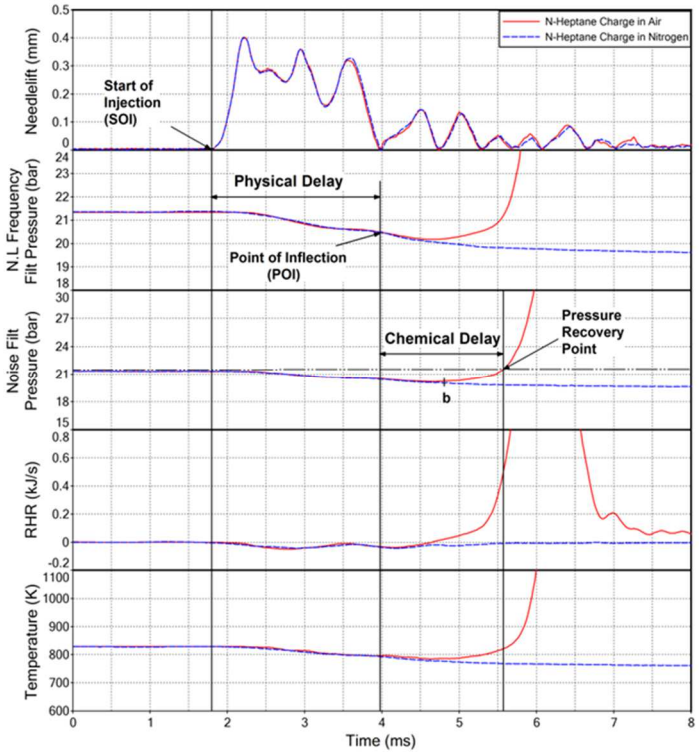

Figure B1: Traces for N.L., pressure, RHR, and temperature for injection of n-heptane in air and in nitrogen environment [3]

A ratio of physical delay time to the total ignition delay time will give us a measure to compare it with data obtained in engines. For ULSD the physical delay time at an intake temperature of 828 K was 3.34 ms out of the total ID time of 4.9 ms [3].

$$Physical\ Delay/Total\ Ignition\ Delay = 3.34/4.9 = 0.6816\ or\ 68.16\ \%$$

In engines the physical delay has been calculated as the time between SOI and Point of Inflection (POI), identified as the point where the second derivative of RHR curve crosses zero and becomes positive [4].

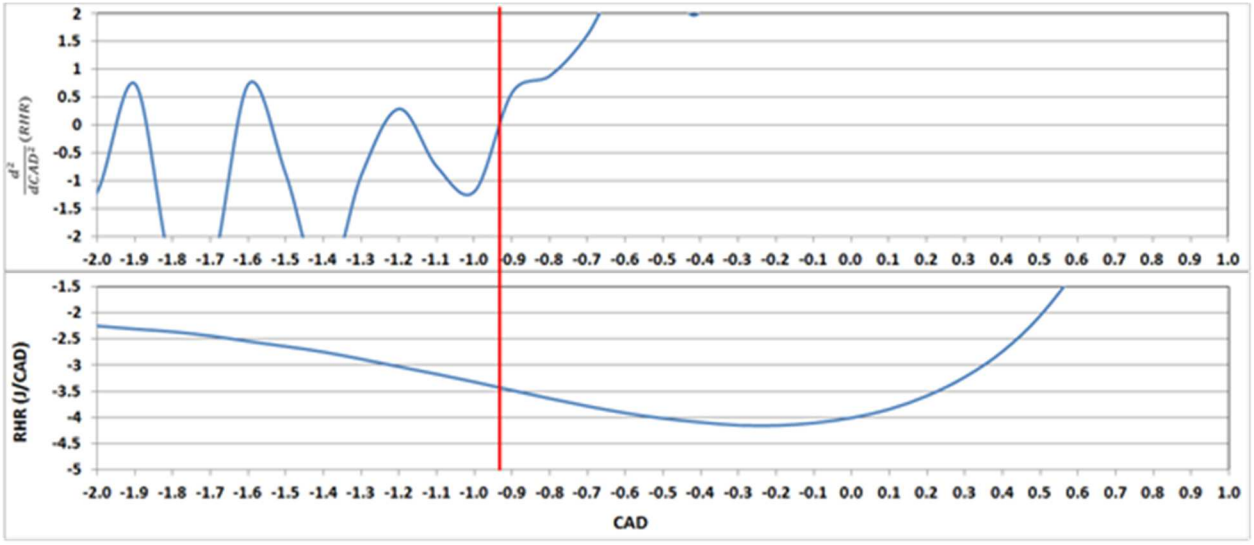

Figure B2: Calculation of Point of Inflection from RHR trace [4]

Applying this definition on our data for ULSD at SOI temperature of 828 K the physical delay time obtained is 2.1 CAD out of the total ID time of 6.5 CAD.

$$Physical\ Delay/Total\ Ignition\ Delay = 2.1/6.5 = 0.3213\ or\ 32.13\ \%$$

Comparing the ratios of the physical delay time to the total ID time in engines and IQT it can be inferred that the physical delay in engines is smaller compared to IQT. As a result, the effect of physical delay on the calculation of activation energy value would also be smaller in engines.

APPENDIX C

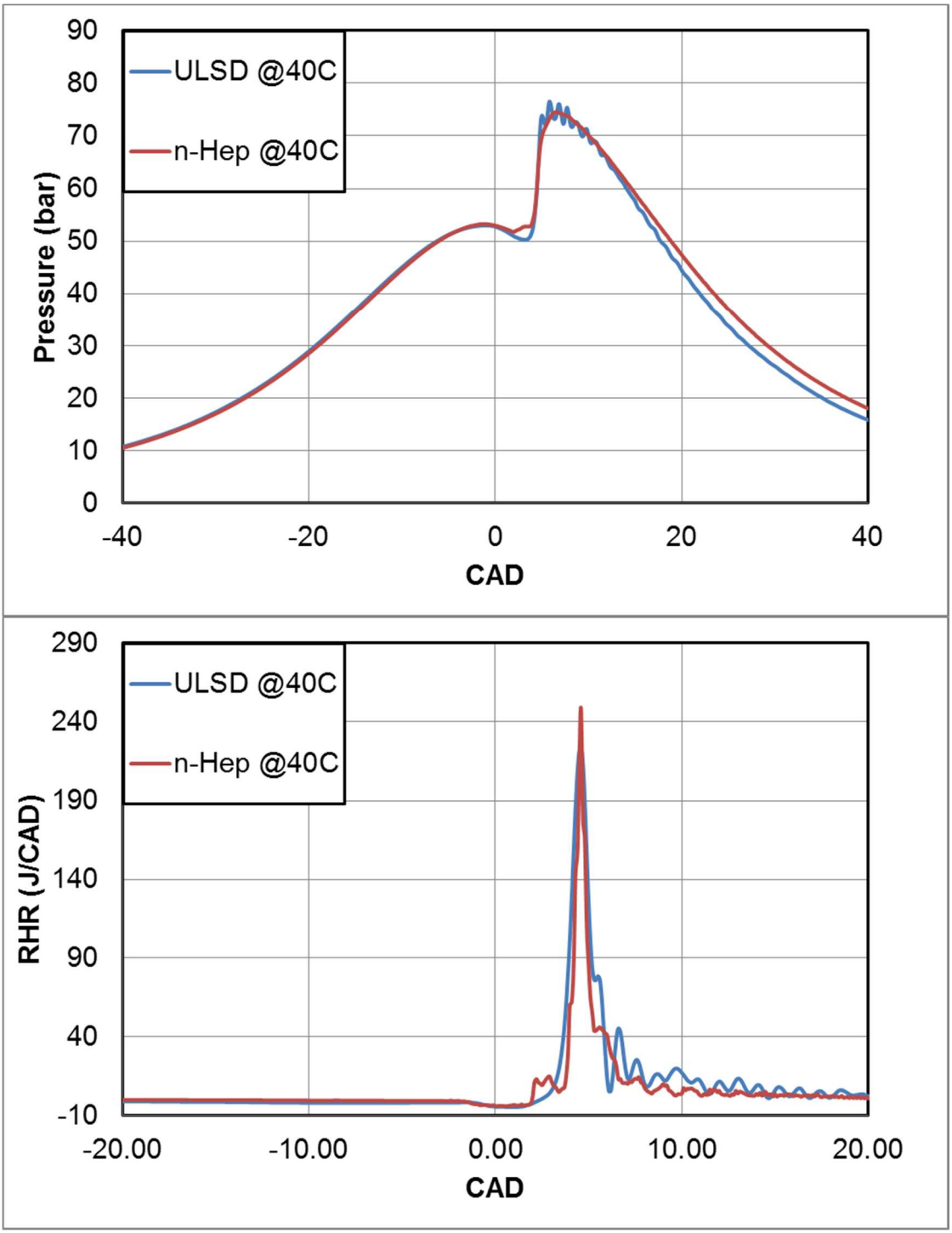

Figure C1: n-heptane simulation model calibration points

REFERENCES

[1] "Improving the Fuel Efficiency of American Trucks - Bolstering Energy Security, Cutting Carbon Pollution, Saving Money and Supporting Manufacturing Innovation," The White House, Washington, 2014.

[2] J. Heywood, "Internal Combustion Engine Fundamentals", McGraw Hill, New York, 1988.

[3] Z. Zheng, "Effect of Cetane Number and Volatility on Autoignition and Combustion of Alternative Fuels and Their Surrogates," PhD, Wayne State University, Detroit, 2014.

[4] C. Jayakumar, "Effect Of Intake Temperature And Boost Pressure On The Auto-Ignition Of Fuels With Different Cetane Numbers And Volatilities," PhD, Wayne State University, Detroit, 2013.

[5] K. C. Tsao, P. S. Myers, and O. A. Uyehara, "Gas Temperature During Compression in Motored and Fired Diesel Engines," SAE Technical Paper 620518, 1962.

[6] S. G. Bauer, "Ignition Lag in Compression Ignition Engines," Engineering, 148(9), p. 368, 1939.

[7] W. T. Lyn, and E. Valdmanis, "The Effects of Physical Factors on Ignition Delay," Paper IME (London) Automotive Division, 1966.

[8] S. Kook, C. Bae, P. C. Miles, D. Choi, and L. M. Pickett, "The Influence of Charge Dilution and Injection Timing on Low-Temperature Diesel Combustion and Emissions," SAE Technical Paper 2005-01-3837, 2005.

[9] "Two-stroke Low Speed Diesel Engines for Independent Power Producers and Captive Power Plants," MAN Diesel, 2009.

[10] T. Takaishi, A. Numata, R. Nakano, and K. Sakaguchi, "Approach to High Efficiency Diesel and Gas Engines," Mitsubishi Heavy Industries Ltd., 2008.

[11] A. Sinha, C. Jayakumar, J. Nargunde, W. Bryzik, N. Henein, and K. Acharya, "Effect of Biodiesel and its Blends on Particulate Emissions from HSDI Diesel Engine," SAE Technical Paper 2010-01-0798, 2010.

[12] M. Dahodwala, V. Nagaraju, K. Acharya, W. Bryzik, and N. Henein, "Effect of Using Biodiesel (B-20) and Combustion Phasing on Combustion and Emissions in a HSDI Diesel Engine," SAE Technical Paper 2011-01-1203, 2011.

[13] J. Nargunde, "Auto-Ignition, Combustion And Emission Characteristics Of Soybean Biodiesel, Jet Propellant (jp-8) Fuel And Ultra Low Sulfur Diesel In A Single Cylinder Diesel Engine," MS, Wayne State University, Detroit, 2010.

[14] K. Zha, X. Yu, R. Florea, and M. Jansons, "Impact of Biodiesel Blends on In-cylinder Soot Temperature and Concentrations in a Small-Bore Optical Diesel Engine," SAE Technical Paper 2012-01-1311, 2012.

[15] B.-Q. He, J.-X. Wang, X.-G. Yan, X. Tian, and H. Chen, "Study on Combustion and Emission Characteristics of Diesel Engines Using Ethanol Blended Diesel Fuels," SAE Technical Paper 2003-01-0762, 2003.

[16] C. Kumar, M. Athawe, Y. V. Aghav, M. K. Gajendra Babu, and L. M. Das, "Effects of Ethanol Addition on Performance, Emission and Combustion of DI Diesel Engine Running at Different Injection Pressures," SAE Technical Paper 2007-01-0626, 2007, 2007.

[17] T. A. Nevius, D. Rauker, and S. T. Porter, "Investigation of Direct-Injected Ethanol and Diesel Fuel Blends on Gaseous and Particulate Emissions in a Medium-Duty Diesel Engine," SAE Technical Paper 2013-01-1141, 2013.

[18] K. Nord, D. Haupt, P. Ahlvik, and K.-E. Egebäck, "Particulate Emissions From an Ethanol Fueled Heavy-Duty Diesel Engine Equipped With EGR, Catalyst and DPF," SAE Technical Paper 2004-01-1987, 2004.

[19] S. H. Park, J. Cha, and C. S. Lee, "Impact of biodiesel in bioethanol blended diesel on the engine performance and emissions characteristics in compression ignition engine," Applied Energy, 99, pp. 334-343, 2012.

[20] C. Jayakumar, Z. Zheng, U. Joshi, W. Bryzik, N. Henein, and E. Sattler, "Effect of Intake Pressure and Temperature on the Auto-Ignition of Fuels with Different Cetane Number and Volatility," SAE Technical Paper 2012-01-1317, 2012.

[21] K. Wadumesthrige, N. Johnson, M. Winston-Galant, E. Sattler, N. Bezaire, S. Zeng, S. Salley, and K. Y. Ng, "Performance, Durability, and Stability of a Power Generator Fueled with ULSD, S-8, JP-8, and Biodiesel," SAE Technical Paper 2010-01-0636, 2010.

[22] R. M. George, T. Badawy, and N. Henein, "Experimental Study for the Effect of Fuel Properties on the Ion Current, Combustion, and Emission in a High Speed Diesel Engine," SAE Technical Paper 2014-01-1263, 2014.

[23] Z. Zheng, T. Badawy, N. Henein, E. Sattler, and N. Johnson, "Effect of Cetane Improver on Autoignition Characteristics of Low Cetane Sasol IPK Using Ignition Quality Tester (IQT)," J. Eng. Gas Turbines Power, 136(8), 2013.

[24] K. Zha, X. Yu, M.-C. Lai, and M. Jansons, "Investigation of Low-Temperature Combustion in an Optical Engine Fueled with Low Cetane Sasol JP-8 Fuel Using OH-PLIF and HCHO Chemiluminescence Imaging," SAE Technical Paper 2013-01-0898, 2013.

[25] K. Kitano, S. Misawa, M. Mori, I. Sakata, and R. H. Clark, "GTL Fuel Impact on DI Diesel Emissions," SAE Technical Paper 2007-01-2004, 2007.

[26] M. Oguma, S. Goto, and Z. Chen, "Fuel Characteristics Evaluation of GTL for DI Diesel Engine," SAE Technical Paper 2004-01-0088, 2004.

[27] M. Oguma, S. Goto, K. Oyama, K. Sugiyama, and M. Mori, "The Possibility of Gas to Liquid (GTL) as a Fuel of Direct Injection Diesel Engine," SAE Technical Paper 2002-01-1706, 2002.

[28] P. Schaberg, J. Botha, M. Schnell, H.-O. Hermann, N. Pelz, and R. Maly, "Emissions Performance of GTL Diesel Fuel and Blends with Optimized Engine Calibrations," SAE Technical Paper 2005-01-2187, 2005.

[29] S. Kook, and L. M. Pickett, "Soot Volume Fraction and Morphology of Conventional, Fischer-Tropsch, Coal-Derived, and Surrogate Fuel at Diesel Conditions," SAE Technical Paper 2012-01-0678, 2012.

[30] P. Schihl, L. Hoogterp-Decker, and E. Gingrich, "The Ignition Behavior of a Coal to Liquid Fischer-Tropsch Jet Fuel in a Military Relevant Single Cylinder Diesel Engine," SAE Technical Paper 2012-01-1197, 2012.

[31] H. B. Dixon, L. Bradshaw, and C. Campbell, "Firing of gases by adiabatic compression. Part I. Photographic analysis of flame.," Journal of Chemical Society, Transactions, 55(2), pp. 2027-2035, 1914.

[32] C. J. Hawks, "Some experimental work in connection with diesel engine - fuel oil in diesel engines," Engineering, 110, pp. 127-131, 1920.

[33] A. Otto, "Combustion of Liquid Fuels in Diesel Engine", National Advisory Committee for Aeronautics Technical Memo, 1924.

[34] K. Neuman, "Experiments on Self Ignition of Liquid Fuels", National Advisory Committee for Aeronautics Technical Memo, 1926.

[35] F. Sass, "Ignition and Combustion Phenomena in Diesel Engines", National Advisory Committee for Aeronautics Technical Memo, 1928.

[36] J. Tausz, and F. Shulte, "Determination of ignition points of liquid fuels under pressure", National Advisory Committee for Aeronautics Techical Memo, 1925.

[37] J. Tausz, and F. Schulte, "Ignition Points and Combustion Reactions in Diesel Engines", National Advisory Committee for Aeronautics Technical Memo, 1928.

[38] J. Tausz, and F. Schulte, "Ignition Points and Combustion Reactions in Diesel Engines", National Advisory Committee for Aeronautics Technical Memo, 1928.

[39] A. M. Rothrock, "The NACA apparatus for studying the formation and combustion of fuel sprays and the results preliminary tests", National Advisory Committee for Aeronautics Report, 1932.

[40] A. M. Rothrock, and C. D. Waldron, "Fuel vaporization and its effect on combustion in a high speed CI engine", National Advisory Committee for Aeronautics Technical Notes, 1932.

[41] C. Miller, "Slow-motion Study of Injection and Combustion of Fuel In a Diesel Engine," SAE Technical Paper 450235, 1945.

[42] W. Wenzel, "Ignition Process in Diesel Engines," NACA Technical Memo No., 797, 1936.

[43] T. Yu, O. A. Uyehara, P. S. Myers, R. N. Collins, and K. Mahadevan, "Physical and Chmeical Ignition Delay in an Operating Diesel Engine Using the Hot-Motored Technique," SAE Technical Paper 560061, 1956.

[44] R. Hurn, J. Chase, C. Ellis, and K. Hughes, "Fuel Heat Gain and Release in Bomb Ignition," SAE Technical Paper 560062, 1956.

[45] El Wakil, M. Myers, P. S. Myers, and O. A. Oyehara, "Fuel Vaporization and Ignition Lag in Diesel Combustion," SAE Technical Paper 560063, 1956.

[46] G. Sitkei, "Uber den dieselmotorisehen Zundverzug," M . T . Z . , Jahrg 24, Heft 6, 1963.

[47] W. T. Lyn, and E. Valdmanis, "The Effects of Physical Factors on Ignition Delay," Paper IME (London), Automobile Div., 1966.

[48] N. A. Henein, "A Mathematical Model for the Mass Transfer and Combustible Mixture Formation Around Fuel Droplets," SAE Technical Paper 710221, 1971.

[49] P. S. Pederson, and B. Quale, "A Model for the Physical Part of the Ignition Delay in a Diesel Engine," SAE Technical Papers 740716, 1974.

[50] T. W. R. III, "Correlation of Physical and Chemical Ignition Delay to Cetane Number," 1985.

[51] P. F. Flynn, R. P. Durrett, G. L. Hunter, A. O. z. Loye, O. C. Akinyemi, J. E. Dec, and C. K. Westbrook, "Diesel Combustion: An Integrated View Combining Laser Diagnostics, Chemical Kinetics, And Empirical Validation," SAE Technical Paper 1999-01-0509, 1999.

[52] J. Dec, "A Conceptual Model of DI Diesel Combustion Based on Laser-Sheet Imaging*," SAE Technical Paper 970873, 1997.

[53] W. Hwang, J. Dec, and M. Sjöberg, "Spectroscopic and chemical-kinetic analysis of the phases of HCCI autoignition and combustion for single- and two-stage ignition fuels," Combustion and Flame, 154(3), pp. 387-409,, 2008.

[54] J. Chen, T. Litzinger, and H. Curran, "The Lean Oxidation of Iso-Octane | at Elevated Pressures," SAE Technical Paper 2005-01-3734, 2005.

[55] C. K. Westbrook, "Chemical kinetics of hydrocarbon ignition in practical combustion systems," Proceedings of the Combustion Institute, 28(8), pp. 1563-1157, 2000.

[56] E. J. Silke, W. J. Pitz, C. K. Westbrook, M. Sjöberg, and J. E. Dec, "Understanding the Chemical Effects of Increased Boost Pressure under HCCI Conditions," SAE Int. J. Fuels Lubr. 1(1):12-25, 2009.

[57] K. Kuwahara, and H. Ando, "Role of Heat Accumulation by Reaction Loop Initiated by H2O2 Decomposition for Thermal Ignition," SAE International, 2007.

[58] M. Yao, and Z. Zheng, "An Investigation on a New Reduced Chemical Kinetic Model of n -heptane for HCCI Combustion," Proceedings of the Institution of Mechanical Engineers Part D Journal of Automobile Engineering, 220(7), pp. 991-1002, 2006.

[59] M. Yao, Z. Zheng, S. Xu, and M. Fu, "Experimental Study on the Combustion Process of Dimethyl Ether (DME)," 2003.

[60] G. D. Boerlage, and J. J. Broeze, "The Ignition Quality of Fuels in Compression Ignition Engines," Engineering, pp. 603-606, 687-689, 755-757, 1931.

[61] G. D. Boerlage, and J. J. Broeze, "Ignition Quality of Diesel Fuels as Expressed in Cetane Numbers," SAE Journal, 31, p. 283, 1932.

[62] H. H. Wolfer, "Ignition Lag in the Diesel Engine," VDI --- Forschumgshelft(392), 1938.

[63] J. Small, "Vagaries of Internal Combustion," Engineer, 164, pp. 642-668, 1937.

[64] F. A. F. Schmidt, "Theoretical and Experimental Study of Ignition Lag and Engine Knock", National Advisory Committee for Aeronautics Technical Memo, 1939.

[65] S. G. Bauer, "Ignition Lag in Compression Ignition Engines," Engineering, 148(368-369), 1939.

[66] A. C. West, and D. Taylor, "Ignition Lag in a Supercharged C. I. Engine," Engineering, pp. 281-282., 1941.

[67] E. Starkman, "Ignition Delay in Diesel Engines," Trans. American Institute of Chemical Engr., 42, pp. 107-120, 1946.

[68] M. A. Elliott, "Combustion of Diesel Fuel," SAE Quarterly Trans., 3, pp. 490-515, 1949.

[69] R. Mueller, "Untersuchung des Verbrennungsvergangs deutscher Schwerole in einer Versuchsbombe , 1, 1936, pp. 1-10," Kraftfahretech, Forschungsarb. No. 3, pp. 1-10, 1936.

[70] W. Jost, "Explosion and Combustion Processes in Gases", McGraw Hill, New York, 1946.

[71] R. W. Hurn, and K. J. Hughes, "Combustion Characteristics of Diesel Fuels as Measured in a Constant-Volume Bomb," SAE Quarterly Trans., 6, pp. 24-35, 1952.

[72] F. H. Garner, F. Morton, J. B. Saunby, and G. H. Grigg, "Preflame Reactions in Diesel Engines," Journal of Inst. of Petroleum, 43, pp. 124-130, 1957.

[73] F. H. Garner, F. Morton, and J. B. Saunby, "Preflame Reactions in Diesel Engines, Part V," Journal of the Institute of Petroleum, 47, pp. 175-193, 1961.

[74] K. C. Tsao, P. S. Myers, and O. A. Uyehara, "Gas Temperatures during Compression in Motored and Fired Diesel Engines," SAE Technical Paper 620518, 1962.

[75] W. T. Lyn, and E. Valdmanis, "The Application of High Speed Schlieren Photography to Diesel Combustion Research," F. L. of Photographic Science, 10, pp. 74-82, 1962.

[76] N. A. Henein, and J. A. Bolt, "Ignition Delay in Diesel Engines," SAE Technical Paper 670007, 1967.

[77] N. A. Henein, and J. A. Bolt, "The Effect of Some Engine Variables on Ignition Delay and Other Combustion Phenomena in a Diesel Engine," Proceedings of the Institution of Mechanical Engineers, 184(310), pp. 130-136, 1969.

[78] N. A. Henein, and J. A. Bolt, "Correlation of Air Charge Temperature and Ignition Delay for Several Fuels in a Diesel Engine," SAE Technical Paper 690262, 1969.

[79] F. W. Stringer, A. E. Clarke, and D. J. S. Clarke, "Spontaneous Ignition of Hydrocarbon Fuels in a Flowing System," Proceedings of the Institution of Mechanical Engineers, 184(10), pp. 212-225, 1970.

[80] H. Hiroyasu, and T. Kadota, "Evaporation and Spontaneous Ignition Delay of a Fuel Droplet and Spray in High Pressure Gaseous Environments," Department of Mechanical Engineering, Hiroshima University, Hiroshima, Japan, 1977.

[81] T. W. R. III, and B. Stapper, "Diesel Fuel Ignition Quality as Determined in a Constant Volume Combustion Bomb," SAE Technical Paper 870586, 1987.

[82] T. W. R. III, and T. J. Callahan, "Engine and Constant Volume Bomb Studies of Diesel Ignition and Combustion," 1988.

[83] N. A. Henein, and Y. Akasaka, "Effect of Physical Properties and Composition on Fuels on Autoignition and Cetane Rating," 1987.

[84] Soon-Ik Kwon, M. Arai, and H. Hiroyasu, "Effect of Temperature and Pressure on Ignition Delay in Direct Injection Diesel Engine," MESJ, 24, 1990.

[85] J. Taylor, R. McCormick, and W. Clark, "Report on the relationship between molecular structure and compression ignition fuels, both conventional and HCCI," NREL/MP-540-36726, National Renewable Energy Laboratory, 2004.

[86] J. Taylor, "Using IQT measurements, develop simplified kinetic expressions for ignition of fuels that could be used in HCCI engine models," NREL/MP-540-40755, National Renewable Energy Laboratory, 2006.

[87] G. Bogin, A. M. Dean, M. A. Ratcliff, J. Luecke, and B. T. Zigler, "Expanding the Experimental Capabilities of the Ignition Quality Tester for Autoigniting Fuels," SAE Int. J. Fuels Lubr., 3(1), pp. 353-367, 2010.

[88] D. A. Rothamer, and L. Murphy, "Systematic study of ignition delay for jet fuels and diesel fuel in a heavy-duty diesel engine," Proceedings of the Combustion Institute, 34(2), pp. 3021-3029, 2013.

[89] I. Singh, "Parametric analysis of combustion and engine-out emissions in a single cylinder HSDI diesel engine," Mechanical Department, Wayne State University, 2009.

[90] K. Acharya, "Effect of The Percentage of Soybean Biodiesel in Blends with ULSD on Autoignition, Combustion and Emissions in a Single Cylinder HSDI Diesel Engine," MS, Wayne State University, Detroit, 2009.

[91] C. Jayakumar, Z. Zheng, U. M. Joshi, N. Henein, W. Bryzik, and E. Sattler, "Effect of inlet Air Temperature on Auto-Ignition of Fuels with Different Cetane Number and Volatility," ICEF2011-60141, pp. 261-272, 2011.

[92] Z. Zheng, P.-I. Lee, A. Shrestha, T. Badawy, M.-C. Lai, N. Henein, and E. Sattler, "Role of Volatility in the Development of JP-8 Surrogates for Diesel Engine Application," SAE International, 2014.

[93] ASTM International, "Standard Test Method for Cetane Number of Diesel Fuel Oil," D613 – 10a, 2010.

[94] ASTM International, "Standard Test Method for Determination of Ignition Delay and Derived Cetane Number (DCN) of Diesel Fuel Oils by Combustion in a Constant Volume Chamber," D6890 – 10a, 2010.

[95] A. J. Donkerbroek, M. D. Boot, C. C. M. Luijten, N. J. Dam, and J. J. ter Meulen, "Flame lift-off length and soot production of oxygenated fuels in relation with ignition delay in a DI heavy-duty diesel engine," Combustion and Flame, 158(3), pp. 525-538, 2011.

[96] K. Zaidi, G. E. Andrews, and J. H. Greenhough, "Diesel Fumigation Partial Premixing for Reducing Ignition Delay and Amplitude of Pressure Fluctuations," SAE Technical Paper 980535, 1998.

[97] D. N. Assanis, Z. S. Filipi, S. B. Fiveland, and M. Syrimis, "A Predictive Ignition Delay Correlation Under Steady-State and Transient Operation of a Direct Injection Diesel Engine," Journal of Engineering for Gas Turbines and Power, 125(2), p. 450, 2003.

[98] R. P. Rodríguez, R. Sierens, and S. Verhelst, "Ignition delay in a palm oil and rapeseed oil biodiesel fuelled engine and predictive correlations for the ignition delay period," Fuel, 90(2), pp. 766-772, 2011.

[99] W. F. Colban, P. C. Miles, and S. Oh, "Effect of Intake Pressure on Performance and Emissions in an Automotive Diesel Engine Operating in Low Temperature Combustion Regimes," SAE Technical Paper 2007-01-4063, 2007.

[100] Y. V. Aghav, V. M. Thatte, M. N. Kumar, P. A. Lakshminarayanan, and M. K. G. Babu, "Predicting Ignition delay and HC emission for DI diesel engine encompassing EGR and Oxygenated fuels," SAE Technical Paper 2008-28-0050, 2008.

[101] D. B. Lata, and A. Misra, "Analysis of ignition delay period of a dual fuel diesel engine with hydrogen and LPG as secondary fuels," International Journal of Hydrogen Energy, 36(5), pp. 3746-3756, 2011.

[102] L. Murphy, and D. Rothamer, "Effects of Cetane Number on Jet Fuel Combustion in a Heavy-Duty Compression Ignition Engine at High Load," SAE Technical Paper 2011-01-0335, 2011.

[103] J. Cowart, M. Carr, P. Caton, L. Stoulig, D. Luning-Prak, A. Moore, and L. Hamilton, "High Cetane Fuel Combustion Performance in a Conventional Military Diesel Engine," SAE Technical Paper 2011-01-0334, 2011.

[104] D. Han, A. M. Ickes, S. V. Bohac, Z. Huang, and D. N. Assanis, "Premixed low-temperature combustion of blends of diesel and gasoline in a high speed compression ignition engine," Proceedings of the Combustion Institute, 33(2), pp. 3039-3046, 2011.

[105] A. Janssen, S. Pischinger, and M. Muether, "Potential of Cellulose-Derived Biofuels for Soot Free Diesel Combustion," SAE Int. J. Fuels Lubr., 3(1), pp. 70-84, 2010.

[106] C. Jayakumar, J. Nargunde, A. Sinha, N. A. Henein, W. Bryzik, and E. Sattler, "Effect of Swirl and Injection Pressure on Performance and Emissions of JP-8 Fueled High Speed Single Cylinder Diesel Engine," Journal of Engineering for Gas Turbines and Power, 134(2), p. 022802, 2012.

[107] "CONVERGE theory manual Version 2.1.0," CONVERGE Science Inc., 2013.

[108] H. J. Curran, P. Gaffuri, W. P. Pitz, and C. K. Westbrook, "A Comprehensive Modeling Study of n-Heptane Oxidation," Combustion and Flame, 114, pp. 149-177, 1998.

[109] A. Shrestha, "JP-8 Surrogates for Diesel Engine Application: Development, Validation, and CFD Simulation," PhD, Wayne State University, Detroit, 2014.

[110] T. Minagawa, H. Kosaka, and T. Kamimoto, "A Study on Ignition Delay of Diesel Fuel Spray via Numerical Simulation," 2000.

ABSTRACT

QUANTIFICATION OF AUTO-IGNITION IN DIESEL ENGINES

by

UMASHANKAR JOSHI

AUGUST 2015

Advisor: Dr. Naeim Henein

Major: Mechanical Engineering

Degree: Doctor of Philosophy

Efforts have been made previously by researchers to quantify the auto-ignition quality of fuels by calculating global activation energy using Arrhenius plots with data measured for the ignition delay period (ID). Large variation in the activation energy of fuels has been observed even for fuels with closer CN values. More recently, the activation energy values obtained by Kook et al in (2005) on an optical engine do not agree with data obtained in an identical metallic engine by Jayakumar using fuels of same CN.

The disparity in their results can be attributed to the differences in ignition delay (ID) and effective temperature definitions used. Most researchers agree upon the start of ID time as the start of injection (SOI). The main point of disagreement has been in defining the end of ID period which is considered to be the start of combustion (SOC).

As a result, numerous definitions for the ID period have been used by researchers which lead to variation in calculation of activation energy value. In addition, in heterogeneous combustion equipment to account for changes in charge temperature due to fuel evaporation and piston movement (in engines) an effective temperature value is used. Different definitions for the effective temperature have been reported in the literature. This leads to more variations in the activation energy value calculation. Furthermore, it was observed that engine test conditions and the temperature regime in which the tests are done would also affect the calculation of activation energy value.

This dissertation examines the effects of ignition delay definitions, effective temperatures, engine conditions and temperature regimes on the global activation energy. Moreover, homogeneous charge test data has shown presence of a NTC regime in which the activation energy value can be either positive, negative or zero. However, heterogeneous test data from literature has always shown positive values for activation energy. This dissertation has also explained the reasons behind such a behavior.

AUTOBIOGRAPHICAL STATEMENT

I was born in a family of farmers, who did terrace farming in the foothills of the Himalayas. My grandparents did their best to provide better education to their children, and my father managed to complete his graduation. On the other hand, my mother wasn't that lucky and in a big family didn't get the opportunity to study beyond the third grade. However, both my parents have always encouraged me to strive for higher education as if to fulfill their dreams through me, especially my mother.

The search for better education took me all over India. After my birth in Kolkata, in eastern India, my family moved to Nainital which is in northern India. Nainital has some of the best schools in India but not many good colleges for higher education. By the time I was about to finish my high school I had to move to Mumbai, in western India. I completed my engineering from Pune University which is at four hours' drive from Mumbai. My journey for education did not stop there and brought me to pursue Masters in Mechanical engineering at Wayne State University, Detroit in 2007. I never thought I would be pursuing PhD after completing my Masters, but when the opportunity came I grasped it with both hands.

It would be a lie if I said it was just education which brought me to America. The constantly changing of cities and places has made me yearn for more travels and journeys. Studying in a different country gives you the chance to see different cultures and meet new people. This desire coupled with an opportunity to study at a prestigious university made me to choose WSU. I believe "Life is a journey" and we should all enjoy it.